

Chaos on Quantum Graphs with Andreev Scattering

Inaugural-Dissertation
zur
Erlangung des Doktorgrades
der Mathematisch-Naturwissenschaftlichen Fakultät
der Universität zu Köln

vorgelegt von
Burkhard E. R. Seif
aus Freiburg im Breisgau

Köln 2003

Berichterstatter: Prof. Dr. M. Zirnbauer
Prof. Dr. F. von Oppen

Tag der mündlichen Prüfung: 19. Mai 2003

Contents

1. Introduction	9
1.1. Superconductivity	10
1.1.1. Microscopic theory of superconductivity	10
1.1.2. The Bogoliubov-deGennes formalism	11
1.1.3. Andreev scattering	12
1.2. Random-matrix theory	17
1.2.1. Gaussian Wigner-Dyson ensembles	17
1.2.2. Circular Wigner-Dyson ensembles	18
1.2.3. A brief historical survey	19
1.2.4. The novel symmetry classes beyond Wigner-Dyson	19
1.3. Periodic-orbit theory	24
1.4. Periodic-orbit theory meets RMT – Berry’s diagonal approximation	31
1.5. The form factors of the new ensembles	33
1.6. Quantum graphs	34
2. Andreev quantum graphs – a numerical analysis	41
2.1. Motivation – random boundary conditions on Schrödinger graphs	42
2.2. Setting up the Andreev graph	44
2.3. Ensemble average generated by random boundary conditions on the vertices	49
2.4. The numerical routine for computing the spectrum	51
2.5. Comparison of numerical results with RMT predictions	54
2.6. Periodic orbit contributions	58
2.7. Concluding remarks and summary	60

3. Andreev Star Graph	61
3.1. Set-up and formalism of the Andreev star graph	63
3.1.1. Star graph with preserved spin-rotation invariance; classes C and CI	63
3.1.2. Star graph without spin-rotation invariance – classes D and $DIII$	68
3.1.3. Requirements on the Andreev scatterers by symmetry	69
3.2. Andreev Star Graph with symmetries of class C	72
3.3. Andreev Star Graph with symmetries of class CI	79
3.4. Andreev Star Graph with symmetries of class D	83
3.5. Andreev Star Graph with symmetries of class $DIII$	88
3.6. The numerical routine used in computing the form factor	98
3.7. Andreev Billiards	99
3.8. Summary	102
A. The superconducting-normalconducting (SN) interface	105
B. Method of stationary phase	109
C. The trace formula for quantum graphs	111
D. Monotonic anti-clockwise movement of eigenphases $\theta_n(E)$	115
E. The Schur orthogonality relations	117
F. Form factors of the new ensembles	119
Bibliography	122

Preface

The subject of this thesis belongs to the realm of mesoscopic physics and lies at the crossroads of two fascinating branches in physics: superconductivity and quantum chaos.

The field of mesoscopic physics involves the study of systems of sizes in between the microscopic and macroscopic world. In this range, quantum interference effects arise when the phase coherence length exceeds the system size. In order to achieve coherence of the quantum mechanical phase, the system is cooled to such low temperatures [of $\mathcal{O}(1K)$] that electron-phonon interactions and inelastic electron-electron interactions are frozen out [1]. Observing the fascinating phenomena due to quantum phase coherence has been made possible by the rapid advances of nanotechnology in fabricating mesoscopic structures over the last decades. This experimental headway – hand in hand with progress on the side of theoretical physics – has made mesoscopic research a very active field.

By superconductivity, we refer to the phenomenon that the electrical resistivity of a specimen drops to zero when cooled below a certain temperature. This striking phenomenon was first discovered by Kamerlingh Onnes in 1911. Theoretical explanations of the experimental findings were given by the phenomenological Ginzburg-Landau theory and the microscopic theory of Bardeen, Cooper and Shrieffer in the 1950s. The field of superconductivity underwent a renaissance when Bednorz and Müller discovered high-temperature cuprate superconductors in 1986, spurring renewed interest and activity in the field.

Quantum Chaos is the quantum mechanics of classically non-integrable systems. While chaos in classical mechanics can be described by properties of trajectories in phase space, the quantization of phase space in quantum mechanics calls for an alternative approach for a study of chaos. In the quantum case, the knowledge about the underlying classical dynamics of the system is encoded in the energy spectrum.

The current thesis analyzes spectral properties of mesoscopic systems with two components where a superconductor is in contact with a normal metal with underlying non-integrable classical mechanics. In referring to their two components, such systems are termed superconducting-normalconducting hybrid systems. The phenomenology of such hybrid systems is reigned by the additional charge conjugation symmetry, as electrons and holes are coupled by the superconducting order parameter. This coupling is achieved by the scattering mechanism at the interface between superconductor and normal metal which

goes under the name of Andreev reflection. This is why such normal-metal billiards adjacent to a superconductor have been termed Andreev billiards.

A single spectrum (i.e. the positions of the individual energy eigenvalues) depends on the details of the system under scrutiny (like the geometry of the system). Evaluating an individual spectrum is of little interest to the scientist interested in the *universal* laws of physics. Instead of a single system, one evaluates an *ensemble* of systems where the averaging procedure may run over different system geometries.

The present thesis is organized in three chapters.

The first chapter is an introduction to the concepts needed in formulating the problem and the methods employed for its solution. This covers topics of as wide a range as superconductivity, random-matrix theory, periodic-orbit theory and its application to spectra in order to obtain universal results. The section on random-matrix theory mainly dwells on the new symmetry classes [2] relevant for the analysis of superconducting-normalconducting hybrid systems. Besides, we introduce the spectral quantity of the new ensembles under scrutiny – the form factor as the Fourier transform of the quantum spectrum. The introductory chapter is concluded by a presentation of the model of choice for the formulation of a solution – quantum graphs.

The second chapter offers a numerical treatise on quantum graphs which include the Andreev scattering mechanism characteristic for superconducting-normalconducting hybrid systems; this led us to the coinage of the term “Andreev quantum graphs”. The necessary ensemble average over the different realizations of the ensemble of graphs is generated by choosing various boundary (scattering) conditions on the graph. The numerical results are compared to predictions of random-matrix theory while non-universal features are accounted for by periodic-orbit theory.

The third chapter offers both an analytical and a numerical solution for the spectral quantities of the new ensembles with the aid of periodic-orbit theory. By mimicking the geometry of an Andreev billiard, one is led to the setup of Andreev graphs with a star structure (where Andreev scattering takes place at the periphery). For this specific star topology of quantum graphs, the form factor of the spectrum is calculated for all of the symmetry classes C , CI , D , and $DIII$. A generalization of these findings for star graphs to Andreev billiards is given for symmetry classes C and CI .

For a more cohesive presentation of the main text, some technicalities and details of calculations are then presented in the appendices A – F.

1. Introduction

The basis for the current thesis is the symmetry classification formulated by Altland and Zirnbauer treating normal-conducting mesoscopic systems in contact with a superconductor [2]. If the underlying dynamics is chaotic, the quasi-particle energy spectrum shows novel universal level statistics. The aim of the thesis is a semiclassical interpretation of this level statistics.

An outline of the systems studied and the methods and concepts employed in the thesis is given in the current introductory chapter. The survey of the topics treated is organized as follows:

We start the introduction with an explanation of the actual physical system under scrutiny. The topical system is the so-called Andreev billiard which is a generalization of a conventional billiard. Its distinguishing feature is that part of the boundary is formed by a superconductor. Consequently, we must start with a brief introduction to superconductivity and its treatment on a mean-field level by the Bogoliubov-deGennes formalism. One may say that the Andreev billiard is one representative of superconducting-normalconducting hybrid systems which form the “playground” for an application of the ideas of [2].

The Andreev billiards studied belong to a larger group of systems with the common property that they are quantum systems whose classical analogues are non-integrable. The field of physics studying those quantum systems goes under the name of “quantum chaos”. After a very brief introduction to quantum chaos, our attention turns to a powerful technique of theoretical physics – random-matrix theory. This theory can be applied in the so-called *ergodic* regime where the system is given enough time such that the degrees of freedom equilibrate and the entire phase-space is explored uniformly. In this range, spectral properties can be described by a model Hamiltonian with *random* entries and by taking only the fundamental *symmetries* into account. A brief overview of Wigner’s and Dyson’s pioneering ideas [3, 4] is given, followed by a concise presentation of the historical development of random-matrix theory. We then turn to the new universality classes beyond the Wigner-Dyson set-up. Important here are the chiral classes which model the Dirac operator in the presence of a random gauge field [5, 6] and the work by Altland and Zirnbauer which finds its application in the context of superconductivity [2, 7].

Following the chapter on random-matrix theory, we present yet another theoretical concept successful in the description of chaotic systems: periodic-orbit

theory pioneered by Gutzwiller [8]. This theory provides a relation between classical and quantum mechanics for those systems whose classical motion is non-integrable. The Gutzwiller trace formula links the quantum spectrum of a system to classically allowed paths and their properties. Its range of validity is the *semiclassical regime* where typical actions are large compared to Planck's quantum of action \hbar . This is why the associated field of research is also referred to as semiclassics.

Periodic-orbit theory was subsequently employed by Berry to compute a statistical quantity bilinear in the density of states of a chaotic system, the form factor [9]. By his calculation, random-matrix theory predictions were reproduced, while at the same time the limits of validity of the random-matrix approach were clarified. Berry's work [9] is motivation for the present thesis insofar as it demonstrates how random-matrix theory predictions can be explained within the framework of periodic-orbit theory.

The model we chose for the evaluation of our Gutzwiller type trace formula is the *quantum graph*. Kottos and Smilansky [10] were the first to study the spectral statistics of these simple quantum systems, offering insights into the connection between random-matrix theory and the underlying classical mechanics of the quantum graph system. As quantum graphs are extremely powerful and transparent in the spectral analysis based on periodic orbits, we conclude this introduction by a presentation of the seminal contribution of [10, 11] to the field of quantum chaos.

The task of the thesis can also be formulated in the following way. In the same way as Berry [9] gave insight into the validity of the Wigner-Dyson ensembles on the basis of Gutzwiller's trace formula, we set out for an explanation of universal spectral features of the novel symmetry classes [2] within periodic-orbit theory.

1.1. Superconductivity

1.1.1. Microscopic theory of superconductivity

The present work is based on a self-consistent field method approach rather than on the microscopic theory of superconductivity. Yet some remarks on the microscopic theory seem appropriate as the theory by Bardeen, Cooper and Schrieffer (BCS for short) [12] revolutionized the understanding of superconductivity. Cooper observed that the ground state of a free electron gas becomes unstable in the presence of an attractive interaction and that pairs of electron build bound states – what has come to be known as Cooper pairs [13]. BCS introduced a ground state wave function describing a coherent state of Cooper pairs and fixed the details of the wave function by a variational calculation. Yet this approach is valid only if momentum is a good quantum number i. e., in the case of spatially homogeneous systems. In the case of a nonuniform system – for example at boundaries of the superconductor or at scattering centers –

an alternative approach proves to be fruitful. These situations can be dealt with by the Bogoliubov method, which generalizes the Hartree-Fock equations to include the superconducting pair potential. Besides, the Bogoliubov method is better suited to handle excitations than the variational BCS method.

1.1.2. The Bogoliubov-deGennes formalism

In this section, we present the key steps of the mean field approximation to treat superconductors. We lean on deGennes' account of the method [14]. The Bogoliubov-deGennes (BdG) Hamiltonian is written in a second quantized form as the sum

$$\hat{H} = \hat{H}^{(1)} + \hat{H}^{(2)} \quad (1.1)$$

of the one-particle Hamiltonian

$$\hat{H}^{(1)} = \int d^d r \psi_\sigma^\dagger(\mathbf{r}) \left[\underbrace{\left(\frac{1}{2m} (\mathbf{p} - e\mathbf{A})^2 - \mu \right)}_{h_0} \delta_{\sigma\tau} + V_{\sigma\tau}(\mathbf{r}) \right] \psi_\tau(\mathbf{r}) \quad (1.2)$$

and the two-particle interaction:

$$\hat{H}^{(2)} = \frac{1}{2} \int d^d r \int d^d r' \psi_\delta^\dagger(\mathbf{r}) \psi_\gamma^\dagger(\mathbf{r}') U_{\delta\gamma,\sigma\tau}^{(2)}(\mathbf{r}, \mathbf{r}') \psi_\sigma(\mathbf{r}') \psi_\tau(\mathbf{r}). \quad (1.3)$$

$\psi_\delta(r)$ is the electronic (fermionic) field, where the index δ labels the spin. Einstein's summation convention is implied. μ stands for the chemical potential such that energies are measured relative to the Fermi energy. Interactions with an external field, such as spin-orbit scattering, are comprised in V . In the spirit of a mean field approximation, the quartic product of fields in $\hat{H}^{(2)}$ is decoupled by neglecting fluctuations. With a spin-independent contact type of interaction $U_{\delta\gamma,\sigma\tau}^{(2)}(\mathbf{r}, \mathbf{r}') = -g \delta_{\sigma\gamma} \delta_{\tau\delta} \delta(\mathbf{r} - \mathbf{r}')$, the order parameter is

$$\Delta_{\sigma\tau}(\mathbf{r}) := -\frac{g}{2} \langle \psi_\sigma(\mathbf{r}) \psi_\tau(\mathbf{r}) \rangle. \quad (1.4)$$

This possibility of non-vanishing expectation values (1.4) is the key feature of the mean field theory of superconductivity. The resulting effective one-particle Hamiltonian is given by:

$$H_{\text{eff}} = \int d^d r \left[\psi_\sigma^\dagger(\mathbf{r}) h_{0\sigma\tau}(\mathbf{r}) \psi_\tau(\mathbf{r}) + \Delta_{\sigma\tau}(\mathbf{r}) \psi_\sigma^\dagger(\mathbf{r}) \psi_\tau^\dagger(\mathbf{r}) + \Delta_{\sigma\tau}^*(\mathbf{r}) \psi_\tau(\mathbf{r}) \psi_\sigma(\mathbf{r}) \right]. \quad (1.5)$$

This Hamiltonian is diagonalized by a generalized Bogoliubov transformation [15, 16] of the form

$$\psi_\sigma(\mathbf{r}) = \sum_n u_{n\sigma}(\mathbf{r}) \gamma_n + v_{n\sigma}^*(\mathbf{r}) \gamma_n^\dagger \quad (1.6)$$

where the operators γ_n^\dagger and γ_n (which obey fermion anti-commutation rules) and the coefficients $u_{n\sigma}(\mathbf{r})$ and $v_{n\sigma}(\mathbf{r})$ are introduced. From the commutator of H_{eff} with the field $\psi_\sigma(\mathbf{r})$

$$[H_{\text{eff}}, \psi_\sigma(\mathbf{r})] = h_0 \psi_\sigma(\mathbf{r}) + V_{\sigma\tau}(\mathbf{r})\psi_\tau(\mathbf{r}) + \Delta_{\sigma\tau}(\mathbf{r})\psi_\tau^\dagger(\mathbf{r}), \quad (1.7)$$

one obtains, by use of the equation of motion $[H_{\text{eff}}, \gamma_n] = -E_n\gamma_n$, the expansion (1.6) and its hermitian conjugate the spin-generalized Bogoliubov equations:

$$\begin{bmatrix} h_0 + V_{\uparrow\uparrow} & V_{\uparrow\downarrow} & \Delta_{\uparrow\uparrow} & \Delta_{\uparrow\downarrow} \\ V_{\downarrow\uparrow} & h_0 + V_{\downarrow\downarrow} & \Delta_{\downarrow\uparrow} & \Delta_{\downarrow\downarrow} \\ -\Delta_{\uparrow\uparrow}^* & -\Delta_{\uparrow\downarrow}^* & -h_0^* - V_{\uparrow\uparrow}^* & -V_{\uparrow\downarrow}^* \\ -\Delta_{\downarrow\uparrow}^* & -\Delta_{\downarrow\downarrow}^* & -V_{\downarrow\uparrow}^* & -h_0^* - V_{\downarrow\downarrow}^* \end{bmatrix} \begin{bmatrix} u_\uparrow(\mathbf{r}) \\ u_\downarrow(\mathbf{r}) \\ v_\uparrow(\mathbf{r}) \\ v_\downarrow(\mathbf{r}) \end{bmatrix} = E \begin{bmatrix} u_\uparrow(\mathbf{r}) \\ u_\downarrow(\mathbf{r}) \\ v_\uparrow(\mathbf{r}) \\ v_\downarrow(\mathbf{r}) \end{bmatrix}. \quad (1.8)$$

where all matrix entries are $N \times N$ -dimensional arrays. The N -dimensional vectors $u_{\uparrow/\downarrow}(\mathbf{r}), v_{\uparrow/\downarrow}(\mathbf{r})$ have as entries the coefficients $u_{n\sigma}(\mathbf{r}), v_{n\sigma}(\mathbf{r})$ ($1 \leq n \leq N$) of the expansion (1.6) truncated when $n = N$. Besides, we note that $\Delta_{\sigma\tau}^T = -\Delta_{\tau\sigma}$ from the definition (1.4) and the expansion (1.6). By use of $2N \times 2N$ -dimensional arrays, we find a more succinct notation of the Bogoliubov-deGennes Hamiltonian (in line with the formalism on which the work in [2] is based):

$$\mathcal{H} = \begin{bmatrix} \hat{h} + \hat{V} & \Delta \\ -\Delta^* & -\hat{h}^T - \hat{V}^T \end{bmatrix} \quad (1.9)$$

with the $2N \times 2N$ arrays $\Delta = -\Delta^T$, $\hat{h} = \hat{h}^\dagger$, and $\hat{V} = \hat{V}^\dagger$.

In cases of preserved spin-rotation invariance, this invariance enforces vanishing entries (in the subblocks $V_{\uparrow\downarrow}, V_{\downarrow\uparrow}, \Delta_{\uparrow\uparrow}, \Delta_{\downarrow\downarrow}$) such that two commuting subblocks arise in the Hamiltonian on the left-hand side in eq. (1.8) (see also treatment of class C in section 1.2.4). If only one of these subblocks is taken into account and spin indices are suppressed, the resulting matrix form of the Hamiltonian is $2N \times 2N$ -dimensional:

$$\mathcal{H} = \begin{bmatrix} \hat{h} + \hat{V} & \Delta \\ \Delta^* & -\hat{h}^T - \hat{V}^T \end{bmatrix} \quad (1.10)$$

where the arrays Δ and $\hat{h} + \hat{V}$ are $N \times N$ -dimensional.

In the Russian literature, the effective (mean-field) Hamiltonian (1.5) is known as the Bogoliubov or Gorkov Hamiltonian after its inventors. In the Anglo-Saxon literature, the denotation Bogoliubov-deGennes Hamiltonian is commonly used paying tribute to the popularization of the mean field description by de Gennes. This information on nomenclature is found in [17].

1.1.3. Andreev scattering

All systems under scrutiny in the current thesis have in common the fact that they are hybrid systems comprised of a superconductor adjacent to a normal-conducting metal. By the vicinity of the superconductor, superconducting characteristics are imparted on the electrons in the normal-conducting region. First,

the scattering phenomena at an interface between superconductor and normal-conducting metal are explained – these phenomena go under the name of *Andreev scattering*. Then we introduce the so-called *Andreev billiard*, where part of the boundary of the billiard region is made up of a superconductor.

The interface between a superconductor and a normal-conducting metal (SN-interface)

The basic coupling process at the interface between a normal-conducting metal and a superconductor (SN-interface) is called *Andreev reflection*. It is named after Andreev who discovered how the reflection of quasi-particle excitations leads to an additional thermal resistance of the SN-heterosystem [18]. This scattering process is described as follows. Let us assume an electron with energy E far below the order parameter $E \ll \Delta$ is incident from the normal-conducting region. When this electron impinges on the interface, it represents a forbidden quasi-particle state for the superconducting region and cannot enter the superconductor. With no quasi-particle state accessible, it may be retroreflected off the boundary back into the normal-conducting region as a *hole*. The charge balance shows that a net charge of $2e$ is transferred across the interface. This charge is converted to a Cooper pair and contributes to the condensate current.¹ This situation is illustrated in figure 1.1. We give a brief summary of the features of Andreev scattering that are of relevance throughout the main body of the work:

- *All three* components of the velocity change sign when the quasi-particle is Andreev scattered at the interface. The hole is reflected back along the path of the incoming electron. This is why one speaks of “retro-reflection“ in contrast to ordinary “specular reflection”.
- An electron with energy $+E$ above the Fermi energy is converted into a hole with energy $-E$ below the Fermi energy (and vice versa).
- The hole acquires a phase $-\pi/2 - \varphi$, where φ is the phase of the order parameter of the superconductor at the interface. It is obvious from eq. (1.4) that the phase φ of the order parameter is a *gauge dependent* quantity.

¹A current produced by a specified level occupied with an electron is precisely the same as the current that would be produced if the specified level were unoccupied and all other levels in the band were occupied but with particles of charge *opposite* to the charge of the electron. Thus, even though the only charge carriers are electrons, we may for convenience consider the current to be carried entirely by fictitious particles of *positive* charge that fill all those levels in the band that are *unoccupied* by electrons. These fictitious particles are called *holes* [19]. In this picture, the initial situation is a filled band with an excess electron just above the band edge in the normalconducting region. The final situation on the side of the normalconducting metal is given by a full band with one level unoccupied just beneath the band edge (two electrons enter the superconductor as one Cooper pair). If one regards the final situation on the side of the normal metal in the hole picture, it is given by an empty band with one level occupied by a hole.

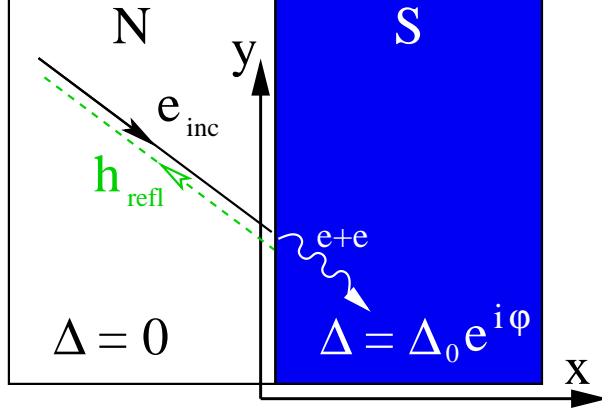


Figure 1.1.: At the SN-interface a normal-conducting metal (labeled by “N” in the figure) and a superconductor (labeled by “S”) meet. The Andreev reflection of an incident electron is shown. The reflected quasi-particle is a *hole* that *retraces* the path of the incoming electron. The net current flow of $2e$ across the interface is converted to a condensate current.

It will be shown in section 3.1.1 that all *physical properties* calculated are *gauge independent*. When a hole is incident on the interface and consequently an electron is scattered back, the outgoing electron acquires the phase $-\pi/2 + \varphi$. Such phases (transferred on the quasi-particles by the superconductor) play a prominent role in the main body of the work when it comes to the construction of ensemble averages.

A detailed calculation backing these summarizing statements is given in appendix A. Here, we briefly discuss the most remarkable feature that *all* components of the velocity are inverted. Although striking at first sight, the retro-reflection can be understood when we discuss momentum conservation for the component parallel to the interface and the necessary momentum transfer perpendicular to the interface.

Translational invariance along the interface entails that the component of momentum parallel to the interface is conserved. As the mass of the hole is opposite to the electron mass, the velocities parallel to the interface have to change sign too, such that the parallel component of momentum is conserved.²

Now consider the momentum component perpendicular to the interface. In order to scatter an incident electron back as an *electron*, the interface would have to transfer roughly twice the Fermi momentum $2\hbar k_F$. This is the momentum

²The statement about opposite (effective) masses of electrons and holes in the BdG formalism is best understood from the BdG Hamiltonian (1.10) and the form of the free one-particle Hamiltonian h_0 in eq. (1.2): $h_0 = (\mathbf{p} - e\mathbf{A})^2/2m - \mu$. The electron (hole) dynamics is governed by h_0 ($-h_0^*$), such that the *mass and charge* of the hole and the electron have opposite relative signs.

needed to transfer the electron from one side of the Fermi sphere to the opposite side. However, we must take into account that the step-like switch from zero order parameter to the bulk value Δ – as shown in figure 1.1 – is an idealisation known in the literature as “rigid boundary condition” [20]. As discussed by Beenakker in [20], it is the pairing interaction $g(\mathbf{r})$ (in $\Delta(\mathbf{r}) = -g(\mathbf{r}) \langle \psi(\mathbf{r})\psi(\mathbf{r}) \rangle$) that is absent in the normal region ($g(\mathbf{r}) = 0$ for $x < 0$) and which leads to a vanishing order parameter $\Delta(\mathbf{r})$ in the normal region. However, the value of $\langle \psi(\mathbf{r})\psi(\mathbf{r}) \rangle$ varies on the length scale $\xi = \hbar v_F / \Delta \gg k_F^{-1}$. Thus, the SN-boundary is too “soft” to generate enough momentum transfer for the reversal of the electron’s momentum. The necessary momentum transfer for the Andreev scattering from electron to hole requires only $\Delta p_\perp \approx (E/E_F) p_F \ll p_F$, where E is the excitation energy measured from the Fermi edge.

Normal backscattering is possible if an atomic-scale potential is present at the interface. Impurities at the interface give rise to such a potential. For the work in chapter 3 of the thesis, we assume clean interfaces without impurities. In this case, quasi-particle conversion at the interface is complete, i. e. *every* electron is scattered back as a hole (and vice versa).

Andreev billiard

In a conventional billiard, particles are confined by a step-like, one-particle potential to some region where they propagate ballistically. These billiards have been topics in quantum chaos research for more than a decade now [21]. Andreev billiards are a generalization of these conventional billiards. They were first studied in [22]. In an Andreev billiard, parts of the boundary of the billiard region are formed by an SN-interface described in the previous subsection. The presence of the SN-interface drastically changes the dynamics in the billiard. First, we discuss the billiard with *no* magnetic field present. Then electrons (holes) sufficiently close to the Fermi energy ($E \ll |\Delta| \ll \mu$) are retro-reflected as holes (electrons) and retrace the original trajectory backwards. The consequence of this mechanism on the orbits of a chaotic billiard is drastic, as essentially all trajectories eventually hit any given part of the boundary. Thus, if the chaotic billiard is coupled to a superconductor, *any* quasi-particle hits the SN-interface in the end, leading to a periodic orbit bouncing back and forth between two points on the SN-interface. Consequently, a conventional chaotic billiard with zero magnetic field that is coupled to a superconductor has a combined electron-hole dynamics that is no longer chaotic, since the resulting trajectories are all periodic. The combined electron-hole motion is integrable regardless of the shape of the billiard. This situation has been sketched in figure 1.2.

It has been pointed out in [23] that the gap induced in the spectrum of a billiard coupled to a superconductor is sensitive to whether the classical dynamics of the (normal) billiard is integrable or chaotic: a gap opens when the classical dynamics is chaotic, it closes if the billiard geometry leads to integrable dynamics.

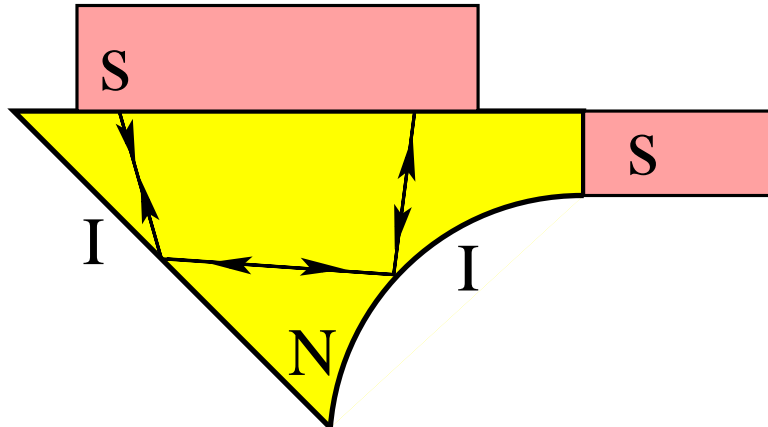


Figure 1.2.: The Andreev billiard has two components. The normalconducting region (labeled “N”) bounded by an insulator (labeled “I”) has underlying chaotic classical mechanics. Adjacent to that normalconducting region are (here, two) superconductors (labeled “S”). The process of *Andreev reflection* takes place at the interface between those distinct regions, converting quasi-particle types: particles (holes) are scattered back to become holes (particles).

In the case of the billiard with *integrable* dynamics, the density of states vanishes linearly with E which can be understood by means of Bohr-Sommerfeld quantization argument. The behaviour of the density of states $\rho(E) \propto E$ can be deduced from a *power-law distribution* $P(s) \propto s^{-3}$ of classical path lengths s for very long paths $s \rightarrow \infty$.

For systems with underlying *chaotic* dynamics, the *hard gap* in the density of states (i. e. the strict vanishing of the density for energies E close to the Fermi surface ($E \rightarrow 0$)) could, so far, not have been reproduced using the concept of classical trajectories. Instead, one has chosen an alternative method, leaving aside the approach based on orbits. Starting with the microscopic Green function for the BdG equation (1.9), one is led in the semiclassical (long-wavelength) limit to the so-called Eilenberger equation [24] (a Boltzmann-type equation for superconductors) when an additional impurity average has been carried out.³ In the solution of the Usadel equation [25] (a limiting case of the Eilenberger equation), the *hard gap* becomes manifest.

Andreev billiards are by no means a theoretical concept without interest to the experimentalist community. An Andreev billiard has been realized in a periodic array of antidots by placing disks of superconducting niobium on an InAs quantum well containing a two-dimensional electron gas [26]. It has been shown experimentally that the known magneto-resistance behaviour of an antidot array are modified if one has retroreflection instead of specular reflection.

³Impurities were not considered in the above discussion of billiards.

1.2. Random-matrix theory

The study of random matrices was initiated by the pioneering work of Wigner [3] leading to Dyson’s classification of complex quantum systems according to their behaviour under time reversal and spin rotation [4]. The name “random-matrix theory” alludes to the bold pioneering idea to replace the Hamiltonian of a physical system by a matrix whose entries are drawn at random. By this reductionist approach – valid in the ergodic regime where the wave function explores the phase-space uniformly – the statistical features of the spectrum of a complex system is solely determined by the underlying fundamental symmetries.

We present the two most prominent *ensembles* within the so-called Wigner-Dyson *symmetry classes*: the Gaussian Wigner-Dyson ensembles and the Circular Wigner-Dyson ensembles. The symmetry class is characterised by the index β with the various possibilities compiled in the following chart:

symmetry class (vulgo)	symmetry class (Cartan)	Gaussian ensemble	Circular ensemble	β	time-reversal	spin-rotation
orthogonal	AI	GOE	COE	1	✓	✓
unitary	A	GUE	CUE	2	–	–/✓
symplectic	AII	GSE	CSE	4	✓	–

The labels “orthogonal”, “unitary”, and “symplectic” refer to the group which diagonalizes the corresponding Hamiltonian in the Gaussian ensemble. The classification by symmetric spaces following Cartan is an anticipatory remark explained in subsection (1.2.4). The abbreviations ‘G(O,U,S)E’ are standard in the field for Gaussian (Orthogonal, Unitary, Symplectic) Ensemble. Likewise, ‘C(O,U,S)E’ stand for Circular (Orthogonal, Unitary, Symplectic) Ensemble, respectively. The value of the so-called Dyson index β depends on the symmetries present or broken in the physical system. After these preliminary remarks, we now turn to the definition of the respective ensembles.

1.2.1. Gaussian Wigner-Dyson ensembles

The Gaussian ensembles in the space of matrices \mathcal{H} are named by their defining Gaussian probability distribution:

$$P(\mathcal{H}) d\mathcal{H} \propto \exp \left[-N\beta \operatorname{tr}(\mathcal{H}^2)/(4v^2) \right] d\mathcal{H} \quad (1.11)$$

where $d\mathcal{H}$ is the flat measure (a product over the independent differentials) and v^2 sets the variance. N refers to the matrix dimension of \mathcal{H} : for GOE and GUE, \mathcal{H} is an $N \times N$ -matrix while for GSE, \mathcal{H} is $2N \times 2N$ -dimensional. As a matter of convenience, we write \mathcal{H} in GSE as a $N \times N$ -matrix with entries \mathcal{H}_{nm} being

2×2 -matrices themselves. It is demanded that the probability distribution $P(\mathcal{H})$ is invariant under every transformation

$$\mathcal{H} \rightarrow U\mathcal{H}U^{-1}, \quad (1.12)$$

with the properties of U depending on the symmetries of \mathcal{H} , resp. on the Dyson index β as outlined in detail below:

β	entries of \mathcal{H}	transformation U
1	$\mathcal{H}_{nm} = \mathcal{H}_{mn} = \mathcal{H}_{nm}^*$	orthogonal: $U \in O(N)$
2	$\mathcal{H}_{nm} = (\mathcal{H}^\dagger)_{nm} = \mathcal{H}_{mn}^*$	unitary: $U \in U(N)$
4	$\mathcal{H}_{nm} = \mathcal{H}_{nm}^{(0)} \mathbb{1}_2 + i \sum_i \mathcal{H}_{nm}^{(i)} \sigma_i$	symplectic: $UU^R = \mathbb{1}$

Table 1.1.: The various symmetries of the Hamiltonian \mathcal{H} (labeled by the Dyson-index β) call for different diagonalizing matrices U .

Note added to table 1.1 for the symplectic case where $\beta = 4$: U is symplectic $UU^R = \mathbb{1}$. Here U^R is the dual of U defined by $U^R = ZU^T Z^{-1}$, where Z is block-diagonal: $Z_{nm} = \delta_{nm} \sigma_y$. Here, and in the table, σ_i are the Pauli matrices.

The requirement that the probability distribution $P(\mathcal{H})$ be invariant under every transformation (1.12) assures that all basis states (and therefore all states) behave in the same way, i. e. that none of them plays a particular role. As a second defining property of the ensembles, one demands that the various matrix elements \mathcal{H}_{nm} are *independent random* variables. One can show that these two requirements define the respective ensemble, leading to the probability distribution (1.11).⁴

All information about the eigenvalues is contained in the joint probability distribution of the eigenvalues. This distribution is found by transforming the volume element $d\mathcal{H}$ to the corresponding quantity in terms of eigenvalues E_i ("radial degrees of freedom") and eigenvectors ("angular degrees of freedom"):

$$P_{N\beta}(E_1, \dots, E_N) \propto \exp \left[-\frac{1}{4v^2} \sum E_i^2 \right] \prod_{j>i} |E_i - E_j|^\beta. \quad (1.13)$$

1.2.2. Circular Wigner-Dyson ensembles

When the approach by the *circular* ensembles is chosen, one specifies the system not by the Hamiltonian \mathcal{H} but by a unitary $N \times N$ (scattering) matrix S with eigenvalues $\exp(i\vartheta_j)$ ($1 \leq j \leq N$). In fact, the precise connection between the matrix S and hamiltonian \mathcal{H} need not be specified but one can imagine a definite relation, for instance $S = \exp(i\mathcal{H}t)$. The symmetry relations on the Hamiltonian \mathcal{H} (laid down in table 1.1) can directly be translated into conditions

⁴The values of the mean and the variance of the distribution are not fixed by the two requirements cited.

on the unitary matrix S . Sparing the reader details which are not of major concern for the main body of the work, we merely cite the joint probability density function of eigenvalues $\exp(i\vartheta_j)$ for the *circular* ensembles (which is to be compared to the *Gaussian* case (1.13)):

$$P_{N\beta}(\vartheta_1, \dots, \vartheta_N) \propto \prod_{j < k} |\exp(i\vartheta_j) - \exp(i\vartheta_k)|^\beta. \quad (1.14)$$

For the present thesis, the CUE ensemble is of some relevance. For our work in chapter 2, an ensemble of CUE scattering matrices on quantum graphs serves as a paradigm. The explanation will follow at the beginning of chapter 2. For large matrix dimension N , *circular* ensembles are equivalent to *Gaussian* ensembles. Put differently, when the dimension of the matrix tends to infinity $N \rightarrow \infty$, the limiting eigenvalue correlations are identical in the two cases [27].

1.2.3. A brief historical survey

For an appreciation of the present status of the field, we offer a brief historical survey about the impact and success of random-matrix theory.

The first success of the theory was the description of statistics of heavy nuclei in the 1950s and 1960s. Many universal features of nuclear spectral could be explained with the aid of random-matrix theory [21, 27].

A certain renaissance of the theory is due to the paper by Bohigas *et al* [28] inspiring the use of random-matrix theory as a standard tool for analysing fingerprints of classical chaos in quantum systems.

The range of applicability has been enlarged even further with the discovery of new symmetry classes. All the new symmetry classes (“beyond Wigner-Dyson”) have in common the fact that, due to an additional symmetry, their statistics is no longer stationary under shifts of the energy. These classes will be treated in greater detail in the following section.

Finally, defining random-matrix ensembles over the tangent spaces of the large families of Cartan’s symmetric spaces allows for an exhaustive classification of all *universality classes* [29].

It goes without saying that a field as rich as random-matrix theory defies an exhaustive review within a few pages. Therefore we refer to [21, 27, 30–32] and the lecture by Bohigas in [33] for an in-depth discussion.

1.2.4. The novel symmetry classes beyond Wigner-Dyson

It has been realized that Dyson’s classification scheme [4] is not exhaustive. To obtain Wigner-Dyson statistics, it is required that the energy spectrum be *stationary* under shifts of the energy. However, a quantum system may have a symmetry that relates the positive and the negative part of the spectrum.

1. Introduction

These systems are *not* included in Dyson’s classification and give rise to new universality classes only recently discovered.

Three new symmetry classes have been found in the context of low energy QCD, where a (massless) Dirac particle moves in a random gauge field [5, 6]. The Gaussian ensembles of those classes are termed “chiral Gaussian (Orthogonal, Unitary, Symplectic) Ensemble” abbreviated by “chG(O,U,S)E”.

The four remaining classes find physical realization in the context of superconductivity. Examples are quasi-particles in superconducting-normalconducting (SN) hybrid systems [2] or in disordered mesoscopic superconductors [7]. The present work gives a semiclassical interpretation of the universal quantities of these classes.

The classification scheme of all symmetry classes is given in [29] using Cartan’s complete classification of symmetric spaces totalling in ten large classes.⁵ A summary of the classification scheme is shown in table (1.2).

Symmetry class	Name of Gaussian ensemble	Symmetric space (compact type)	α	β
<i>A</i>	GUE	$U(N)$	0	2
<i>AI</i>	GOE	$U(N)/O(N)$	0	1
<i>AII</i>	GSE	$U(2N)/Sp(N)$	0	4
<i>AIII</i>	chGUE	$U(p+q)/U(p) \times U(q)$	$1 + 2 p - q $	2
<i>DI</i>	chGOE	$SO(p+q)/SO(p) \times SO(q)$	$ p - q $	1
<i>CII</i>	chGSE	$Sp(p+q)/Sp(p) \times Sp(q)$	$3 + 4 p - q $	4
<i>D</i>		$SO(N)$	$2 / 0$	2
<i>C</i>		$Sp(N)$	2	2
<i>CI</i>		$Sp(N)/U(N)$	1	1
<i>DIII</i>		$SO(2N)/U(N)$	$5 / 1$	4

Table 1.2.: The classification scheme according to Cartan’s ten symmetry classes. Commonly used names for the Gaussian ensembles are given. The eigenenergy level distribution according to (1.21) depends on the indices α and β . The first (second) value quoted for α applies to odd (even) dimension N .

We want to draw the reader’s attention to the following difference in nomenclature: while in Dyson’s classification the RMT ensemble is named according to the properties of the matrix *diagonalizing* the Hamiltonian, the classification scheme of Altland and Zirnbauer labels the symmetry class according to the properties of the *Hamiltonian itself*. The respective matrix ensemble is classified

⁵Here we do not distinguish between odd and even dimension for classes *D* and *DIII*. The consequences of this distinction have been worked out by Ivanov in [34].

according to Cartan's label of the symmetric space to which the Hamiltonian \mathcal{H} is tangent [29].

Classification scheme using the BdG formalism

The emergence of four distinct classes in the context of superconductivity is readily understood by use of the BdG formalism. The four symmetry classes come about by the combination of conserved or broken symmetry of time-reversal and spin-rotation invariance:

	time-reversal symmetry	spin-rotation invariance
D	–	–
C	–	✓
$DIII$	✓	–
CI	✓	✓

Table 1.3.: The four symmetry classes relevant in the context of superconductivity

The classification of the BdG-Hamiltonian \mathcal{H} according to the symmetries of the system is exemplified in some detail for class C . Here we closely follow the lines of [2] and restrict ourselves to those details which are relevant to the numerical calculations presented in chapter 2.

We start by switching from \mathcal{H} (cf eq. (1.9)) to the antihermitian matrix $X := i\mathcal{H}$:⁶

$$X := i\mathcal{H} = i \begin{bmatrix} h & \Delta \\ -\Delta^* & -h^T \end{bmatrix} \quad \text{with } h = h^\dagger \text{ and } \Delta = -\Delta^T. \quad (1.15)$$

The hermiticity of h and skewness of Δ are succinctly cast in the equations $-X^\dagger = X = -\Sigma_x X^T \Sigma_x$, where $\Sigma_x := \begin{bmatrix} 0 & 1 \\ 1 & 0 \end{bmatrix}$. Considering the blocks $X = \begin{bmatrix} A & B \\ C & D \end{bmatrix}$, the condition $X = -\Sigma_x X^T \Sigma_x$ translates into $B = -B^T$, $C = -C^T$, $D = -A^T$, while $X = -X^\dagger$ implies $A = -A^\dagger$ and $C = -B^\dagger$. So far, no symmetries besides the particle-hole symmetry are involved, so the above statements alone characterize the class with the least degree of symmetry, namely the class D . The restriction to class C is achieved by imposing the additional constraints corresponding to spin-rotation invariance. In the particle-hole space, the generators of spin rotations take the form

$$J_k = \begin{bmatrix} \sigma_k \otimes \mathbb{1}_N & 0 \\ 0 & -\sigma_k^T \otimes \mathbb{1}_N \end{bmatrix} \quad (k = x, y, z). \quad (1.16)$$

Spin-rotation symmetry requires that the Hamiltonian \mathcal{H} and the generators J_k commute: $[\mathcal{H}, J_k] = 0$. This commutation relation imposes additional con-

strains on A , B , and C , yielding the following form for X :

$$X = \begin{bmatrix} a & 0 & 0 & b \\ 0 & a & -b & 0 \\ 0 & -c & -a^T & 0 \\ c & 0 & 0 & -a^T \end{bmatrix} \quad \text{acting on} \quad \begin{bmatrix} p \uparrow \\ p \downarrow \\ h \uparrow \\ h \downarrow \end{bmatrix}. \quad (1.17)$$

For bookkeeping purposes, a vector is supplemented reminding us which quasi-particle types are acted on by the different blocks of X . We can read off directly that X decomposes into two commuting subblocks. One acts on the spin-up particles ($p \uparrow$) and spin-down holes ($h \downarrow$), the other one acts on spin-down particles ($p \downarrow$) and spin-up holes ($h \uparrow$). The two subblocks are related to one another ($b \mapsto -b, c \mapsto -c$), so we can focus on one of them (namely, the subblock acting on $p \uparrow$ and $h \downarrow$) without loss of information:

$$X_{\text{red}} = \begin{bmatrix} a & b \\ c & -a^T \end{bmatrix}. \quad (1.18)$$

The equations satisfied by the larger blocks A , B , C imply in turn $b = +b^T$, $c = +c^T$, $a = -a^\dagger$ and $c = -b^\dagger$. All these conditions can be put in a nutshell:

$$-X_{\text{red}}^\dagger = X_{\text{red}} = -JX_{\text{red}}^T J^{-1} \quad \text{with} \quad J = \begin{bmatrix} 0 & 1 \\ -1 & 0 \end{bmatrix} \otimes \mathbb{1}_N. \quad (1.19)$$

From those equation it is understood that X_{red} is an element of the symplectic Lie algebra $\text{sp}(2N)$. As Cartan used the notation $\text{sp}(2N) = C_N$, the authors of [2] named the present symmetry class “class C ”.

Random-matrix ensembles

The *symmetry classes* are determined by the various symmetries of the physical system. Within each symmetry class one may find integrable or chaotic systems, with rather different spectral characteristics. In the ergodic limit, chaotic systems exhibit the *universal* features of its symmetry class, that is, the spectral features of a “generic” matrix in that class. Those systems then build the corresponding *universality class* [35].

As in the Wigner-Dyson case, one may use the invariant Gaussian ensemble to compute the universal spectral features. The BdG-Hamiltonian is replaced by a random Hamiltonian \mathcal{H} of the appropriate symmetry and a Gaussian probability distribution is chosen:

$$P(\mathcal{H}) d\mathcal{H} \propto \exp[-\text{tr}(\mathcal{H})^2/2v^2] d\mathcal{H}. \quad (1.20)$$

As already explained for the Wigner-Dyson symmetry classes, diagonalizing \mathcal{H} yields the joint probability distribution function of the eigenvalues E_i , which depends on the symmetry indices α, β :

$$P_{N\alpha\beta}(E_1, \dots, E_N) = \prod_{i < j} |E_i^2 - E_j^2|^\beta \prod_k |E_k|^\alpha \exp(-E_k^2/v^2). \quad (1.21)$$

For each class, the indices α and β were given in table (1.3). The strength of repulsion between levels is determined by β . The strength of repulsion from zero (and consequently the spectral properties in the vicinity of zero) is given by α .

The common feature of the new symmetry classes (beyond Wigner-Dyson) is a mirror symmetry in the spectrum: if E is in the spectrum, so is $-E$. Due to this symmetry, all spectra presented in the thesis show only the positive part $E > 0$ of the spectrum without any loss of information.

Impact of the classification scheme in the literature

The widespread attention in the novel symmetry classes is due to their various realizations in disordered systems. A brief survey of their impact in the field of condensed matter physics concludes the section on random-matrix theory.

As an example of a superconducting-normalconducting hybrid system, the excitation spectrum of a vortex is calculated in [36]. A vortex is a tube-like normalconducting region inside a superconductor. The supercurrent circulating around the vortex leads to a variation of the phase of the order parameter, which is a prerequisite for the low end of the spectrum to be faithful to the Gaussian random matrix ensemble developed in [2].

The work in [37] can be understood as an extension of the above-mentioned treatment of the vortex. Here, random-matrix theory is taken as a starting point for the construction of a low-energy effective field theory. This field theory successfully describes noninteracting quasi-particles in an inhomogeneous superconducting state.

A large variety of topics relevant for systems of class D are studied in [38]. From an elaborate field-theoretic formulation, results are derived for the two-dimensional Ising model with disorder together with the physics of quasi-particles in disordered superconductors belonging to class D .

Properties of superconducting phases where the quasi-particles are localized or delocalized are discussed in [39]. Without spin rotation invariance present the systems under scrutiny belong to class D or $DIII$ depending on whether time-reversal symmetry is broken or conserved. An example of a physical realization is provided by a superconductor where the order parameter has triplet symmetry such that quasi-particles can exchange spin with the condensate. Possible implications for the random Ising model are also discussed when the authors undertake an attempt to match the phase diagram for the two-dimensional superconductor with its counterpart for the random bond Ising model.

The contribution of [7] to the research field of disordered superconductors with d -wave order parameter symmetry takes a symmetry oriented stance independently of the current literature of the field. The system treated falls in one of the four symmetry classes C , CI , D or $DIII$, depending on the nature of the

impurities and on whether time-reversal symmetry is present or broken. All four scenarios are given a common root in a field-theoretical description.

Another branch of research addresses network models that are generalizations of the Chalker-Coddington network [40] for the quantum Hall plateau transition. As one allows a particle of either spin to propagate on each bond, the coinage *spin quantum Hall system* has been adopted. Their common property is that they are representatives of symmetry class C . Within this network model, a transition between two insulating phases with quantized Hall conductances was found in [41]. Exponents for the spin quantum Hall transition have been calculated in [42] where the network model was mapped onto a percolation-problem by use of supersymmetry. An alternative derivation of this mapping has been developed and exploited in [43, 44] where sums over classical random walks are evaluated. Those models can be realized in a two-dimensional dirty gapless superconductors [45] when the order parameter has $d_{x^2-y^2} + id_{xy}$ symmetry.

The ideas of the classification in [2, 29] are also taken up in the treatment of the random-bond Ising model in [46, 47]. Here also, the transfer matrix of the two-dimensional Ising model with randomness in exchange interactions is written in terms of fermionic operators. This intermediary formulation is then mapped onto an network model belonging to class D .

1.3. Periodic-orbit theory

Periodic-orbit theory establishes a semiclassical correspondence between the (discrete) quantum spectrum of a Hamiltonian and the periodic orbits of the corresponding classical system. Below we sketch the key ideas of the derivation of the *Gutzwiller trace formula*, which is the cornerstone and founding idea of periodic-orbit theory. Whenever possible, physical concepts are highlighted and less emphasis is placed on the formalism. A complete and detailed discussion is beyond the scope of an introduction but can be found in [21], [32]. A survey of Gutzwiller's pioneering work [8, 48–50] can be found in his textbook [51]. The outline below follows the lines of [17, 21, 48].

For clarity, we offer the following compendium as a brief guideline to the derivation:

- Starting from the Feynman path integral formulation of the time-evolution operator, one derives the semiclassical propagator $K_{sc}(q_A, q_B, t)$.
- Subjecting the semiclassical propagator to a Laplace transform leads to the semiclassical Green function $G_{sc}(q_A, q_B, E)$.
- The imaginary part of the trace of the Green function yields the complete quantum spectrum in terms of the density of states $\rho(E) = \sum_n \delta(E - E_n)$.

The semiclassical approximations undertaken in the derivation of the trace formula are based on the method of *stationary phase approximation* (see appendix B for details). These approximations are based on sound grounds if the typical actions of the classical system are large compared to \hbar , which explains why the approximation is termed *semiclassical*. As a lax notation, one often finds the expression “ $\hbar \rightarrow 0$ ” for this situation.

We begin the derivation with the quantum mechanical propagator $K(q_A, q_B, t) = \Theta(t) \langle q_B | U(t) | q_A \rangle$, where $U(t) = \exp(-i\mathcal{H}t/\hbar)$ is the time-evolution operator generated by the Hamiltonian $\mathcal{H} = \hat{p}^2/2m + \hat{V}(\hat{q})$. Following the Feynman path integral formulation [52], the quantum mechanical propagator $K(q_A, q_B, t)$ is given in Feynman’s famous formulation as a “path integral” or a “sum over histories” [52]:

$$K(q_A, q_B, t) = \lim_{N \rightarrow \infty} \int dq_1 \dots dq_{N-1} \left(\frac{m}{2\pi i \hbar t / N} \right)^{dN/2} \exp \left[\frac{i}{\hbar} W_N \right], \quad (1.22)$$

where the action W_N is an approximation to Hamilton’s principal function:

$$W_N = \sum_{n=1}^N (t_n - t_{n-1}) L \left(\frac{q_n - q_{n-1}}{t_n - t_{n-1}}, q_n, t_n \right). \quad (1.23)$$

Here, $L(q, \dot{q}, t)$ is the classical Lagrangian (the identification of starting point $q_A = q_0$ and end point $q_B = q_N$ in d -dimensional space is understood). The short time limit $|t_B - t_A| \rightarrow 0$ for $K(q_A, q_B, t)$ was already investigated by Pauli (see ref. [6] in [48]):

$$K(q_A, q_B, t) = \frac{1}{(2\pi i \hbar)^{d/2}} D_{BA}^{1/2} \exp [i W_{BA}(t)/\hbar], \quad (1.24)$$

where D_{BA} stands for the determinant of mixed derivatives

$$D_{BA} = (-1)^d \det |\partial^2 W_{BA} / \partial q_{B_j} \partial q_{A_i}| \quad (1.25)$$

and $W_{BA}(t) = \int_0^t d\tau L(q, \dot{q}, \tau)$ for t sufficiently small. With the initial momentum $p_A = -\partial W_{BA} / \partial q_A$, one can interpret the determinant D_{BA} as Jacobian between the range of initial momenta p_A and the volume covered by the endpoints q_B . One can see from Feynman’s formula (1.22) that for $\hbar \rightarrow 0$, the relevant contributions come from paths where $W_{BA}(t) = W_{BC} + W_{CA}$ is stationary under variations with respect to some intermediary coordinate q_C :

$$\frac{\partial W_{BA}(t)}{\partial q_C} = \frac{\partial W_{BC}}{\partial q_C} + \frac{\partial W_{CA}}{\partial q_C} = -p_C^{(BC)} + p_C^{(CA)} = 0. \quad (1.26)$$

This observation on intermediate momenta is the key to an understanding of the semiclassical limit. The stationary phase approximation singles out those trajectories where the initial momentum for the second section $p_C^{(BC)}$ and the

final momentum of the first section $p_C^{(CA)}$ at the link q_C coincide. These are the classically allowed trajectories.

Thus one expects a sum of terms like (1.24) as the general expression for $K(q_A, q_B, t)$ in the semiclassical limit, one for each classical trajectory j from q_A to q_B in time t . By continuity of the result it is required that each term in the sum takes the exact form of (1.24) for t being sufficiently small. For longer times t , the classical trajectory j may pass a so-called *focal point* where the amplitude $|D_{BA}|^{1/2}$ becomes infinite. Yet the expression (1.24) remains valid if for every reduction of rank of the inverse Jacobian $1/D_{BA}$ a phase factor $\exp(-i\pi/2)$ is inserted, leading to the general expression for the *semiclassical* propagator:

$$K_{\text{sc}}(q_A, q_B, t) = \frac{1}{(2\pi i \hbar)^{d/2}} \sum_j |D_{BA,j}|^{1/2} \exp \left[i \frac{W_{BA,j}}{\hbar} - i \frac{\nu_j \pi}{2} \right]. \quad (1.27)$$

Here, the index j counts the different classically allowed trajectories from q_A to q_B and the index ν_j counts all multiplicities of phase factors due to the focal points. The main task (purely classical) when computing the semiclassical propagator $K_{\text{sc}}(q_A, q_B, t)$ is to identify all trajectories connecting q_A and q_B .

Now the second step (outlined in the initial compendium) on the way towards the trace formula is undertaken: the semiclassical Green function $G_{\text{sc}}(q_A, q_B, E)$ is obtained from the semiclassical propagator (1.27) by a Fourier-Laplace transform

$$\begin{aligned} G_{\text{sc}}(q_A, q_B, E) &= \\ &= -\frac{i}{\hbar} \int_0^\infty dt K_{\text{sc}}(q_A, q_B, t) \exp \left[\frac{iEt}{\hbar} \right] \\ &= -\frac{i}{\hbar} \frac{1}{(2\pi i \hbar)^{d/2}} \sum_j \int_0^\infty dt |D_{BA,j}|^{1/2} \exp \left[i \frac{W_{BA,j} + Et}{\hbar} - i \frac{\nu_j \pi}{2} \right]. \end{aligned} \quad (1.28)$$

Again, we emphasize here the line of reasoning of evaluating the propagator (1.28) without keeping track of the detailed prefactors. Two types of contributions to the integral (1.28) are important. One type of contributions arises from the stationary points of the phase (longer orbits), while the other type is due to the infinitesimally short times t (paths of length zero). It will become clear below that this distinction between different types of orbits results in two contributions to the density of states:

$$\rho(E) = \rho_{\text{av}}(E) + \delta\rho(E), \quad (1.29)$$

where $\rho_{\text{av}}(E)$ results from paths of length zero and varies only smoothly with the energy, while $\delta\rho(E)$ provides corrections to the smooth term showing oscillatory behaviour. As we are well within semiclassical reasoning (employing stationary phase arguments), we first evaluate the contributions from longer orbits —

leaving the zero path contribution aside for the time being. We will catch up on the zero length paths in due course.

Thus, we now turn to the evaluation of the contributions from those points where the phase $\Phi(t) = \frac{1}{\hbar}[W_j(q_A, q_B, t) + Et]$ is stationary. The stationarity condition

$$\left. \frac{\partial W_j}{\partial t} \right|_{t=t^*} = -E \quad (1.30)$$

means that the classical trajectory from q_A to q_B during the time t^* , accounted for in the function $W_j(q_A, q_B, t^*)$, belongs to the energy shell $H = E$. The function $W_j(q_A, q_B, t^*) + Et^*$ at the stationary point may be rewritten as $S_j(q_A, q_B, E)$, where $S(q_A, q_B, E) = \int_{q_A}^{q_B} dq p$ is the action of that trajectory. Performing the stationary phase approximation and rearranging the determinant prefactors yields the contributions of “long trajectories” to the semiclassical Green function⁷

$$G_{\text{sc, long traj.}}(q_A, q_B, E) = -\frac{i}{\hbar} \frac{1}{(2\pi i \hbar)^{(d-1)/2}} \sum_j |\Delta_{BA,j}|^{1/2} \exp \left[i \frac{S_j(q_A, q_B, E)}{\hbar} - i \frac{\nu_j \pi}{2} \right]. \quad (1.31)$$

We are now ready to undertake the third point of the compendium, i. e. calculating the spectrum via the trace of the approximated Green function (1.31)

$$\begin{aligned} \rho(E) &= \sum_n \delta(E - E_n) = -\frac{1}{\pi} \text{Im} \sum_n \frac{1}{E + i\epsilon - E_n} \\ &= -\frac{1}{\pi} \text{Im} \text{tr} \left[\frac{1}{E + i\epsilon - \mathcal{H}} \right] = -\frac{1}{\pi} \text{Im} \underbrace{\int dq G(q, q, E)}_{g(E)} \end{aligned} \quad (1.32)$$

where the trace is evaluated as an integral over the diagonal of the propagator. By inserting the contributions (1.31) for $G(q, q, E)$ in (1.32), one obtains:

$$g(E) = -\frac{i}{\hbar} \frac{1}{(2\pi i \hbar)^{(d-1)/2}} \sum_j \int dq |\Delta_{BA,j}|^{1/2} \exp \left[i \frac{S_j(q, q, E)}{\hbar} - i \frac{\nu_j \pi}{2} \right]. \quad (1.33)$$

For the last time we apply a the stationary-phase approximation to that integral:

$$0 = \left(\frac{\partial S}{\partial q_A} + \frac{\partial S}{\partial q_B} \right) \Big|_{q_A=q_B=q} = (-p_A|_q + p_B|_q). \quad (1.34)$$

This is the central result: the contributing paths are periodic not only in coordinate space but also in *momentum* space. In the semiclassical limit, only orbits periodic in *phase space* contribute to the density of states.

⁷The prefactor $|\Delta_{BA,j}|^{1/2}$ contains the determinant $\Delta_{BA} = \begin{vmatrix} -\partial_E^2 S & -\partial_{q_A, E}^2 S \\ -\partial_{q_B, E}^2 S & -\partial_E^2 S \end{vmatrix}$ evaluated for the path j .

For evaluation of the integral (1.34), one chooses a coordinate system with q_{\parallel} pointing in the \dot{q} direction of the orbit and $(d - 1)$ perpendicular coordinates $q_{\perp,i}$ with $1 \leq i \leq d - 1$ (the fixed point has the coordinates $q_{\parallel} = q_{\perp,i} = 0$). Expanding $S(q, q, E)$ in this coordinate system to second order leads to:

$$S(q, q, E) = S(q_{\parallel}, q_{\parallel}, E) + \frac{1}{2} q_{\perp,i}^T (S_{A_i A_i} + 2S_{A_i B_j} + S_{B_i B_j}) q_{\perp,j} \quad (1.35)$$

where summation over indices i, j is understood, and we used the abbreviation $S_{A_i B_j} = \partial^2 S / (\partial q_{A_{\perp,i}} \partial q_{B_{\perp,j}})$ (analogously for $S_{A_i A_i}$, etc).

The expansion (1.35) in the intrinsic coordinate system is possible only if the periodic orbit is *isolated*. If families of non-isolated orbits exist where the action $S(q, q, E)$ does *not* vary in the perpendicular direction q_{\perp} , the derivation of the integral must be modified. As the action is calculated over a closed orbit, it is independent of q_{\parallel} :

$$S(q_{\parallel}, q_{\parallel}, E) = S(E) = \oint dq p. \quad (1.36)$$

A description of the diligent handling of the prefactors is beyond the scope of an introductory survey. Thus, we content ourselves with communicating the result. The combination of the determinant $|\Delta_{BA,j}|^{1/2}$ in eq. (1.33) with the prefactor stemming from the integral over the perpendicular components q_{\perp} yields

$$\frac{1}{|\dot{q}_{\parallel}|} \frac{(2\pi i \hbar)^{(d-1)/2}}{|\det(M_j - 1)|^{1/2}}. \quad (1.37)$$

The matrix M_j in (1.37) is the *monodromy matrix* M_j of the orbit j , which is of purely classical nature. Let T be the period of the periodic orbit under consideration. A phase space point $x = (\vec{q}, \vec{p})$ along this periodic orbit is a fixed point of the classical evolution operator U^T : $U^T(x) = x$. We first linearize this operator U^T in the vicinity of the fixed point x :

$$U^T(x + y) = U^T(x) + \tilde{M}_j y = x + \tilde{M}_j y. \quad (1.38)$$

We now choose a specific local coordinate system in phase space: we take x_{\parallel} along the orbit, x_E transverse to the energy shell, and x_i transverse to the orbit inside the energy shell ($1 \leq i \leq 2d - 2$). The monodromy matrix M_j is the restriction of \tilde{M}_j to the latter $2d - 2$ -dimensional block; it determines the *stability* of the orbit. Collecting all elements of the saddle point approximation (1.35) to (1.38) for $g(E)$ in (1.33), we find:

$$g(E) = -\frac{i}{\hbar} \sum_j \underbrace{\int \frac{dq_{\parallel}}{|\dot{q}_{\parallel}|}}_{(t_p)_j} \frac{1}{|\det(M_j - 1)|^{1/2}} \exp \left[i \frac{S_j(E)}{\hbar} - i \frac{\mu_j \pi}{2} \right]. \quad (1.39)$$

The remaining integration yields the period $(t_p)_j$ for the primitive orbit, that is the time needed for one passage. The index $\mu_j = \nu_j + \alpha_j$ keeps count of the overall number of non-positive eigenvalues encountered while performing the two saddle point approximations (1.26) and (1.34). This completes the derivation of the fluctuating part $\delta\rho(E)$ of the density of states, which is the backbone of the *Gutzwiller trace formula*:

$$\delta\rho(E) = \frac{1}{\pi\hbar} \sum_j (t_p)_j A_j \cos \left[\frac{1}{\hbar} S_j(E) - \frac{\mu_j\pi}{2} \right]. \quad (1.40)$$

$\delta\rho(E)$ is the fluctuating part of the density of state, reflecting the fact that we only took orbits of non-zero length into account while deriving the semiclassical Green function. We write $A_j = |\det(M_j - 1)|^{-1/2}$ for the stability amplitude describing the linearized flow around the j th orbit. The sum is over all orbits j , including repetitions. The remarkable feature of Gutzwiller's trace formula (GTF) (1.40) is the connection established between the *quantum* spectrum — in the form of $\delta\rho(E)$ — and specific *classical* properties of the periodic orbits, namely the stability A_j , the period $(t_p)_j$, and the so-called Maslov index μ_j .

With the computation of the oscillatory part $\delta\rho(E)$ of the spectrum completed, we are now obliged to make good for the so far omitted part $G_0(q_A, q_B, E)$ of the semiclassical propagator $G_{\text{sc}}(q_A, q_B, E)$ (see eq. (1.28)) stemming from paths with vanishing length $|q_A - q_B| \rightarrow 0$ (i. e., when the stationary phase approximation (1.30) is not applicable). For orbit traversal times $t \rightarrow 0$, we have to resort to the propagator $K_0(q_A, q_B, t)$ for infinitesimal times t (taking only the *direct* path from q_A to q_B into account) known to us from the context of Feynman's path integral formulation:

$$K_0(q_A, q_B, t) = \left(\frac{m}{2\pi i \hbar t} \right)^{d/2} \exp \left[\frac{i}{\hbar} \left(\frac{m(q_B - q_A)^2}{2t} - tV \left(\frac{q_A + q_B}{2} \right) \right) \right] \quad (1.41)$$

which is akin to the expression (1.24) at the beginning of the section. From the Laplace transform of this propagator (1.41), one obtains

$$G_0(q_A, q_B, E) = \frac{1}{(2\pi\hbar)^d} \int d^d p \frac{\exp[ip(q_B - q_A)/\hbar]}{E - \frac{p^2}{2m} - V((q_A + q_B)/2)}. \quad (1.42)$$

Linking this Green function G_0 to the spectrum – as outlined in (1.32) – gives the contribution of the paths of length zero to the spectrum:

$$\rho_{\text{av}}(E) = \int \frac{d^d p d^d q}{(2\pi\hbar)^d} \delta[E - H(p, q)]. \quad (1.43)$$

This smooth part $\rho_{\text{av}}(E)$ of the density of states corresponds to the part of the phase space accessible to a classical particle with energy E . This completes the calculation of the density of states $\rho(E) = \rho_{\text{av}}(E) + \delta\rho(E)$ with the smooth part $\rho_{\text{av}}(E)$ stated in eq. (1.43) and $\delta\rho(E)$ given by a sum over (non-zero length) periodic orbits (1.40) which shows an oscillatory behaviour.

A few remarks are now in place appreciating the outstanding significance of Gutzwiller's trace formula.

While semiclassical quantization of integrable system dates back to Bohr and Sommerfeld, it was Einstein who pointed out the non-applicability of that quantization for non-integrable systems [53].

It is important to note the fundamental difference between the semiclassical approach to an integrable system (à la Bohr-Sommerfeld quantization) and the approach to a non-integrable system (à la Gutzwiller). While the former provides an approximation for *individual* energy levels, the latter is in essence global. Gutzwiller's approach relates the *full* set of periodic orbits to the *full* set of eigenvalues.

On a principal level, the GTF shows how the correspondence principle is at work for non-integrable systems. Classical dynamics is hidden in the quantum spectrum as quantum mechanics turns to classical mechanics in the semiclassical limit. The GTF displays a dependency of the quantum spectrum on the classical orbits and their properties.

The Gutzwiller trace formula as given by eq. (1.40) has serious convergence problems due to the exponential increase in the number of periodic orbits with length. Yet this problem can be overcome by mathematically sound versions of the Gutzwiller trace formula. The general idea, in order to achieve convergence, is to take a convolution of the density of states with a smooth function. This function is demanded to have a Fourier transform with finite support. In this way, one has to deal only with a *finite* number of periodic orbits [54, 55].

Gutzwiller's pioneering idea that the quantum spectrum of non-integrable systems is synthesized by many contributing periodic orbits has found sound experimental affirmation. One example is the spectral analysis of a chaotic billiard realized by an microwave resonator by Stöckmann *et al.* [56], cleverly exploiting the equivalence between the time-independent Schrödinger equation and the Helmholtz equation. Another example when periodic-orbit theory proved successful is the explanation of the spectrum of the hydrogen atom in a strong magnetic field — a paradigm of quantum chaos. The electron's motion in the hydrogen atom is chaotic when the interaction of the electron with the magnetic field is of the same order of magnitude as the Coulomb interaction with the nucleus — which can be realized experimentally in highly excited states, the so-called Rydberg states. On the theoretical side, periodic orbits could be extracted from calculated spectra [57, 58], while on the experimental side, contributions from different classical periodic orbits to the experimental data have been worked out [59]. As a third example for the success of the trace formula, we cite the work by Berry [9] clarifying how random-matrix theory predictions can be understood semiclassically with the aid of periodic-orbit theory. This landmark work of quantum chaos research is one fundamental motivation for the current work and consequently deserves some introduction on its own. We now

give a survey of Berry’s ideas [9] insofar as the present work owes its conceptual basis to Berry.

1.4. Periodic-orbit theory meets RMT – Berry’s diagonal approximation

Random-matrix theory only uses the fundamental symmetries of a system, with the exclusion of any system-specific dynamical property. On the other hand, the Gutzwiller trace formula expresses the spectrum of a quantum mechanical system in terms of the specific properties of that system, namely its periodic orbits. Still, to understand universality of some spectral features (for instance, the short-distance correlations between eigenvalues), one would like to recover the (statistical) random-matrix predictions from the (dynamical) Gutzwiller trace formula of the particular system. A partial answer to this question was given by Berry in his seminal paper [9], bridging the gap between periodic orbits (system-specific) and the random-matrix theory approach (statistical).

When spectral analysis explores the correlations between eigenvalues, one prominent quantity under scrutiny is the two-point correlation function $C(\epsilon) = \langle (\rho(E) - \rho_{\text{av}}(E)) (\rho(E + \epsilon) - \rho_{\text{av}}(E + \epsilon)) \rangle = \langle \delta\rho(E) \delta\rho(E + \epsilon) \rangle$.⁸ For the Wigner-Dyson classes, random-matrix theory makes universal predictions for this quantity in the *ergodic limit* – that is, when the system is given enough time so that the degrees of freedom equilibrate and fill the available phase space uniformly. The Fourier transform

$$K(t) = \int_{-\infty}^{\infty} d\epsilon e^{-2\pi i \epsilon t} C(\epsilon) \quad (1.44)$$

of the spectral two-point correlator is known as the *spectral form factor*. When we refer to the analogous quantity from random-matrix theory, we use an additional subscript $K_{\text{WD}}(t)$ for “Wigner-Dyson”. Berry compares the random-matrix predictions for $K_{\text{WD}}(t)$ with the result obtained through periodic-orbit theory for a chaotic system (which is ergodic with all closed orbits isolated). To that end, the periodic orbit expansion (1.40) is injected in (1.44). The time T_j for the traversal of the j th orbit is given by the energy derivative of the action: $T_j(E) = dS_j(E)/dE$, allowing for the expansion $S_j(E + \epsilon) \approx S_j(E) + \epsilon T_j(E)$. As is common practice in this context, all times are expressed in terms of the *Heisenberg time* T_H : $T_j = \tau_j T_H$. This time T_H and the mean level spacing $1/\rho_{\text{av}}$ are related by the Heisenberg “uncertainty relation”: $T_H/\rho_{\text{av}} = 2\pi\hbar$. Taking these observations into consideration one obtains

$$K_{\text{WD}}(\tau) = \sum_{j,k} \tau_j \tau_k A_j A_k^* \left\langle \exp \left[\frac{i(S_j - S_k)}{\hbar} \right] \right\rangle \delta \left(\tau - \frac{\tau_j + \tau_k}{2} \right). \quad (1.45)$$

⁸The brackets denote averaging over an energy window.

Again the brackets denote an average over some energy window. It is legitimate to take only the diagonal contributions with $i = j$ into account, as non-diagonal contributions with $i \neq j$ (where $|S_i - S_j| \gg \hbar$) cancel each other by destructive interference. Yet, this is a good approximation only for times τ short enough $\tau \ll 1$, as the periodic orbits proliferate exponentially with length in chaotic systems. This approximation scheme is called the *diagonal approximation*. For systems without time-reversal symmetry one finds within that approximation:

$$K_{\text{WD,diag}}(\tau) = \sum_j \tau_j^2 |A_j|^2 \delta(\tau - \tau_j). \quad (1.46)$$

Formally, this quantity gives the length spectrum of the periodic orbits, which are specific to the system. However, physically one may slightly smooth the delta peaks into a function of width $\Delta\tau$ (equivalently, one averages over the time τ in a window of width $\Delta\tau$). Due to the proliferation of long periodic orbits, the sum then loses track of the original peaks (except for the few shortest orbits), but may be estimated by using classical sum rules over long periodic orbits. Precisely, once the periodic orbits are long enough to explore the whole energy shell uniformly, the sum rule by Hannay and Ozorio de Almeida [60] (in this form found in [61]):

$$\sum_j |A_j|^2 f(\tau_j) \approx \int \frac{d\tau}{\tau} f(\tau) \quad (1.47)$$

can be applied. One then obtains the famous result

$$K_{\text{WD,diag}}(\tau) = \tau \quad (1.48)$$

valid for $\tau_c < \tau \ll 1$.⁹ Bearing in mind that the form factor $K_{\text{WD}}(\tau)$ is the Fourier transform of the two-point correlator, the relation (1.48) obviously cannot hold for τ arbitrarily large. Indeed, large times $\tau \gg 1$ correspond to minute energy differences ϵ much smaller than the mean level spacing; therefore, the correlator $C(\epsilon)$ shrinks to a δ -function $\delta(\epsilon)$ (as every eigenvalue is perfectly correlated with itself). Simultaneously, the condition $|S_i - S_j| \gg \hbar$ (necessary to justify the diagonal approximation) breaks down for large times τ , due to the proliferation of long orbits. This leads to

$$K_{\text{WD}}(\tau) \rightarrow 1 \quad \text{for } \tau \gg 1. \quad (1.49)$$

Consequently, the diagonal approximation must break down for large times. We spare the reader the (very simple) graphical representation of the closed form of the two-point correlator $K_{\text{GUE}}(\tau) = \min(\tau, 1)$ for systems with time-reversal symmetry broken; instead, we refer the reader to figure 2.1 in section 2.1 at the

⁹Below the lower bound of validity τ_c , the delta peaks are still well-separated, meaning that two successive times $|\tau_{j+1} - \tau_j| > \Delta\tau$. In that range, the formula (1.47) does not apply as yet.

beginning of chapter 2 where the dashed curve indicates the random-matrix theory prediction for the form factor.

A first extension of the results presented here beyond the diagonal approximation can be found in [62]. The limitations of the diagonal approximation are highlighted when contrasted with works including non-diagonal terms. As an example, we mention the description of Anderson localization within periodic-orbit theory [63]: the quantum phenomenon of Anderson localization can be reproduced by periodic-orbit theory only by taking correlations between periodic orbits into account, that is going beyond the diagonal approximation.

Very recently, an important step beyond Berry's was achieved by Sieber *et al*, as the first semiclassical off-diagonal correction to Berry's diagonal approximation was computed for a uniformly hyperbolic system [64]. They discovered that for systems with time-reversal invariance, long periodic orbits with a self-crossing in configuration space are accompanied by partner orbits which have nearly the same action. Such an orbit and its partner differ only in that the partner narrowly avoids the crossing. Everywhere else in configuration space, the two partner orbits are very close. It was found that action differences between the partner orbits become smaller than Planck's constant \hbar in the limit of small crossing angles. Taking their interference into account, Sieber *et al* computed the first correction to Berry's approximation. Their findings of a contribution of $-2\tau^2$ of the loop partner orbits to the GOE form factor $K_{\text{GOE}}(\tau)$ are in agreement with the random-matrix prediction $K_{\text{GOE}}(\tau) = 2\tau - \tau \log(1 + 2\tau) = 2\tau - 2\tau^2 + \mathcal{O}(\tau^3)$ for $\tau < 1$. The implications of the described (off-diagonal) loop partner trajectories onto the conductance of a clean chaotic mesoscopic system was studied in [65], while generalizations of the original ideas of Sieber *et al* can be found in [66].

1.5. The form factors of the new ensembles

In order to formulate the principal task of the present thesis, we need to redefine the form factor (1.44) when studying systems that lie in one of the new symmetry classes C , CI , D , and $DIII$. The main difference between the new classes and the well known Wigner-Dyson classes is that the low-energy behaviour of the density of states $\langle \rho(E) \rangle$ is not translationally invariant any more but instead has specific characteristics in the close vicinity of the Fermi energy. That is, the ergodic limit of the new symmetry classes differs from the Wigner-Dyson case by the fact that even the *average density of states* $\langle \rho(E) \rangle$ is universal (in the RMT sense) close to the Fermi energy μ (which is equivalent to $E = 0$). This is why the spectral form factor will be defined now as the Fourier transform of the spectral *one-point* function, instead of the *two-point* function for the Wigner-Dyson case. In fact, we define the form factor $K(t)$ as the Fourier

transform of the averaged deviation from the mean density $\langle \delta\rho(E) \rangle$:¹⁰

$$K(t) = 2 \int_{-\infty}^{\infty} dE e^{-2\pi i Et} \langle \delta\rho(E) \rangle. \quad (1.50)$$

We refrain from calling $\langle \delta\rho(E) \rangle$ a “fluctuating part”, as it is not only fluctuating for energies E well off the Fermi energy, but also describes the marked drop or enhancement in the spectral density near $E = 0$. Taking a chaotic system belonging to any of the new symmetry classes, one expects to recover a universal behaviour for the averaged deviation from the mean density $\langle \delta\rho(E) \rangle$ in the vicinity of the Fermi level. This behaviour can be predicted within the framework of Gaussian random-matrix ensembles. Calculations based on these Gaussian ensembles [2] yield the following spectral form factors:¹¹

$$\begin{aligned} K^C(t) &= -\Theta(1-t), & K^D(t) &= \Theta(1-t), \\ K^{CI}(t) &= -\frac{1}{\pi t} \int_{\max(1-t, t-1)}^{1+t} ds \frac{\sqrt{1-(s-t)^2}}{\sqrt{(s+t)^2-1}}, & \text{and} \\ K^{DIII}(t) &= -\Theta(t-1) \frac{t}{\sqrt{t^2-1}} + \frac{1}{2\pi t} \int_{\max(2-t, t-2)}^{2+t} ds \frac{\sqrt{(s+t)^2-4}}{\sqrt{4-(s-t)^2}}. \end{aligned} \quad (1.51)$$

We omit a graphical presentation of the formfactors (1.51) within the current discourse as these universal predictions are shown in figures (3.4, 3.5, 3.7, 3.12) whereupon they are compared to the numerical calculation.

In view of these universal predictions from random-matrix theory, we formulate succinctly the goal of the present work. In the same way as Berry [9] gave a semiclassical interpretation of the spectral form factor $K_{\text{WD}}(t)$ (1.44) of chaotic quantum systems in the GUE universality class, we set out on a semiclassical explanation of the corresponding quantities (1.51) for the new ensembles pioneered by Altland and Zirnbauer [2]. The necessary calculation of the density of states from the periodic orbits is by no way an easy task because of the exponential increase in the number of periodic orbits with respect to their lengths. This is why we use the model of quantum graphs, where the bookkeeping of the periodic orbits is comparatively easy.

1.6. Quantum graphs

As quantum graphs are the key model used in the present thesis, they merit some introductory remarks. Graphs are the outcome of modeling physical systems with the radically reductionist idea that particle propagation is allowed

¹⁰The spectral density $\rho(E) = \rho_{\text{av}} + \delta\rho(E)$ may be split in a part ρ_{av} which is constant on scales much larger than the mean level spacing and a deviation $\delta\rho(E)$ therefrom. Suppressing the constant part ρ_{av} in the definition (1.50) amounts to omitting a δ -function in the form factor $K(t)$.

¹¹In [2] the spectral density $\langle \rho(E) \rangle$ is calculated. The algebraic manipulations leading to the expressions for the spectral form factors (1.51) are documented in appendix F.

only on one-dimensional wires (channels) which are interconnected to each other at nodes (or vertices). Prominent examples of the use of quantum graphs before their introduction to the world of quantum chaos — also under the name of “network models” — are found in [67] where a multichannel theory of a wire is constructed, or in [40] where Chalker and Coddington use a network model for the analysis of localization in the integer quantum hall effect. Their network model [40] is used in [68] for the analysis of the metal-insulator transition in a disordered electronic system. Other examples of such network models are generalizations of the one-dimensional Kronig-Penney model studied in [69, 70]. The design of those models shares many common features with the set-up of quantum graphs in [10, 11].

The introduction of quantum graphs in the context of quantum chaos is due to Kottos and Smilansky [10, 11]. Their success is based on the fact that graphs are relatively simple examples of systems where the underlying classical dynamics is chaotic. The connection between random-matrix theory and the underlying classical dynamics is studied with the help of an exact trace formula for the quantum spectrum. The invaluable advantage for the periodic-orbit theory on graphs is the relative ease in classifying all periodic orbits.

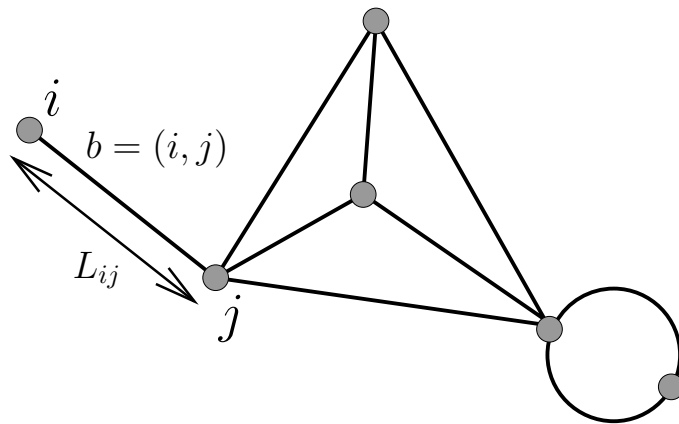


Figure 1.3.: A general graph structure: the tetrahedron with one dangling line and one loop as presented by [10]. For details on the labels and the set-up of the graph we refer to the text.

Graphs consist of V vertices connected by bonds. The information about which vertices i and j are connected is encoded in the connectivity matrix C_{ij} ($1 \leq i, j \leq V$): it takes the value $C_{ij} = 1$ if the vertices i and j are connected by a bond $b = (i, j)$ and zero otherwise. The valency v_i of a vertex i is given by the total number of bonds $v_i = \sum_{j=1}^V C_{ij}$ connected to this vertex. The bond directed from i to j is denoted by $b = (i, j)$ and \overleftarrow{b} stands for the reverse (j, i) . The positive direction on the bond $b = (i, j)$ is defined from $\min(i, j)$ to $\max(i, j)$. The metric information about distances between vertices i and j is

stored in the length matrix L_{ij} ($1 \leq i, j \leq V$). An example of a generic graph with $V = 6$ with detailed labeling of bond $b = (i, j)$ is given by figure 1.3.

On each bond b one considers the time-independent Schrödinger equation:¹²

$$\left(-i\frac{d}{dx} - \mathbf{A}_b\right)^2 \psi_b(x) = k^2 \psi_b(x) \quad b = (i, j) \quad (1.52)$$

with $\hbar = 1$ and $m = 1$. The general solution to (1.52) is the superposition

$$\psi_{b=(i,j)} = a_{i,j} \exp[i(k + \mathbf{A}_{i,j})x_{i,j}] + a_{j,i} \exp[i(k + \mathbf{A}_{j,i})(L_{i,j} - x_{i,j})] \quad (1.53)$$

of two counter-propagating waves. The coefficients $a_{i,j}$ are arranged in a $2B$ -dimensional vector $\mathbf{v} \equiv (a_{b_1^{\rightarrow}}, \dots, a_{b_B^{\rightarrow}}, a_{b_1^{\leftarrow}}, \dots, a_{b_B^{\leftarrow}})$. This vector \mathbf{v} is an element in the $2B$ -dimensional space of *directed bonds*. Boundary conditions are imposed on the free wave solution (1.53) at the vertices, ensuring current conservation. For a single vertex j where v_j bonds meet, the most general boundary condition is imposed in terms of a unitary $v_j \times v_j$ vertex-scattering matrix $\sigma^{(j)}$. Incoming and outgoing components of the wave function are related by¹³

$$a_{j,l} = \sum_{m=1}^{v_j} \sigma_{l,m}^{(j)} \exp[i(k + \mathbf{A}_{jm})L_{jm}] a_{m,j}. \quad (1.54)$$

If the matching conditions (1.54) are met for every vertex j , one has found a stationary state of the graph. In this case, all vertex conditions (1.54) can be cast in a single eigenvalue equation

$$\mathbf{v} = S_B(k)\mathbf{v}. \quad (1.55)$$

Nontrivial solutions to this equation require that the secular equation

$$\zeta_B(k) = \det(1 - S_B(k)) = 0 \quad (1.56)$$

be solved. The central quantity $S_B(k)$, on which most investigations in the current thesis are based, is the unitary *bond-scattering matrix*. It acts on the space of the directed bonds. $S_B(k)$ groups all vertex scattering conditions (1.54) together. We spare the reader the details in the current introductory chapter, as the systematics of constructing the matrix $S_B(k)$ is explained for the actual systems of interest in section 2.2 of the thesis.

The concept of an *orbit* on the graph is explained in the following. On the graph, an itinerary is defined by a possible sequence of vertices i_1, i_2, \dots ($i_m \in [1, V]$). For a *periodic* orbit with period n one has $i_k = i_{k+n}$ for all k . A periodic orbit of length n can be uniquely defined by the sequence of n vertex labels i_1, i_2, \dots, i_n where any cyclic permutation of the sequence defines the same periodic orbit.

¹²The vector potential is denoted by \mathbf{A} , as the letter A is reserved for the stability amplitudes as introduced in the Gutzwiller trace formula (1.40).

¹³The indices l and m label all the vertices connected to j .

This sequence is referred to as the *code* of the periodic orbit. An orbit is termed *primitive periodic orbit* if the defining sequence of vertices is not the repetition of a shorter sequence. From the concept of a graph orbit as explained above follows the fact that for graphs, the concepts of closed trajectories and periodic orbits are identical.

The derivation of a trace formula for the graph starts from the secular equation (1.56). The complex valued function $\zeta_B(k)$ is split into a real amplitude and a phase factor (ϕ_i are the eigenphases of $S_B(k)$, $1 \leq i \leq 2B$):

$$\zeta_B(k) = \exp \left[\frac{i}{2} \sum_{i=1}^{2B} \phi_i(k) \right] 2^{2B} \prod_{i=1}^{2B} \sin \left(\frac{\phi_i(k)}{2} \right). \quad (1.57)$$

It is shown in appendix C that the imaginary part of the logarithmic derivative of the last product (which is real for k real) is a sum over δ -peaks localized at the points where the secular equation (1.56) is fulfilled. This leads to the following expression for the density of states $\rho(k)$, pivotal for all work within the current thesis:

$$\rho(k) = \frac{1}{2\pi} \frac{d}{dk} \left[\sum_{i=1}^{2B} \phi_i(k) \right] + \frac{1}{\pi} \lim_{\varepsilon \rightarrow 0} \text{Im} \frac{d}{dk} \sum_{n=1}^{\infty} \frac{1}{n} \text{tr} S_B(k + i\varepsilon)^n. \quad (1.58)$$

The first term containing derivatives of eigenphases ϕ_i yields the smooth part ρ_{av} of the spectral density, whereas the second term with the sum over traces gives the fluctuating part $\delta\rho(k)$. The details of the derivation of the spectral density (1.58), starting from the quantization conditions, are given in appendix C. The trace $\text{tr} [S_B(k)]^n$ is given by a sum over periodic loops (orbits) p of period n on the graph:

$$\text{tr} S_B(k)^n = \sum_{p \in P_n} n_p A_p^r \exp [(ikl_p + i\mathbf{A}b_p)r] \\ \text{with } A_p = \prod \sigma_{i_1, i_2} \cdots \sigma_{i_n, i_1}. \quad (1.59)$$

The sum is over the set P_n of all orbits of total length $n = rn_p$ composed of r repetitions ($r \geq 1$) of primitive periodic orbits of length n_p . l_p gives the total length of the primitive orbit, b_p gives the directed length taking positive and negative directions of bonds into account (for simplicity the vector potential \mathbf{A}_{ij} on all bonds b_{ij} is chosen to be equal $\mathbf{A}_{ij} = \mathbf{A}$). The stability amplitude A_p is composed of the scattering amplitudes of all n_p passed vertices. The structural similarity of the trace formula (1.58) along with (1.59) to the Gutzwiller trace formula for chaotic systems (1.40) is striking. Yet, as the quantization (1.56) condition is exact, this trace formula also is exact, instead of semiclassically exact. Due to that fact, quantum graphs are extremely powerful and transparent in the semiclassical analysis of universal spectral statistics.

An introduction to quantum graphs is not complete unless complemented by a brief overview of the classical dynamics associated with a graph. A rudimentary

phase-space description is given by the graph version of the so-called Poincaré section (which is a common tool for the investigation of dynamical systems, see e. g. [71]):

$$\left\{ \begin{array}{l} \text{position} \\ \text{momentum} \end{array} \right\} \Leftrightarrow \left\{ \begin{array}{l} \text{current vertex index } i_m \\ \text{next vertex index } i_{m+1} \end{array} \right\}. \quad (1.60)$$

The set of all vertices (positions) with directions to the next vertex (momentum) is equivalent to the set of $2B$ directed bonds. The evolution on this Poincaré section can be defined with help of the transition *probabilities* $P_{kl} = |S_B(k)_{kl}|^2$ between bonds k and l . One then obtains a Markovian master equation for the classical probability $\rho_k(t)$ to occupy the bond k at time t :

$$\rho_k(t+1) = \sum_l P_{kl} \rho_l(t). \quad (1.61)$$

While the motion on the bonds themselves is one-dimensional and simple, the vertices connecting multiple bonds lead to chaos. At each vertex, a Markovian choice determines onto which bond the particle is scattered. Thus, chaos on graphs originates from the multiple connectivity at the bonds of the system. As a difference with usual Hamiltonian systems, the dynamics on the graph is not deterministic, but stochastic by essence.

All graphs presented in this introductory chapter are governed by a Schrödinger operator (see eq. (1.52)). This is why we refer to such graphs in the main body of the thesis as Schrödinger graphs to discern them from graphs where superconducting elements play a role.

To finish, we offer a brief tour d'horizon of the achievements in the field of quantum chaos using quantum graphs.

A striking proof that spectral statistics of quantum graphs is well reproduced by random-matrix theory is provided in [10, 11]. To that end, the distribution $P(s)$ for spacings $s_n = x_{n+1} - x_n$ between nearest neighbours of quantal levels is computed. This distribution $P(s)$ is known for integrable systems as well as for systems in the Wigner-Dyson universality classes. The agreement of the data obtained for a tetrahedron quantum graph (four vertices, all interconnected) and the RMT prediction in [10, 11] is excellent. Another testing field for the universality of quantum graphs is the computation of two-point spectral correlations functions and the related form factor (which is a graph version of the form factor defined in (1.44)). Evaluation of these quantities for appropriate graphs again show excellent agreement with the RMT predictions [10, 11, 72, 73].

The concept of quantum graphs introduced here may be extended by attaching infinite leads at the vertices [74]. These *non-compact* graphs display features characterizing scattering systems whose underlying classical dynamics is chaotic [74–76]. In this framework, the distributions of resonances, partial delay times, scattering amplitudes and resonance widths have been computed and compared to the corresponding RMT predictions [76, 77].

Anderson localization on graphs is understood by taking classical correlations between orbits into account. It has been shown in [63] that by grouping together the periodic orbits of equal length that are *not* related by an exact symmetry (as in Berry's [9] diagonal approximation), one is able to explain the phenomenon of localization.

For systems with time-reversal symmetry, the RMT prediction for the form factor $K_{\text{GOE}}(\tau) = 2\tau - \tau \log(1 + 2\tau)$ for $\tau < 1$ has been approximated by Berry [9] within the diagonal approximation, yielding the leading term $K_{\text{GOE}}(\tau) = 2\tau + \mathcal{O}(\tau^2)$.¹⁴ The leading off-diagonal correction to this approximation has been computed for graphs along the lines of and extending [64], yielding $-2\tau^2$ as the next order. The contributions to this $-2\tau^2$ -term are pairs of self-intersecting orbits that differ from each other only in the orientation of a single loop. Recovery of the RMT result for the GOE form factor to *third* order has been shown for certain types of quantum graphs in [78].

With regard to the role attributed to star graphs in chapter 3 of the thesis, the results on star graphs (one central scatterer, many peripheral scatters, see chapter 3 for details) with Neumann boundary conditions at the central scatterer are of relevance. An analysis of the two-point spectral statistics in [79], [80] shows that the form factor $K(t)$ is neither that of an integrable system nor that of a non-integrable system in the ergodic limit (which would follow random-matrix theory predictions).

It is this wide scope of topics treated with success in the framework of quantum graphs which suggests that the semiclassical analysis of spectral properties of the recently discovered symmetry classes might be worthwhile.

We have now presented all the necessary ingredients – physical concepts and mathematical methods alike – and are ready to start the presentation of the actual work. The quantum graphs treated in the following have Andreev reflection as a new ingredient. They provide a powerful tool for a semiclassical analysis of the universal spectral features of the new symmetry classes [2].

¹⁴The factor of 2 here in $K_{\text{GOE}}(\tau)$ in comparison to $K_{\text{GUE}}(\tau) = \tau$ in (1.48) reflects the fact that the number of orbits related by an exact symmetry here is double the number in systems where time-reversal symmetry is broken (GUE).

2. Andreev quantum graphs – a numerical analysis

So far, quantum graphs have been used only for the study of spectral properties of systems with dynamics governed by a Schrödinger operator. This fruitful endeavour has produced a wide range of new semiclassical understanding of spectral Wigner-Dyson statistics provided by random-matrix theory. A brief synopsis of those results was given in the introductory chapter 1.6.

With the discovery of the four new universality classes [2], one might raise the question: Is it possible to include the relevant features of superconducting-normalconducting hybrid systems in the framework of quantum graphs? The question is answered in the positive by quantum graphs incorporating the process of *Andreev reflection*. Henceforth, such graphs will be termed *Andreev graphs*. Can one recover the *universal* spectral results of the new symmetry classes, when the spectrum of such an *Andreev graph* in the ergodic limit is computed?

As an answer, the present chapter offers a numerical treatise on the spectrum of an *Andreev graph* with the symmetries of class C . In the following, we give a guideline to the structure of the present chapter.

We start in section 2.1 with a brief account on the method of generating an ensemble average for graphs by imposing random boundary conditions at the scattering vertices. This idea has its origin in work on graphs with Schrödinger dynamics [73].

In the subsequent section 2.2, we pave the way for an implementation of *Andreev scattering* on the quantum graph. To that end, the notions of quantum graphs (laid out in the introductory chapter 1.6) have to be adapted to the situation of a multi-component wave function on the bonds of the graph. The constituents of the *Andreev graph*, as generalizations of their counterparts in Schrödinger graphs, are explained.

With the actual set-up of the *Andreev graph* completed, we explain the implementation of the ensemble average by the random choice of vertex scattering matrices in section 2.3. For an Andreev graph with broken time-reversal symmetry and preserved spin-rotation invariance, the scattering matrices at the vertex must be drawn from the *circular ensemble of type C* [81]. This symmetry class is chosen as it is easiest from the technical point of view. Defining

the vertex scattering matrices in section 2.3 completes the construction of the Andreev graph.

We subsequently turn to the construction of the numerical algorithm used for the computation of the eigenvalues of the Andreev graph in section 2.4. This routine exploits the unitarity of the bond-scattering matrix (defined in eq. (2.8)) and the representation of the quantization condition (2.12) in terms of eigenphases of the scattering matrix. The principal ideas of the algorithm are outlined. Rigorous tests are described, which the routine passed faultlessly, before it was used for Andreev graphs.

The central section 2.5 of this chapter presents the numerical results computed for different Andreev quantum graphs. The systems of choice are *fully-connected* Andreev graphs where all vertices are connected with each other. Different sizes of graphs are studied with the range $V = 4, \dots, 8$ for the number of vertices V . The numerical data are compared with the appropriate random-matrix theory predictions for class C and good agreement is found.

Admittedly, the congruence of numerical data and RMT prediction is not exact; yet, taking into account that the quantum graph is a dynamical system, these deviations come as no surprise. The deviations from the *universal* random-matrix expectation are due to short periodic orbits. The fingerprint of these orbits and their contribution to the spectral density is analyzed in section 2.6. This analysis is based on the Fourier transform of the spectral density, which exhibits peaks at lengths identical to the lengths of the respective periodic orbits.

A brief summary and concluding remarks are given in the final section 2.7.

2.1. Motivation – random boundary conditions on Schrödinger graphs

First, we familiarize ourselves with the different possibilities in generating an ensemble average when computing averaged spectral quantities on quantum graphs.

In the first publications on the spectral statistics of quantum graphs [10, 11] with Schrödinger dynamics, the authors compute spectral fluctuations such as the two-point correlation function for the eigenphase spectrum of the appropriate bond-scattering matrix. To that end, the correlation function is averaged over an appropriately chosen range of wave numbers k .

An alternative method to generate an ensemble of graphs was introduced in [73]. There, the ensemble is generated by randomizing the vertex-scattering matrices $\sigma^{(i)}$. These scattering vertices are drawn from the CUE ensemble (which we touched upon in the introductory section 1.2.2). At the same time, all bond lengths l_{ij} and connectivities c_{ij} between vertices are kept constant.

It has been shown in [73] that such an ensemble of fully connected quantum graphs approaches universal random-matrix predictions with increasing system size.

The numerical results for the ensemble average of the form factor – the Fourier transform of the two-point correlation as defined by eq. (1.44) – is in good agreement with the random-matrix prediction.¹ In fact, the agreement between the predictions of RMT and the numerical results computed by randomizing the vertex-scattering matrices $\sigma^{(i)}$ becomes progressively better when the number of vertices V increases.

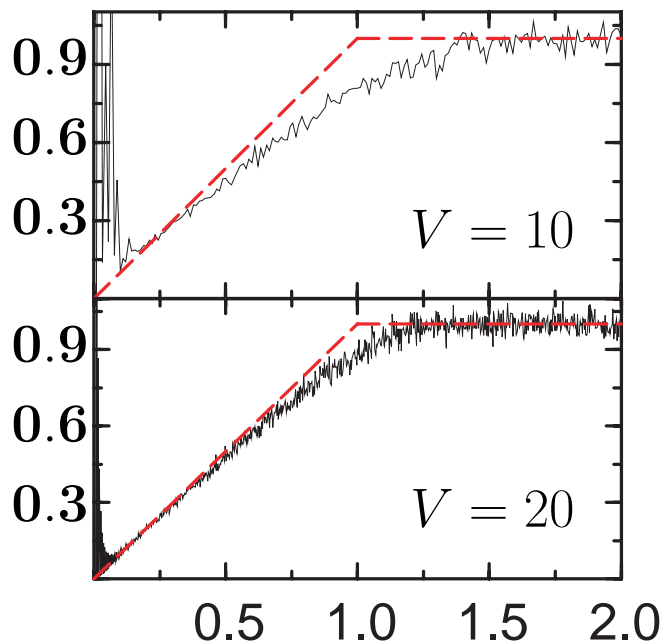


Figure 2.1.: The form factor of the eigenphase spectrum of S_B for a fully connected Schrödinger graph with $V = 10, 20$ taken from [73]. The abscissa is given in units of the Heisenberg time. The dashed lines give the RMT expectation for the form factor $K(\tau)$. The data show the form factor $K(\tau)$ averaged over the boundary conditions at the vertices (see text). Agreement of the numerical data with RMT prediction is progressively better for larger V . Figure taken from [73].

For a visualization, we cite the figure 2.1 illustrating the numerical calculation of the form factor in [73].

The method of choice in generating an ensemble average for the Andreev graphs in the present chapter is in close analogy to the averaging procedure over scattering matrices presented in [73].

¹For the present context, the energy variable E is replaced by the angle φ .

2.2. Setting up the Andreev graph

In this section, the necessary definitions and main properties of the Andreev quantum graph are given. With this set-up, we generalize the successful concept of quantum graphs in order to be able to apply it to superconducting-normalconducting hybrid systems. The new ingredient we introduce is *Andreev reflection* at the vertices of the graph. This type of graph incorporating Andreev reflection is called the *Andreev graph* from now onwards.

As with their Schrödinger counterparts, Andreev graphs too consist of V vertices which are connected by B bonds. The valency v_i is defined as the number of bonds meeting at that vertex i . For simplicity, only a single bond is allowed between two vertices.

The connecting bond between the vertices i and j is denoted by $\overrightarrow{b} = (i, j)$. Sometimes a direction needs to be assigned to the bond. Then $\overrightarrow{b} = (i, j)$ implies that $i < j$. When a “time reversed” notation is needed, where the first index is the larger, we use $\overleftarrow{b} = (j, i)$ with $j > i$. Only graphs without loops are considered (a loop is a bond with coinciding endpoints). The information as to which vertices are connected is stored in the *connectivity matrix* $C_{i,j}$, a symmetric square matrix of size V . One has $C_{i,j} = C_{j,i} = 1$ if the vertices i and j are connected and $C_{i,j} = 0$ if no bond exists in between these two vertices.

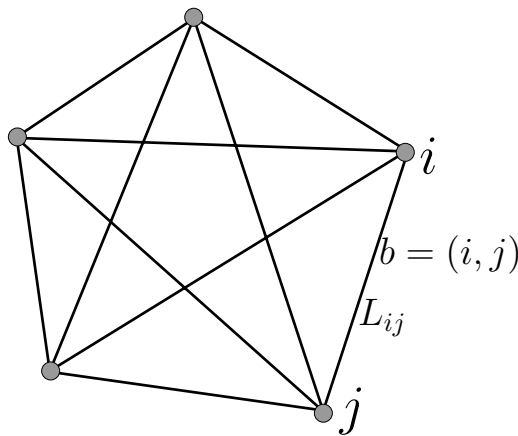


Figure 2.2.: Fully connected Andreev graph with $V = 5$ vertices. For details of the set-up, we refer to the text. The vertices i and j and the bond $b = (i, j)$ of length L_{ij} are labeled explicitly.

In terms of the connectivity matrix $C_{i,j}$, the valency v_i of the vertex i is given by $v_i = \sum_j^V C_{i,j}$ and the overall number of bonds is given by $B = \frac{1}{2} \sum_{i,j=1}^V C_{i,j}$. In the present chapter, we consider only *fully connected* graphs. These are graphs where all V vertices are connected to one another. In this case, all non-diagonal entries $C_{i,j}$ ($i \neq j$) are equal to one while all diagonal entries $C_{i,i} = 0$ vanish. An example of such a fully connected graph is drawn in figure 2.2.

A coordinate $x_{i,j}$ is assigned to each bond $b = (i, j)$ indicating the position on the bond. $x_{i,j}$ ($x_{j,i}$) measures the distance from the vertex i (j) along the bond. The length of the bond $b = (i, j)$ is denoted by $L_{i,j}$. All the metric information about the distances between the vertices i and j are stored in the length matrix $L_{i,j}$ – as in the case of Schrödinger graphs. For the fully connected Andreev graph (as shown in figure 2.2) where the ensemble average is generated by randomizing the vertex-scattering matrices, all bond lengths L_b can be chosen equal [73]. For simplicity, we choose $L_b = 1$.

The essential new ingredient we introduce to the world of quantum graphs is *Andreev reflection*. It is at the vertices where the Andreev scattering processes take place. By Andreev reflection, the quasi-particle character can be changed from electron-like to hole-like and vice versa. The bonds interconnecting the vertices display no superconducting features as they are regions with vanishing order parameter $\Delta = 0$. As the bonds themselves are *not* superconducting, the Bogoliubov-deGennes (BdG) operator on the Andreev graph has non-vanishing entries only on the diagonal. It is only via the boundary conditions imposed on the vertices that the electron and the hole wave functions are coupled.

The total wave function Ψ has B components $\Psi_{b_1}(x_{b_1}), \Psi_{b_2}(x_{b_2}), \dots, \Psi_{b_B}(x_{b_B})$. The index b_i with $1 \leq b_i \leq B$ labels the B different undirected bonds. Each of these components $\Psi_{b=(i,j)}$ is itself a wave function on a bond $b = (i, j)$. As our interest in this chapter focuses on symmetry class C , i.e., where time-reversal symmetry is broken yet spin-rotation invariance is present, the wave function on each bond is represented by a two-element column vector:

$$\Psi_b(x_{i,j}) = \begin{bmatrix} e_b(x_{i,j}) \\ h_b(x_{i,j}) \end{bmatrix} \quad (2.1)$$

which is a solution of the Bogoliubov-deGennes (BdG) equation with vanishing order parameter $\Delta = 0$:

$$\begin{bmatrix} \hat{h} & 0 \\ 0 & -\hat{h}^T \end{bmatrix} \Psi_b(x_{i,j}) = E \Psi_b(x_{i,j}) \quad \text{with} \quad \hat{h} = -\frac{\hbar^2}{2m} \frac{d^2}{dx_{i,j}^2} - \mu. \quad (2.2)$$

Here, μ is the chemical potential and E the energy measured from the Fermi energy. The BdG equation with vanishing order parameter (2.2) trivially decouples into two Schrödinger type equations for the electron amplitude $e_b(x_{i,j})$ and the hole amplitude $h_b(x_{i,j})$, respectively. The electron's (hole's) wave number k^+ (k^-) depends linearly on the energy E in the vicinity of the Fermi wave number:

$$\hbar k^\pm(E) = \sqrt{2m} \sqrt{\mu \pm E} \approx \hbar k_F \pm \sqrt{\frac{m}{2\mu}} E =: \hbar(k_F \pm k), \quad (2.3)$$

where we have introduced k as measuring the difference of the wave number k^\pm from the Fermi wave number k_F . Both components of the solution to equation

(2.2) are superpositions of two counter-propagating waves:

$$\Psi_b(x_{i,j}) = \begin{bmatrix} e_{i,j} e^{ik^+ x_{i,j}} + e_{j,i} e^{ik^+(L_{i,j}-x_{i,j})} \\ h_{i,j} e^{-ik^- x_{i,j}} + h_{j,i} e^{-ik^-(L_{i,j}-x_{i,j})} \end{bmatrix}. \quad (2.4)$$

Here, $e_{i,j}$ ($e_{j,i}$) is the amplitude for electron excitations moving on the directed bond $b = (i, j)$ from vertex i to vertex j (from vertex j to vertex i). Likewise, $h_{i,j}$ ($h_{j,i}$) is the amplitude for hole propagation from vertex i to vertex j (from vertex j to vertex i). The entirety of all coefficients $e_{i,j}$ and $h_{i,j}$ is arranged in a $4B$ -dimensional vector $\mathbf{v} \equiv (e_{\overline{b_1}}, \dots, e_{\overline{b_B}}, e_{\overline{b_1}}, \dots, e_{\overline{b_B}}, h_{\overline{b_1}}, \dots, h_{\overline{b_B}}, h_{\overline{b_1}}, \dots, h_{\overline{b_B}})^T$. By this arrangement, the matrices acting on \mathbf{v} have a particle-hole partition structure.

Boundary conditions are imposed on the free wave solution (2.4) at the vertices. These boundary conditions ensure current conservation at the vertices. For the vertex j , where v_j bonds meet, the most general boundary condition is imposed in terms of a unitary $2v_j \times 2v_j$ vertex-scattering matrix $\sigma_{l,m}^{(j)\tau_1, \tau_2}(E)$. The indices l and m label all the vertices connected to j , τ_1 and τ_2 label the quasi-particle type, where e stands for electron-like and h for hole-like excitation. The incoming and outgoing components of the wave function at the vertex j are related by²

$$\begin{bmatrix} e_{j,l} \\ h_{j,l} \end{bmatrix} = \sum_{m=1}^{v_j} \begin{bmatrix} \sigma_{l,m}^{(j)e,e} & \sigma_{l,m}^{(j)e,h} \\ \sigma_{l,m}^{(j)h,e} & \sigma_{l,m}^{(j)h,h} \end{bmatrix} \begin{bmatrix} e^{ik^+ L_{m,j}} e_{m,j} \\ e^{-ik^- L_{m,j}} h_{m,j} \end{bmatrix}. \quad (2.5)$$

From the vertex-scattering relation (2.5), an intuitive picture of the effect of the vertex-scattering matrix can be read off [72]. The coefficient $e_{m,j}$ ($h_{m,j}$) is the amplitude of an electron (hole) coming from vertex m incident on vertex j . On arriving at vertex j , the electron (hole) has acquired a phase $e^{ik^+ L_{j,m}}$ ($e^{-ik^- L_{j,m}}$). It is scattered onto the bonds connected to the vertex j with the quasi-particle type and scattering amplitude assigned by the appropriate scattering matrix entry. The resulting new amplitude $e_{j,l}$ ($h_{j,l}$) is a superposition of all contributions from quasi-particle amplitudes which are incident on vertex j and are scattered by the vertex-scattering matrix of this vertex.

Our specific choice for the vertex-scattering matrices $\sigma^{(j)}$ will be discussed in detail when the generation of the ensemble of graphs is explained in the subsequent section 2.3.

When the boundary conditions (2.5) are fulfilled at every vertex j , the state described by the corresponding set of coefficients $e_{i,j}$ and $h_{i,j}$ is *stationary*. Combining all boundary conditions of the V vertices (as given by eq. (2.5)) yields a set of altogether $4B$ linear equations for the coefficients $e_{i,j}$ and $h_{i,j}$.

Starting with these $4B$ linear equations, we now derive the secular equation for the total *Andreev* quantum graph. This equation is analogous to the secular

²For brevity, a possible energy dependence of the scattering matrix entries $\sigma_{l,m}^{(j)\tau_1, \tau_2}(E)$ is suppressed.

equation (1.56) which was introduced for Schrödinger graphs in section 1.6. As this eigenvalue problem is the cornerstone in the theory of quantum graphs, the construction of the secular equation is sketched in some detail. We restrict the presentation to the first row of eq. (2.5) – this is sufficient in clarifying the idea. After introducing the connectivities $C_{j,m}, C_{l,j}$, eq. (2.5) states (note that the sum over m now includes *all* vertices):

$$e_{j,l} = \sum_{m=1}^V \sigma_{l,m}^{(j)e,e} C_{j,m} C_{l,j} e^{ik^+ L_{m,j}} e_{m,j} + \text{terms}(h_{m,j}). \quad (2.6)$$

From this, the most general expression for coefficients $e_{j,l}$ ($h_{j,l}$ likewise) of any directed bond $b = (j,l)$ (which are not necessarily connected by a common vertex) is easily constructed:

$$e_{j,l} = \sum_{m=1}^V \sum_{k=1}^V \sigma_{l,m}^{(k)e,e} C_{k,m} C_{l,k} \delta_{k,j} e^{ik^+ L_{m,k}} e_{m,k} + \text{terms}(h_{m,k}). \quad (2.7)$$

Altogether, for the fully connected Andreev graph without any loops, $V(V-1) = 2B$ such relations exist for electron amplitudes $e_{j,l}$ and another $2B$ for the hole amplitudes $h_{j,l}$. These $4B$ equations can be cast in the compact form of an eigenvalue equation for the unitary $4B \times 4B$ *bond-scattering matrix* $S_B(E)$:

$$\mathbf{v} = S_B(E) \mathbf{v}. \quad (2.8)$$

The *bond-scattering matrix* $S_B(E)$ has partitions according to the particle-hole symmetry of the problem:

$$S_B(E) = \begin{bmatrix} S^{e,e} & S^{e,h} \\ S^{h,e} & S^{h,h} \end{bmatrix} = \begin{bmatrix} D^{e,e} & 0 \\ 0 & D^{h,h} \end{bmatrix} \begin{bmatrix} T^{e,e} & T^{e,h} \\ T^{h,e} & T^{h,h} \end{bmatrix}. \quad (2.9)$$

Each of the partition blocks of size $2B \times 2B$ acts on the space of *directed bonds*. For the single entries of the partitions S^{τ_1, τ_2} , we use the convention that the matrix element $S_{m'l',lm}^{\tau_1, \tau_2}$ describes the transition amplitude for a quasi-particle of type τ_2 incident from the directed bond (m,l) to become a quasi-particle of type τ_1 on the directed bond (l',m') . τ_1, τ_2 stand for quasi-particle types e or h .

The individual entries of the matrices $D^{e,e}, D^{h,h}$, which are diagonal in the directed bond space, store all metric information about the graph:

$$\begin{aligned} D^{e,e}_{ij,kl}(k^+) &= \delta_{i,k} \delta_{j,l} e^{ik^+ L_{i,j}} & \text{and} \\ D^{h,h}_{ij,kl}(k^-) &= \delta_{i,k} \delta_{j,l} e^{-ik^- L_{i,j}} \end{aligned} \quad (2.10)$$

The unitary transition matrix T depends on the connectivity of the graph and on the scattering potentials at the vertices. For each partition T^{τ_1, τ_2} (where τ_1, τ_2 again label the quasi-particle type), the individual entries read:

$$T_{lj,km}^{\tau_1, \tau_2} = \sigma_{l,m}^{(k)\tau_1, \tau_2} C_{l,k} C_{k,m} \delta_{k,j}. \quad (2.11)$$

The structure of this matrix is readily understood. Transition from one directed bond onto another can occur only if the two bonds meet at a common vertex such that one is incoming to and the other outgoing from the same vertex. If the bonds meet this condition, the corresponding entry of the vertex-scattering matrix gives the phase and absolute value of the transition amplitude.

The unitarity of the bond-scattering matrix $S_B(E)$ follows from the unitarity of the vertex scattering matrices $\sigma^{(j)}$. This connexion becomes transparent once the unitarity condition is written down by explicitly using the matrix indices $(S_B S_B^\dagger)_{ac} = \sum_b (S_B)_{ab} (S_B^*)_{cb} = \delta_{ac}$. The matrix indices here comprise both the directed bond space and the quasi-particle type. The unitarity of the bond-scattering matrix implies that all its eigenvalues lie on the unit circle in the complex plane. This will be exploited when the eigenvalue spectrum of the graph is computed numerically.

We come back to the eigenvalue equation (2.8) and its significance for the energy spectrum of the quantum graph. For non-trivial \mathbf{v} , solutions to the eigenvalue equation (2.8) exist if and only if the secular equation

$$\det(\mathbb{1} - S_B(E)) = 0 \tag{2.12}$$

is fulfilled. As the bond-scattering matrix $S_B(E)$ depends parametrically on the energy E , one has to probe for which values of the energy E the secular equation (2.12) is satisfied. The set of matching values $\{E_n\}$ ($n \in \mathbf{N}$, $E_1 < E_2 < \dots$) makes up the energy spectrum of the Andreev quantum graph. As the secular equation (2.12) determines the eigen-energies, it is often referred to as the “quantization condition” for the graph. As stressed by the pioneers of the spectral statistics of quantum graphs [10, 11], the quantization condition (2.12) is exact as no approximation has been made at any point of the derivation.

The secular equation has the usual form of a quantization condition in the scattering approach [82]. Yet, it cannot be associated with an actual scattering system in the usual sense where the scattering matrix acts on asymptotic solutions in the leads [82–84]. Here the scattering matrix $S_B(E)$ acts on the directed bond space.

The bond-scattering matrix $S_B(E)$ may be considered as a time evolution operator for discrete time steps. We assume an arbitrary graph wave function Ψ represented by its coefficient vector \mathbf{v} and apply the bond-scattering matrix repeatedly:

$$\mathbf{v}(n) = S_B^n(E)\mathbf{v}(0), \text{ with } n = 0, 1, 2, \dots \tag{2.13}$$

Obviously, the solutions of the eigenvalue equation (2.8) are stationary with respect to this time evolution. The index n in (2.13) counts the number of vertices crossed by the quasi-particle.

The secular equation (2.12) serves as a natural starting point for the spectral theory of the Andreev graph. The derivation of a Gutzwiller type trace formula

for spectral density $\langle \rho(E) \rangle$ has its origin in the quantization condition (2.12). The details of the derivation of the graph version of the Gutzwiller trace formula are outlined in appendix C.

Likewise, the numerical analysis of the quantum graph spectrum $\{E_n\}$ – the topic of the present chapter – also starts with the secular equation (2.12). The numerical techniques employed in obtaining an arbitrary sequence of eigenvalues E_n ($n = 1, 2, \dots$) starting from the secular determinant will be presented in section 2.4.

2.3. Ensemble average generated by random boundary conditions on the vertices

In this section, we explain how the ensemble of Andreev graphs is generated by randomizing the vertex-scattering matrices $\sigma^{(j)}$ ($j = 1, \dots, V$). The topology of the graph is constant throughout, i.e. for every system size, the Andreev graph is fully connected.

For each configuration of the ensemble, the scattering matrices $\sigma^{(j)}$ are generated independently for each vertex j . The Andreev quantum graph is constructed such that it models a superconducting-normalconducting hybrid system *with* particle-hole symmetry and spin-rotation invariance but *without* time-reversal symmetry. According to the classification scheme of [2] which we reviewed in section 1.2.4, the Andreev graph is of symmetry class C . The symmetry class C has the advantage of being the easiest technically.

In the same way as Kottos *et al* [73] choose random matrices from the CUE for the ensemble average over scattering matrices of the Schrödinger graph, we have to choose the scattering matrices $\sigma^{(j)}$ from the corresponding circular ensemble of type C [81]. For the symmetry class C , the unitary scattering matrix $\sigma^{(j)}$ is drawn from the symplectic group $\text{Sp}(2N)$ [81]. The BdG-Hamiltonian $i\mathcal{H}$ of the same symmetry class lies in the symplectic Lie algebra $\text{sp}(2N)$, as demonstrated in section (1.2.4). Consequently, exponentiation is the link between scattering matrix $\sigma^{(j)}$ and the Hamiltonian \mathcal{H} :

$$\sigma^{(j)} = \exp(i\mathcal{H}). \quad (2.14)$$

By replacing the BdG-Hamiltonian \mathcal{H} with an appropriately chosen random matrix, one could subsequently generate the unitary scattering matrix $\sigma^{(j)} \in \text{Sp}(2N)$ by the exponential map (2.14). Although possible in principle, the generation of the scattering matrix $\sigma^{(j)}$ by way of the matrix exponential is too costly numerically. Instead, we generate a random matrix $U \in \text{Sp}(2N)$ by diagonalizing a random matrix $X = i\mathcal{H} \in \text{sp}(2N)$:

$$X = U^{-1}\Lambda U \quad \text{with } \Lambda = i\sigma_z \otimes \text{diag}(\lambda_1, \dots, \lambda_N). \quad (2.15)$$

The matrix U is unitary and in the symplectic group $\text{Sp}(2N)$: $(U^\dagger)^{-1} = U = J(U^{-1})^T J^{-1}$, where J is the symplectic unit matrix as defined in eq. (1.19). The dimension $2N$ of the matrices X and U depends on the number of bonds v_j meeting at the vertex j : $N = v_j$.

After these preliminary remarks, we itemize the steps for generating the random scattering matrices $\sigma^{(j)}$ ($j = 1, \dots, V$) in the following outline:

- The matrix X with the characteristics for the symmetry class C

$$X = \begin{bmatrix} a & b \\ -b^\dagger & -a^T \end{bmatrix} \quad \text{with } a = -a^\dagger, b = +b^T \quad (2.16)$$

is chosen with random entries. All independent entries are distributed according to a Gaussian probability distribution with mean 0 and standard deviation 1. Due to the symmetry restriction for the $N \times N$ partitions a and b , the following entries can be chosen independently: $\text{Re } a_{ij}, \text{Im } a_{ij}$ with $i > j$, $\text{Im } a_{ii}$ and $\text{Re } b_{ij}, \text{Im } b_{ij}$ with $i \geq j$, with the indices $1 \leq i, j \leq N$. Their number adds up to $(2N + 1)N$, as required for the matrix $X \in \text{sp}(2N)$ [85]. The choice of the Gaussian probability distribution is standard in the field and in line with the principle of least information contained in the distribution [21].

- On diagonalizing this random matrix X , one obtains a matrix $U \in \text{Sp}(2N)$ according to eq. (2.15).
- The diagonalization (2.15) does not, however, define the matrix U in a unique way. With U , any matrix $U \sigma_z \otimes \text{diag}(e^{i\varphi_1}, \dots, e^{i\varphi_N})$ is a solution to (2.15) with $\varphi_1, \dots, \varphi_N \in [0, 2\pi[$. The numerical routine for the diagonalization singles out one special choice of U by convention. This bias needs to be lifted by subjecting U to the multiplication:

$$U \rightarrow U \sigma_z \otimes \text{diag}(e^{i\varphi_1}, \dots, e^{i\varphi_N}) \quad (2.17)$$

with phases $\varphi_i, \dots, \varphi_N$ chosen at random within the interval $[0, 2\pi[$.

For an interpretation, we recall the joint probability distribution for the eigenvalues (1.21) for symmetry class C :

$$\exp(-\text{tr } X^2/v^2) \prod dX_{ij} \propto \prod_{k=1}^N \lambda_k^2 \exp\left[-\frac{\lambda_k^2}{v^2}\right] \prod_{i<j} (\lambda_i^2 - \lambda_j^2)^2 dU. \quad (2.18)$$

Generating the random matrix U via diagonalization of X corresponds to a transit from the left hand side of (2.18) to the right hand side, where the eigenvalues λ_i (in the diagonal matrix Λ) and the independent elements of U are the new variables.

Usually in random-matrix theory, one is interested in the characteristics of the eigenvalues λ_i and the angular degrees of freedom in U (which do *not* depend

on the eigenvalues) are absorbed in some normalisation constant. However, here we discard any interest in the eigenvalues λ_i and benefit from the fact that U is evenly distributed with respect to the angular degrees of freedom. As the statistical weight depends only on the eigenvalues and no preference with respect to the "angle variables" is introduced, generating U via diagonalization from the randomly chosen matrix X provides the correct Haar measure dU for the unitary symplectic group $\text{Sp}(2N)$.

Before incorporating the matrix $U \in \text{Sp}(2N)$ as scattering matrix $\sigma^{(j)}$ on the graph, it is tested to check that the probability distribution for U is indeed in agreement with a distribution according to the group's invariant Haar measure dU . Group theory provides the following relations for a matrix U distributed according to the Haar measure of the group G (here $G = \text{Sp}(2N)$):

$$\int_G dU U_{ij} = 0 \quad \text{and} \quad \int_G dU U_{ij}(U^{-1})_{lk} = \frac{\delta_{ik}\delta_{jl}}{2N}. \quad (2.19)$$

The integration is understood to be handled entry-by-entry. For a proof of these relations (2.19), we refer to appendix E. It has been tested that the numerically generated matrices U fulfill these relations. Although not sufficient, passing the test posed by the relations (2.19) is a *necessary* condition that the matrix U is distributed according to the Haar measure.

2.4. The numerical routine for computing the spectrum

In this section we present the conceptual idea for the numerical computation of the complete spectrum $\{E_n\}$ of an Andreev quantum graph.

The most naive approach of finding the solutions to the secular equation (2.12) is the search for simultaneous zeros of the real and imaginary parts of the determinant $\det(1 - S_B(E))$.

However, as a matter of principle, no grid on the energy axis can be chosen fine enough such that it is guaranteed that no zero is lost. For any resolution of the energy axis, two adjacent eigenvalues can always lie closer together than the chosen grid size. In that case, the existence of this pair of zeros would pass unnoticed.

Here comes in useful the unitarity of the bond-scattering matrix $S_B(E)$, confining its eigenvalues to the unit circle. We denote the eigenvalues of $S_B(E)$ by $e^{i\theta_i(E)}$ where $i = 1, \dots, 4B$. $\theta_i(E)$ are the so-called eigenphases of the unitary matrix $S_B(E)$. A solution of the secular equation (2.12) is equivalent to $S_B(E)$ having an eigenvalue $+1$. That is, the quantization condition is equivalent to

$$\theta_i(E) = 2\pi n \quad \text{with} \quad n \in \mathbb{Z} \quad \text{and} \quad 1 \leq i \leq 4B. \quad (2.20)$$

Monitoring the movement of the eigenphases $\theta_i(E)$ on the unit circle as the energy E increases is the key for a faultless computation of all energy eigenvalues

$\{E_n\}$. The method is best explained with help of figure (2.3). Two “snapshots” of the $4B$ (here $B = 2$) eigenphases θ_i on the unit circle in the complex plane are shown for two different energies E : phases for the lower energy E_0 have dashed “spokes” while the eigenphases with somewhat higher energy $E_0 + \Delta E$ have solid “spokes”. Every eigenphase $\theta_i(E)$ constantly moves anti-clockwise with increasing energy E . For the detailed proof of $d\theta_i/dE > 0$, we refer to appendix D. Detecting an energy eigenvalue – for which $\theta_i(E) = 0 \bmod 2\pi$ –

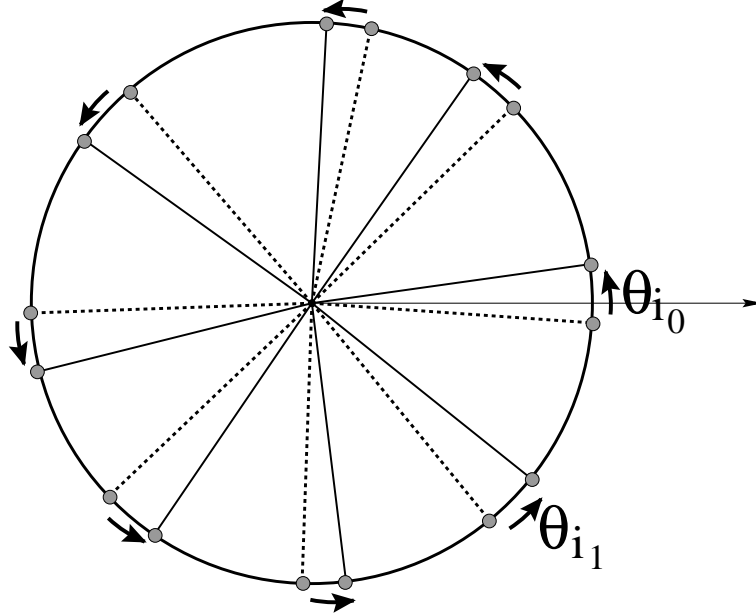


Figure 2.3.: The eigenphases θ_i on the unit circle for energy E_0 (dashed spokes) and energy $E_0 + \Delta E$ (solid spokes).

amounts to tracking the passage of an eigenphase past the angle zero when the energy is increased by a step ΔE . Consequently, the main focus lies on monitoring the eigenphase θ_{i_0} closest to the zero angle approaching the positive real axis from below. Once such a passage has been detected on increasing the energy from E_0 to $E_0 + \Delta E$, the existence of a zero of the continuous function $\theta_{i_0}(E)$ within the interval $[E_0, E_0 + \Delta E]$ is guaranteed.

It is important to note that the numerical calculation can only provide “stroboscopic pictures” of the eigenphases at given points of the energy. That is why the energy step size ΔE must be small enough, such that the attribution is unambiguous as to which “dashed” eigenphase for energy E rotates onto which “solid” eigenphase for energy $E + \Delta E$. This attribution is indicated by the arrows in figure 2.3.

By construction of the algorithm and due to the fact that all eigenphases $\theta_i(E)$ increase permanently with increasing energy E , the routine can never show a spurious level at a certain energy.

This leaves us to exclude the second possible source of error – failing to detect a given eigenvalue. This might happen if the step size ΔE is chosen to be too large. More precisely – using the nomenclature of the figure 2.3 – the “dashed” eigenphase θ_{i_1} for energy E_0 could rotate that far so as to become the “solid” eigenphase θ_{i_0} for energy $E_0 + \Delta E$ instead of ending as the “solid” θ_{i_1} . This would result in a failure in detecting one of the two energy eigenvalues within the interval $[E_0, E_0 + \Delta E]$.

To prevent this, the algorithm implemented constantly monitors the phase difference $\theta_{i_0} - \theta_{i_1}$ and allows only energy step sizes ΔE such that the identification of the phases is unambiguous:

$$\theta_{i_0} - \theta_{i_1} \gg \Delta E \frac{d\theta_{i_0}}{dE}. \quad (2.21)$$

In fact, the algorithm was calibrated to allow step sizes

$$\Delta E = \frac{\theta_{i_0} - \theta_{i_1}}{M \frac{d\theta_{i_0}}{dE}} \quad \text{with } M = 20. \quad (2.22)$$

Choosing an appropriate value for M is a problem of optimization: the larger our choice of M , the smaller the step sizes undertaken and consequently less fault-prone is the routine. Yet on the other side, unnecessarily large values of M (i. e. small step sizes) waste computer time. Choosing $M = 20$ turned out to be the optimal value. A rigorous test of the routine was undertaken. It follows the publication [11] and detects any missing or spurious levels. To that end, the difference between the exact spectral counting function $N(E; E_0) = \int_{E_0}^E dE \rho(E)$ and the smooth spectral counting function $\overline{N}(E; E_0) = \int_{E_0}^E dE \rho_{av}(E)$ is calculated. The quantity

$$\delta_{\text{level}} = N(E; E_0) - \overline{N}(E; E_0) \quad (2.23)$$

is expected to fluctuate around zero. Any missing or redundant level would be detected by an offset of ± 1 . The small insert of figure 2.4 at the top-right corner shows such a situation where one eigenvalue has been lost. As evidence that the routine constructed for this thesis works faultlessly, we cite the main part of figure 2.4 where δ_{level} fluctuates as expected.

Before applying the routine to the case of Andreev graphs, it was extensively tested on Schrödinger graphs. Freezing the additional degrees of freedom for the time being, the distribution $P(s)$ of the spacings $s_n = x_{n+1} - x_n$ of the nearest neighbour of quantal levels is computed along the lines of Kottos *et al* in [10, 11]. This nearest neighbour spacing distribution $P(s)$ is a most convenient and widely used statistical test of whether a given system follows random-matrix theory predictions or not. We computed a total of about 12000 eigenvalues for a single realization of a fully connected Schrödinger graph with $V = 4$ vertices and found good agreement with the random-matrix theory expectations. This finding gave further substantial proof of the soundness of the algorithm.

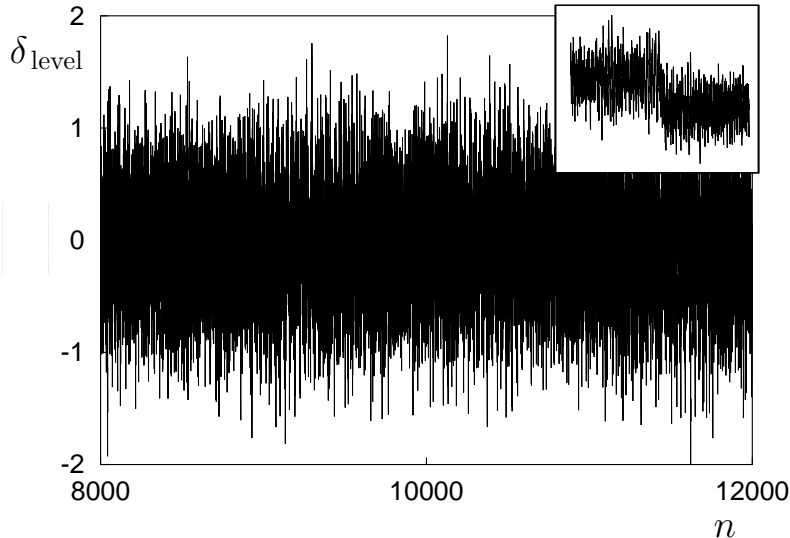


Figure 2.4.: The quantity $\delta_{\text{level}} = N(E; E_0) - \overline{N(E; E_0)}$ plotted against the label n counting the energy eigenvalues. The scanned energy region comprises 4000 eigenvalues, starting high above the Fermi edge. The simulation has been done for a fully connected Andreev graph as depicted in figure 2.2. The insert at the top-right corner shows the fingerprint a lost eigenvalue leaves on the quantity δ_{level} .

2.5. Comparison of numerical results with RMT predictions

We now present the results obtained for the spectral statistics of an ensemble of fully connected Andreev graphs. The analysis is done for varying graph sizes with the number of vertices ranging from $V = 4$ to $V = 8$.

As with the spectral statistics of the Schrödinger graph studied by Kottos and Schanz in [73] and reviewed in the section 2.1, it is fair to assume that the averaged spectral density of the Andreev graph tends to the *universal* predictions of random-matrix theory for class C in the limit of very large system sizes.

However, for the comparison of the numerical results of the class C type Andreev graphs with random-matrix theory, we take a slightly different approach which spares us the costly numerical calculation of ever larger systems. This is possible because of the variety of results known for class C . As mentioned earlier, the circular ensemble of type C is built by drawing scattering matrices S at random from the symplectic group $\text{Sp}(2N)$. The eigenphase correlations of the circular random-matrix ensemble of type C have been computed in the large- N limit by use of a supersymmetry technique [86]. The same calculation also yields

results for *finite* N (see [87] and citation [10] in [43]). It is this prediction for the eigenphase density for *finite- N* circular random-matrix ensembles of type C which is the cornerstone of our analysis:

$$\rho_N(\varphi) = \frac{2N+1}{2\pi} - \frac{\sin[(2N+1)\varphi]}{2\pi \sin \varphi}. \quad (2.24)$$

The phase φ indicates the angular position of an eigenvalue on the unit circle. The index N refers to the dimension of the matrices drawn at random from the symplectic group $\text{Sp}(2N)$. From what we have learned about the directed bond space in section 2.2, it is clear that the dimension N must be identified with the total number of directed bonds $N = V(V-1)$, where V denotes the overall number of vertices. Comparing the numerical results to the random-matrix prediction for finite N (2.24) has the enormous advantage that rather small system sizes suffice to prove that the limiting statistics for Andreev graphs are indeed universal for $N \rightarrow \infty$. This spares us the costly computation of very large systems.

As the dimension N varies for different sizes of the Andreev graph, the comparison of the numerical quantum graph spectra with the exact random-matrix result (2.24) calls for rescaling of the density $\rho(\varphi)_N$.

The mean density of eigenphases is given by $\nu = N/\pi$, as the $2N$ eigenphases lie on the unit circle with circumference 2π . The abscissa is rescaled such that it is given as a multiple x of the mean spacing $1/\nu$ between eigenphases $x = \varphi/\nu$. Likewise, the absolute value of the eigenphase density varies for different N . For the comparison of cases with different dimension N , the rescaling of the ordinate with the mean level spacing π/N is useful. The rescaled eigenphase density $R_N(x)$ as a function of the dimensionless parameter x is given by:

$$R_N(x) = 1 + \frac{1}{2N} - \frac{\sin(2\pi x + \pi x/N)}{2N \sin(\pi x/N)}. \quad (2.25)$$

As expected, this expression (2.25) coincides in the limit $N \rightarrow \infty$ with the *universal* spectral density of the *Gaussian* random-matrix ensemble of type C [2].

We start the presentation of results with the smallest possible fully connected graph showing quantum chaos – the graph with $V = 4$ vertices. The top-left figure shows the random-matrix theory prediction for the eigenphase density $\rho_N(\varphi)$ defined in (2.24) for $N = V(V-1) = 12$ in the interval $[0, \pi[$. On the top right of figure 2.5, the numerical results obtained for an ensemble of 48000 configurations of the Andreev graph are shown, with arbitrary units on the abscissa. After rescaling the numerical data such that it has level spacing of unity, it is compared to the random-matrix prediction $R_N(x)$ for $N = 12$ defined in (2.25) in the bottom picture of figure 2.5. We emphasize that at no stage are there any *free parameters* involved.

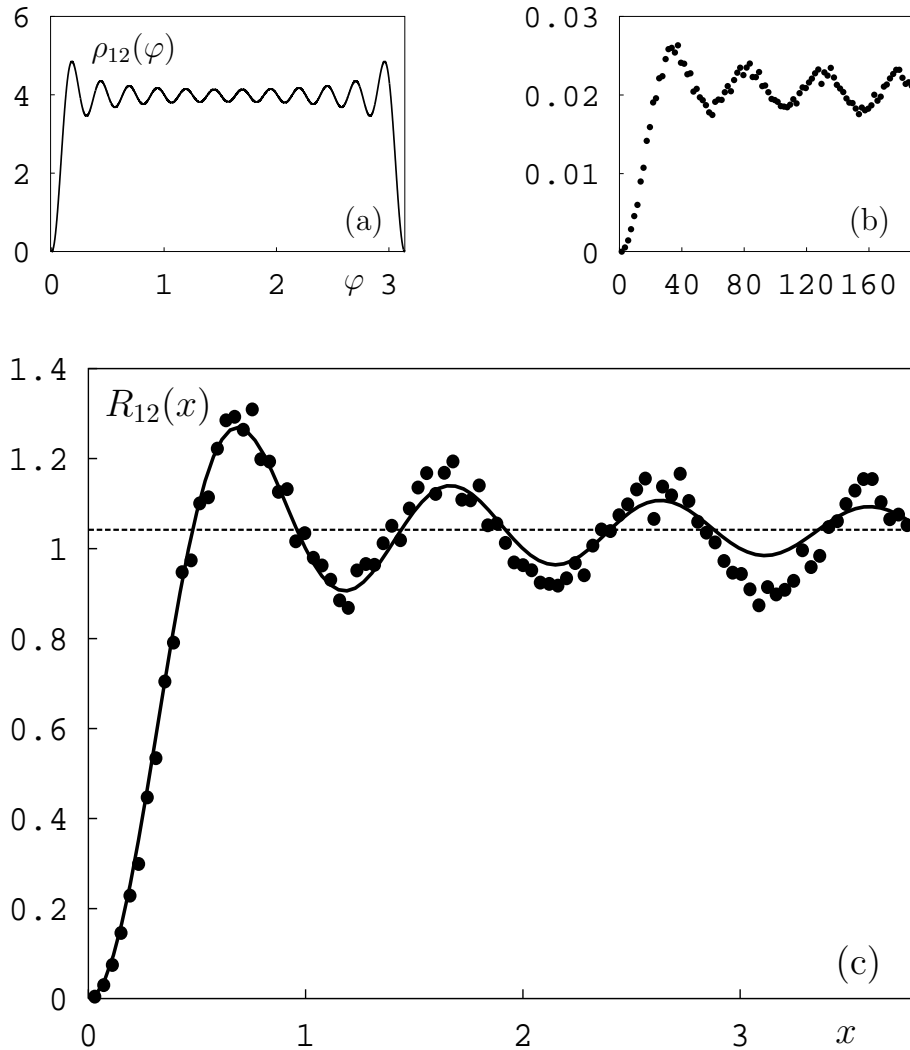


Figure 2.5.: The comparison of RMT prediction with numerical results. Figure (a) shows the RMT prediction for the eigenphase density $\rho_{12}(\varphi)$ as defined by (2.24). Figure (b) shows the numerical data obtained by an ensemble average over 48000 configurations of the fully connected Andreev graph with $V = 4$ vertices (with arbitrary units on the abscissa). When plotted against the mean level spacing x (see text for details about the rescaling), the numerical results show good agreement with the RMT prediction $R_{12}(x)$ defined in (2.25), as depicted in figure (c). The dashed line indicates the limiting value $1 + 1/(2N)$ of the distribution (2.25). For further details of the analysis, we refer to the text.

In general, we find good agreement between the numerical data and the random-

matrix theory prediction. Though, from the second maximum onward, we observe an onset of deviation between the numerical data and the RMT prediction in figure 2.5 (c). These deviations exceed the statistical error margin and cannot be ironed out by further averaging. We offer the interpretation that these differences originate from the fact that a graph is a dynamical system where the short time dynamics (stemming from the short periodic orbits) is *non-universal*. A more quantitative argumentation discerning between universal and non-universal behaviour – in analogy to the Wigner-Dyson case – is given in the following. From the form of the spectral density $\delta\rho(k) = \sum_j A_j \exp(ikl_j)$ (simplification of the trace formula (1.40)), we can read off that every orbit of length l adds an oscillatory contribution with a period $\Delta k = 2\pi/l$ to the density of states $\delta\rho(k)$. Thus, the long orbits determine the short range behaviour of the eigenvalues. In this range, random-matrix theory predictions are on sound grounds. In contrast, the short orbits are responsible for the behaviour of eigenvalues further apart. With the length of the shortest orbit given by l_{\min} , we can expect that for a wave number difference $\Delta k \gtrsim 2\pi/l_{\min}$ random-matrix theory will no longer be applicable.

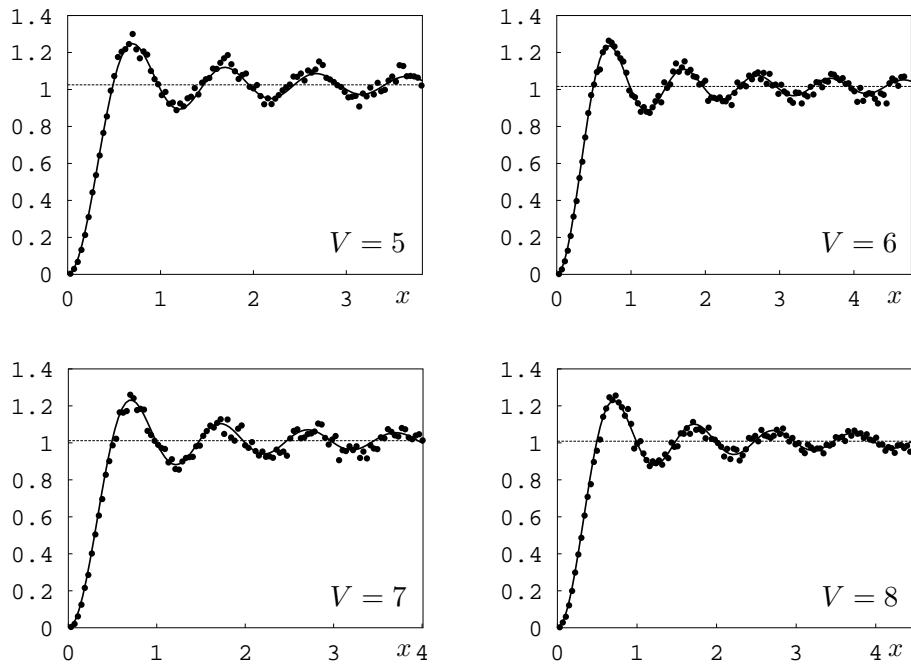


Figure 2.6.: Gallery of numerical results for Andreev graphs with varying total number of vertices V ranging from 5 to 8. The full curve shows the random-matrix prediction for $R_N(x)$ with $N = V(V - 1)$. For every graph size shown, the numerical data is based on an ensemble of 36000 configurations and has been rescaled as in the $V = 4$ case. The value $1 + \frac{1}{2N}$, about which the distribution $R_N(x)$ fluctuates, is indicated by the dashed horizontal line.

With this insight, we give an estimate for when we expect the breakdown of random-matrix theory predictions in the present context. From what we learn in the appendix C (in the paragraphs beneath eq. (C.9)), the mean spacing between eigenvalues for the type *C* Andreev graph is $\pi/2L_{\text{tot}}$, where L_{tot} is the total length of the graph. Thus, the estimate for the validity range of random-matrix theory in units of mean level spacings is given by $\Delta k \times 2L_{\text{tot}}/\pi = 4L_{\text{tot}}/l_{\text{min}} \approx 2V(V-1)/2 = N$, where every length between any two vertices is set to unity for a rough estimate. For the fully connected Andreev graph with $V = 4$ vertices ($N = 12$), this estimate predicts that significant deviations are visible around the twelfth eigenvalue. In hindsight, this result is not surprising given the drop in $\rho_{12}(\varphi)$ to zero at angle π in the RMT density of states plotted in figure 2.5, part (a). In fact, in the bottom part (c) of figure 2.5 small deviations can be seen starting around the third eigenvalue. However, as the estimate was of the coarsest kind and as the transition from random-matrix behaviour to non-universal statistics is gradual, we content ourselves with this estimate.

In order to supplement the computation for the fully connected Andreev graph with $V = 4$ vertices and to underline the soundness of these results, the spectral density of the same type of graph is also computed numerically for $V = 5, \dots, 8$. The gallery of spectra in figure 2.6 show how the agreement between numerical data and random-matrix theory prediction $R_N(x)$ with $N = V(V-1)$ grows ever better the larger is the system size chosen.

The good agreement between the spectral statistics of the fully connected Andreev graph with varying number of vertices $V = 4, \dots, 8$ and the random-matrix theory predictions $R_N(x)$ given by the definition (2.25) with $N = V(V-1)$ is the key result of the present chapter. This consistency of the numerical data and the random-matrix theory predictions exemplified in figures 2.5 and 2.6 proves that the statistics of the fully connected Andreev graph with the random scattering matrices $\sigma^{(j)} \in \text{Sp}(2v_j)^3$ approaches the *universal* limit of class *C* for $N \rightarrow \infty$.

As stressed before, the Andreev graph with random scattering matrices on the vertices – though *universal* in the limiting case of very large graphs – is a dynamical system which can not fully described by random-matrix theory. Fingerprints of the non-universal dynamics of the system can be found in contributions from the shortest periodic orbits – these contributions are the topic of the following section.

2.6. Periodic orbit contributions

In this section, we analyze the spectrum of a specific Andreev graph in terms of periodic orbits. While the computation of the spectrum $\rho(E)$ from the periodic

³ v_j is the number of bonds connected to the vertex j .

orbits of the spectrum is by no means trivial, the inverse procedure is comparatively easy – analyzing a given spectrum in terms of periodic orbits. Such a spectral analysis of the spectral density of a chaotic microwave resonator was carried out by Stöckmann [56] and is described in his monograph [21]. In the footsteps of this work, we analyze the spectrum of a fully connected graph with $V = 4$ vertices with respect to the contributing periodic orbits.

In the spirit of this approach, we extract contributions of different periodic orbits, by subjecting the spectral density $\rho(k)$ to a Fourier transform:

$$\hat{\rho}(l) = \int dk \rho(k) e^{ikl} = \sum_j A_j \delta(l - l_j) \quad (2.26)$$

with $\rho(k)$ expressed by the GTF (1.40) where all factors but the dynamical phase are absorbed in the stability amplitude A_j , and the sum on j labels all periodic orbits j with length l_j .

For the Andreev graph shown in the inset of figure 2.7 (with the bond lengths kept fixed throughout as cited), the absolute square $|\hat{\rho}(l)|^2$ was computed from a sequence of about 8000 eigenvalues $\{k_i\}$ of a single realization:

$$\hat{\rho}(l) = \int dk \rho(k) e^{ikl} = \sum_i \int dk \delta(k - k_i) e^{ikl} = \sum_i e^{ik_i l}. \quad (2.27)$$

The wave number k measures the distance from the Fermi wave number k_F : $k^\pm = k_F \pm k$. The dynamical phase of an orbit of total length l (where l_e (l_h) is the length traversed by electron (hole)) is given by $\exp(ik^+l_e - ik^-l_h) \propto \exp[ik(l_e + l_h)] = \exp(ikl)$.

Clearcut fingerprints of the periodic orbits are found in the numerical results. We now comment on these results obtained for the Fourier transform $|\hat{\rho}(l)|^2$ of the spectrum of the Andreev graph as shown in the inset of figure 2.7. The lengths of the bonds chosen result in definite lengths of the shortest periodic orbits. The peaks in the Fourier transform $|\hat{\rho}(l)|^2$ can be associated with respective periodic orbits. For the shortest periodic orbits, the lengths of the bonds constituting the periodic orbit specify the orbit and are quoted in the vicinity of the corresponding peak. The agreement of the numerical data with the forecast built on periodic-orbit theory is quite good.

The increase of the Fourier transform $|\hat{\rho}(l)|^2$ for small lengths is due to the smooth part of the spectrum ρ_{av} . It has been shown in the introductory chapter 1.3 that orbits of vanishing length build up the smooth part of the spectrum ρ_{av} . We interpret the broadening of the contribution for length zero ($l = 0$) as a result of the finite support in the wave number variable k ; this is unavoidable as only a finite number of eigenvalues were calculated.

A few words should be said about the splitting of the peaks in $|\hat{\rho}(l)|^2$ for the short orbits of total length $L_{\text{tot}} = 20$ and $L_{\text{tot}} = 24$. These orbits are both 2-step orbits with two scattering events at vertices adjacent to bonds of length

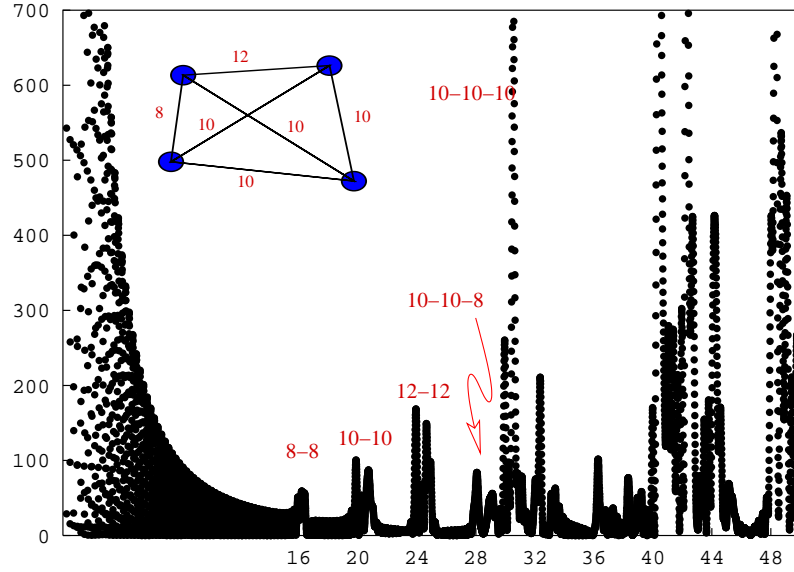


Figure 2.7.: Periodic orbit contributions visible in the absolute square of the Fourier transform $|\hat{\rho}(l)|^2$ of the spectrum.

$L_b = 10$ and $L_b = 12$, respectively. As only *a single* configuration of vertex scattering matrices $\sigma^{(j)}$ is taken into account for the computation of $|\hat{\rho}(l)|^2$, the splitting of peaks could be due to different scattering phases acquired by the different quasi-particle types on these short orbits.

This concludes this section, where we have shown that the Andreev quantum graphs are dynamical systems whose system-specific non-universal fingerprints in the spectrum can be understood with the aid of periodic-orbit theory.

2.7. Concluding remarks and summary

In this chapter, we have shown how Andreev reflection can be incorporated on a quantum graph. The numerical analysis of this toy model for superconducting-normalconducting hybrid systems confirms the expectations on the spectrum from the RMT perspective which takes only the fundamental symmetries of the system into account.

The full strength of quantum graphs will become manifest in the next chapter, where we compute the spectrum of Andreev quantum graphs with the help of a trace formula analogous to the formula presented in (1.59). In this way, we provide a semiclassical interpretation for the RMT findings of the new symmetry classes relevant for superconducting-normalconducting hybrid systems.

3. Andreev Star Graph

The goal of this chapter is the semiclassical calculation of the form factors $K(t)$ of the new ensembles (1.51) with the aid of periodic-orbit theory. This calculation becomes particularly transparent and explicit within the reductionist model of quantum graphs.

As a motivation, we start by presenting the correspondence between the original physical system of the Andreev billiard and the Andreev quantum graph model. An illustration of the transition to the quantum graph model is given in figure 3.1, showing both the Andreev billiard and the Andreev quantum star graph. One can think of the formation of the quantum graph in the following way. The normalconducting area (with underlying chaotic dynamics) is emulated by the central scatterer and the bonds connected to it. The SN-interface between the superconductor (S) and the normalconducting area (N) is divided into parts – each bond carrying a fragment of the interface at its peripheral end. One way to obtain *universal* spectral results is to have a spatially varying phase of the order parameter of the superconductor. This situation is modeled by an independent stochastic choice of the superconductor order parameter for every peripheral vertex. In the reductionist way described above can one think of the Andreev star graph as a toy model for the Andreev billiard.

The modeling discussed above employs a discretization of configuration space. An alternative approach uses discretization in momentum space [88] and is presented in the following. This alternative construction of the quantum graph identifies the peripheral vertices of the graph with different quantum mechanical channels n in the superconducting leads connected to the normal conducting billiard region. For a lead of width w (with hard walls), one has quantization in the transversal direction with possible transverse wave numbers $n\pi/w$ ($n = 1, 2, \dots, N$, where N is the integer part of $k_F w/\pi$, k_F is the Fermi wave number). Such a mode enters the normal conducting region of the billiard under the angle θ_n where $\pm \sin \theta_n = n\pi/(k_F w)$. Each of the N quantum mechanical channels of the billiard is mapped to a distinct peripheral vertex of the star graph.

After this motivational opener, we present now the outline of this chapter. In the subsequent section 3.1, the formally rigorous set-up of the *Andreev* quantum star graph is provided. First, the star graph versions for systems *with* spin-rotation invariance (class *C* and *CI*) are introduced. Second, star graphs where spin degrees of freedom are taken into account (for the treatment of classes *D* and *DIII*) are introduced. Besides, our choice for the central scatterer is

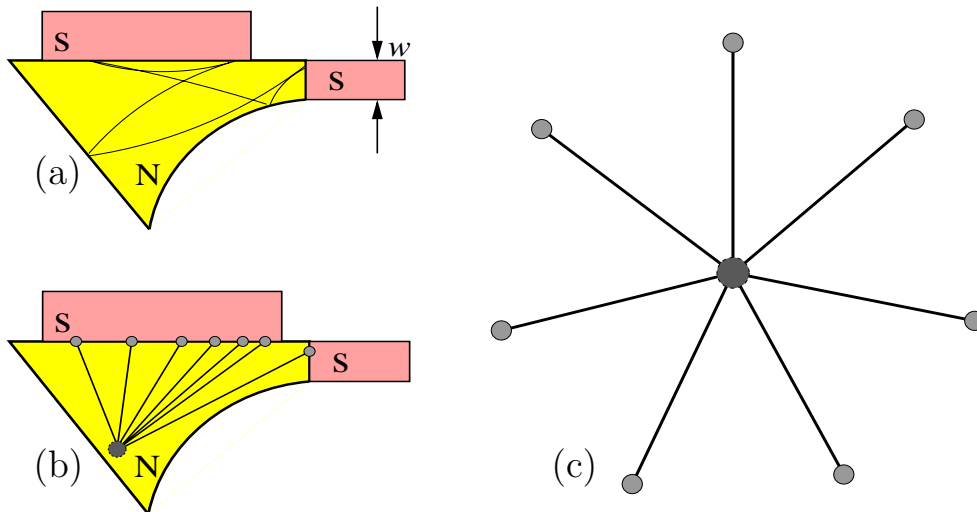


Figure 3.1.: The metamorphosis from Andreev billiard to Andreev quantum star graph. (a) shows the Andreev billiard (in the presence of a magnetic field B) with the sketch of a (very simple) periodic orbit involving two normal and two Andreev reflections. (b) presents the same Andreev billiard where the superimposed graph gives a hint to the modeling process: the central scatterer mimics the chaotic dynamics of the normalconducting region and the peripheral vertices at the outer ends of the separate bonds are fragments of the SN-interface. (c) the Andreev quantum star graph in its own right. The central scatterer has mixing dynamics, the phases of the order parameter at the peripheral vertices can be tuned appropriately in order to model the spatially variant phase of the order parameter. Besides, for the graph model where different transverse momenta modes are mapped to the peripheral vertices, the width w of one superconducting lead attached to the billiard is shown in part (a).

motivated, the gauge invariance of the relevant physical quantities is proven, and the symmetry requirements on the Andreev scatterers at the periphery are explained.

In section 3.2, the calculation of the spectral quantities for the Andreev star graph of class C is presented in some detail, as the calculation for class C serves as a template for the treatment of the star graphs of the remaining symmetry classes CI , D , and $DIII$. As an approximation scheme, we introduce the *self-dual approximation* for evaluating the spectral quantities of the new symmetry classes. This *self-dual approximation* is akin to Berry's diagonal approximation for systems in Wigner-Dyson classes [9].

The subsequent sections 3.3 – 3.5 treat the Andreev star graphs with symmetries of the classes CI , D , and $DIII$.

The analytical calculations are supplemented by numerical calculations for the average spectral density $\langle \rho(k) \rangle$ and its Fourier transform, the form factor $K(t)$. While the results of these numerical calculations are inserted in the sections 3.2 – 3.5, a comprehensive account of the numerical routine for the calculation of the form factor is given in section 3.6.

A brief review on how the findings for the spectral quantities of the Andreev star graph of class C and CI are generalized to Andreev billiards is given in the section 3.7. Hereby, we closely follow the lines of the publication [89]. Concluding remarks in section 3.8 summarize this chapter, where the semiclassical calculation of the form factors of the new ensembles (1.51) is achieved with the aid of periodic-orbit theory for Andreev quantum graphs.

3.1. Set-up and formalism of the Andreev star graph

Depending on the symmetries imposed, the Andreev star graph is a toy model for systems within one of the four symmetry classes C , CI , D , and $DIII$. We begin with the set-up for star graphs in symmetry classes C and CI (subsection 3.1.1). Here spin-rotation invariance is preserved, allowing for a restriction to a single spin sector as described in the introductory section 1.2.4. This renders the treatment of the graph easier from a technical point of view. Subsequently in subsection 3.1.2, the design of star graphs will be extended to systems where spin-rotation invariance is broken (leading to classes D and $DIII$). The symmetry requirements on the Andreev scattering matrices at the periphery are explained in the subsection 3.1.3.

3.1.1. Star graph with preserved spin-rotation invariance; classes C and CI

A star graph consists of a central vertex v_0 and N peripheral vertices v_1, \dots, v_N (see figure 3.1, (c)). The central vertex v_0 is connected to every peripheral vertex v_j by the bond $b_j = b_{[0,j]}$ of length L_j . The bond is attached to the central scatterer at $x_j = 0$ and reaches the peripheral (Andreev) vertex at $x_j = L_j$. The position x_j on the bond b_j is measured starting from the center. The star geometry suggests the following labeling: Amplitudes of quasi-particles on the way to the periphery have the suffix \rightarrow whereas the amplitudes of the quasi-particles incident on the center have the suffix \leftarrow . The wave function has a total of $2N$ components as on each bond b_j ($1 \leq i \leq N$), the two-element column vector

$$\Psi^{(j)}(x_j) = \begin{bmatrix} e_{\rightarrow,i} e^{ik^+ x_i} + e_{\leftarrow,i} e^{ik^+(L_i - x_i)} \\ h_{\rightarrow,i} e^{-ik^- x_i} + h_{\leftarrow,i} e^{-ik^-(L_i - x_i)} \end{bmatrix} \quad (3.1)$$

solves the BdG equation with vanishing order parameter Δ .¹ Here it suffices to remember the linear approximation of the dispersion relation $E(k)$ close to the Fermi surface:

$$\hbar k^\pm(E) = \sqrt{2m} \sqrt{\mu \pm E} \approx \hbar k_F \pm \sqrt{\frac{m}{2\mu}} E = \hbar(k_F \pm k). \quad (3.2)$$

Here, and throughout all subsequent sections, we use the convention that k measures the wave number difference from the Fermi wave number k_F .

The coefficients of the counter-propagating amplitudes $e_{\rightarrow,i}, e_{\leftarrow,i}$ and $h_{\rightarrow,i}, h_{\leftarrow,i}$ (for $1 \leq i \leq N$) form a $4B$ -dimensional vector:

$$\mathbf{v} = \begin{bmatrix} e_{\leftarrow} \\ e_{\rightarrow} \\ h_{\leftarrow} \\ h_{\rightarrow} \end{bmatrix}, \quad (3.3)$$

where e_{\leftarrow} is an N -dimensional vector with entries $e_{\leftarrow,i}$ (likewise for $e_{\rightarrow}, h_{\leftarrow},$ and h_{\rightarrow}).

Two important restrictions are imposed on the star graph model. They are both well motivated on physical grounds and are of great advantage when evaluating periodic-orbit contributions within the graph model. First, the central scatterer preserves the particle type. This is fair to assume as the central scatterer mimics the dynamics in the *normalconducting* region of the Andreev billiard. The second restriction concerns the Andreev reflection at the interface between the normalconducting region (the inner part of the star graph) and the exterior. We restrict ourselves exclusively to Andreev processes with *complete electron-hole conversion*: every electron hitting the periphery is scattered back as a hole and vice versa. This complete transformation is a good approximation for energies $E \ll \Delta_0$ ² (where Δ_0 is the absolute value of the order parameter) when *no impurities* are situated in the interface (see e. g. the appendix of [90]). With our interest being in the level statistics close to the Fermi energy, we are well within the energy regime where the approximation of complete conversion is valid.

These two restrictions can be succinctly cast into boundary conditions at the central vertex and at the peripheral vertices, both of which are specializations of the general form of the vertex-scattering relations presented by eq. (2.5):

$$\begin{bmatrix} e_{\rightarrow,l} \\ h_{\rightarrow,l} \end{bmatrix} = \sum_{m=1}^N \begin{bmatrix} S_{C,lm} & 0 \\ 0 & \overline{S}_{C,lm} \end{bmatrix} \begin{bmatrix} e^{ik^+L_m} e_{\leftarrow,m} \\ e^{-ik^-L_m} h_{\leftarrow,m} \end{bmatrix} \quad (3.4)$$

¹When the order parameter Δ vanishes, the BdG equation decouples into a pair of Schrödinger type equations. This has been discussed in the section 2.2.

²It has already been explained in the introductory chapter 1.1.2 that the energy E is measured from the Fermi energy.

for the central scatterer and for the scatterers at the periphery ($1 \leq m \leq N$):

$$\begin{bmatrix} e_{\leftarrow,m} \\ h_{\leftarrow,m} \end{bmatrix} = \begin{bmatrix} 0 & -ie^{i\varphi_m} \\ -ie^{-i\varphi_m} & 0 \end{bmatrix} \begin{bmatrix} e^{ik^+L_m} & e_{\rightarrow,m} \\ e^{-ik^-L_m} & h_{\rightarrow,m} \end{bmatrix}. \quad (3.5)$$

Here S_C is the scattering matrix associated with scattering at the center and φ_m denotes the phase of the superconducting order parameter. The amplitudes $(e/h)_{(\rightarrow/\leftarrow),m}$ were introduced in eq. (3.1).

In the following, the central scattering matrix S_C is discussed. We explain the special choice taken and discuss its properties. An explicit treatment of the superconducting order parameter φ_m and the values allowed by the respective symmetry is postponed and will follow in subsection 3.1.3.

For the entries of the matrix S_C we choose:

$$S_{C,kl} = \frac{1}{\sqrt{N}} \exp\left(2\pi i \frac{kl}{N}\right). \quad (3.6)$$

In the context of quantum graphs, these matrices were introduced by [91] and subsequently used in [78] and [92]. A vertex, where the scattering is prescribed by a matrix S_C with entries given by eq. (3.6), has been termed Fourier vertex as the entry (3.6) is the Fourier coefficient of a discrete Fourier transform from k to l .

The choice of (3.6) avoids the localization effect found in usual star graphs with Neumann boundary conditions at the central vertex [79], [80].³

Although the outcome of the calculation does *not* depend on the special choice taken for the central scatterer, the choice (3.6) proves advantageous for the calculation and merits some detailed discussion. The different transition probabilities at the central scatterer for either Fourier or Neumann boundary conditions explain the advantage of the form (3.6) when the interest focuses on the ergodic limit where the wave function explores the phase space uniformly. For Neumann boundary conditions, the transition probability for scattering from bond l to bond k is $P_{kl} = (2/N - \delta_{kl})^2$ [11]. Thus, when the number of peripheral vertices N is large, backscattering is strongly favoured. The wave function is trapped which is highly unfavourable if one is interested in the ergodic limit.

The situation is distinctly different in the case of Fourier boundary conditions. With this choice (3.6), the transition probability $P_{kl} = |S_{C,kl}|^2 = 1/N$ is equal for all scattering processes $l \rightarrow k$. The consequence is a swift arrival at the ergodic limit. For instance, we consider the least uniform probability distribution at the initial time step $t = 0$ where an electron is inward moving only on bond b_0 : $\rho_{\leftarrow,b}^e(t = 0) = \delta_{b,b_0}$. After only *one* scattering event,

³An analysis of the two-point spectral statistics [79], [80] demonstrates that the form factor $K(t)$ for the Schrödinger star graph, with Neumann boundary conditions at the central vertex, is neither that of an integrable system nor that of a non-integrable system in the ergodic limit (which would follow random-matrix theory predictions).

one has equal probability to find the electron outward bound on any bond b' : $\rho_{\leftarrow,b'}^e(1) = \sum_b P_{b',b} \rho_{\leftarrow,b}^e(0) = 1/N$. As a consequence, *any* choice of initial probabilities $\rho_{b_j}^e(0)$ (made up from a linear combination of the case explained here) is equilibrated after *one* scattering event in the center. This concludes our comments on the advantage of the Fourier scattering conditions (3.6) in favour of the ergodic limit.

Now, a comment on the partition in (3.4) responsible for the scattering of holes at the center is mandatory. This partition is chosen such that time-reversal symmetry is *not* broken by the central scatterer itself. In our set-up, the decision as to whether time-reversal symmetry is broken or not is *solely* governed by the choice of Andreev phases φ_m at the periphery. In anticipation of table 3.1, where the conditions for a scattering matrix with good time-reversal symmetry are laid down in the last row,⁴ the entries for hole scattering are complex conjugates $\overline{S_{C,lm}}$ of their electron counterparts $S_{C,lm}$.

The complete set of boundary conditions of all vertices can be cast in one single scattering matrix \mathcal{S}_B acting on the $4B$ -dimensional vector of directed-bond-amplitudes $\mathbf{v} = (e_{\leftarrow}, e_{\rightarrow}, h_{\leftarrow}, h_{\rightarrow})^T$ defined in (3.3):

$$\mathcal{S}_B = \begin{bmatrix} 0 & 0 & 0 & \mathcal{L}^+ \text{diag}(-ie^{i\varphi_j}) \\ \mathcal{L}^+ S_C & 0 & 0 & 0 \\ 0 & \mathcal{L}^- \text{diag}(-ie^{-i\varphi_j}) & 0 & 0 \\ 0 & 0 & \mathcal{L}^- \overline{S_C} & 0, \end{bmatrix} \quad (3.7)$$

where $\mathcal{L}^\pm = \text{diag}(e^{\pm ik^\pm L_j})$ stores all metric information (bond lengths L_j) of the graph. Again, the scattering matrix \mathcal{S}_B can be written as a product $\mathcal{S}_B = DT$, where D depends on lengths and T on the boundary conditions of the Andreev star graph.

A simplification with respect to the metric matrices \mathcal{L}^\pm is possible as the spectrum does not depend on the absolute value of the Fermi wave number k_F . Setting $k_F = 0$ in \mathcal{S}_B is equivalent to a unitary transformation $\mathcal{S}_B^{\mathbf{k}_F}(k) = U^\dagger \mathcal{S}_B^{\mathbf{k}_F=0}(k) U$ which has no influence on the quantization (3.11). With the linear expansion (3.2) such that $k^\pm = k_F \pm k$, one can decompose

$$\begin{aligned} \mathcal{L}_{mm}^+ &= \exp(ik^+ L_m) = \exp(ik_F L_m) \exp(ik L_m) = \mathcal{L}_{mm}^0 \mathcal{L}_{mm} \quad \text{and} \\ \mathcal{L}_{mm}^- &= \exp(-ik^- L_m) = \exp(-ik_F L_m) \exp(ik L_m) = \overline{\mathcal{L}_{mm}^0} \mathcal{L}_{mm}. \end{aligned} \quad (3.8)$$

This leads to the unitary transformation

$$\mathcal{S}_B^{\mathbf{k}_F}(k) = U^\dagger \mathcal{S}_B^{\mathbf{k}_F=0}(k) U \quad \text{with} \quad U = \text{diag}(\mathbb{1}, \overline{\mathcal{L}^0}, \mathbb{1}, \mathcal{L}^0) \quad (3.9)$$

and the bond-scattering matrix for $k_F = 0$ takes the form:

$$\mathcal{S}_B^{(\mathbf{k}_F=0)}(k) = \begin{bmatrix} 0 & 0 & 0 & \mathcal{L} \text{diag}(-ie^{i\varphi_j}) \\ \mathcal{L} S_C & 0 & 0 & 0 \\ 0 & \mathcal{L} \text{diag}(-ie^{-i\varphi_j}) & 0 & 0 \\ 0 & 0 & \overline{\mathcal{L} S_C} & 0, \end{bmatrix}. \quad (3.10)$$

⁴For the $2N$ -dimensional central scatterer, the condition of class CI reads $S^{-1\dagger} = S^T = S = \Sigma_y \overline{S} \Sigma_y$ with $\Sigma_y = \sigma_y \otimes 1_N$.

It is understood that this form is used in the following while the superscript ($k_F = 0$) is suppressed. The only dependence of the scattering matrix $\mathcal{S}_B(k)$ on the wave number k comes from the metric matrices $\mathcal{L} = \text{diag}[\exp(ikL_m)]$. With this form (3.10) of the scattering matrix \mathcal{S}_B , the secular equation

$$\det(1 - \mathcal{S}_B(k)) = 0 \quad (3.11)$$

serves as a natural starting point for the spectral theory of the Andreev star graph. Along the lines of reasoning of Kottos *et al* ([10], [11]), we derive a Gutzwiller type trace formula for the deviations of the spectral density from its average value $\langle \delta\rho \rangle$ starting with the quantization condition (3.11).

It is remarkable that only the partitions beneath the diagonal are nonvanishing.⁵ This structure implies that the traces $\text{tr} \mathcal{S}_B^m$ vanish for $n = 4m + 1$, $n = 4m + 2$, and $n = 4m + 3$. Only $n = 4m$ contributes. This algebraic finding is transparent in the light of periodic-orbit theory for the Andreev star graph. For $m = 1$, one can find the following quasi-particle sequence on a periodic orbit: $(e_{\rightarrow}, h_{\leftarrow}, h_{\rightarrow}, e_{\leftarrow})$. Quasi-particle type transformation at the Andreev vertices and scattering at the center take turns. So $n = 4$ is the minimal number of scattering events to close a periodic orbit such that the directed bond *and* the particle type are identical to the starting configuration.

This observation motivates the introduction of a *reduced* bond-scattering matrix

$$S_{B\text{red}}(k) = \mathcal{L}(k) \overline{S_C} \mathcal{L}(k) \text{diag}(-ie^{-i\varphi_j}) \mathcal{L}(k) S_C \mathcal{L}(k) \text{diag}(-ie^{i\varphi_j}), \quad (3.12)$$

where the partitions of (3.10) are ordered by decreasing row index. The product of the individual partition matrices in (3.12) – read in reverse order – indicates the sequence of scattering events on the Andreev star graph. The original quantization condition (3.11) translates into an analogous expression for the *reduced* scattering matrix:⁶

$$\det(1 - S_{B\text{red}}(k)) = 0. \quad (3.13)$$

This quantization condition (3.13), with different choices for the Andreev phases φ_j , is the starting point for computing spectral quantities of the Andreev star graph within the symmetry classes C and CI .

We conclude this section on the set-up of the star graph by an essential remark about the *gauge invariance* of the quantization conditions (3.11) resp. (3.13). Once the gauge invariance of these expressions is shown, all spectral quantities derived therefrom are also gauge invariant.

For the proof of gauge invariance, the dependence of the dynamical phases acquired by the quasi-particles and the dependence of the Andreev phases φ_j on the gauge chosen needs to be taken into account. For the treatment of the

⁵By “beneath the diagonal”, we indicate the partitions $P_{i,j} = P_{(j+1) \bmod 4, j}$ with $1 \leq j \leq 4$.

⁶This can be seen by expanding the logarithm of the determinant in a trace.

dynamical phases, it is best to resort to the formulation (3.7) of the bond-scattering matrix where the dynamical phases acquired by electrons (holes) are comprised in \mathcal{L}^+ (\mathcal{L}^-). Introducing the minimal coupling $-i\partial \rightarrow -i\partial - e\mathbf{A}$ in the original BdG equation (1.9) entails $\mathcal{L}^+ = \text{diag}[\exp(i(k^+ - \mathbf{A})L_j)]$ and $\mathcal{L}^- = \text{diag}[\exp(-i(k^- + \mathbf{A})L_j)]$ for the matrices of the dynamical phases.

Now, the *local* gauge transformation $\psi(x) \rightarrow e^{i\theta(x)}\psi(x)$, $q\mathbf{A}(x) \rightarrow q\mathbf{A}(x) + \partial\theta(x)$ (with $\theta(x)$ an arbitrary space dependent phase and q the charge of the quasi-particle) leads to the following changes for the elements of the matrix (3.7):

$$\begin{aligned}\mathcal{L}^+ &= \text{diag}[\exp(i(k^+ - \mathbf{A})L_j)] \\ &\rightarrow \text{diag}[\exp(i(k^+ - \mathbf{A})L_j) \exp(i\theta_{\text{fin}} - i\theta_{\text{ini}})], \\ \mathcal{L}^- &= \text{diag}[\exp(-i(k^- + \mathbf{A})L_j)] \\ &\rightarrow \text{diag}[\exp(-i(k^- + \mathbf{A})L_j) \exp(-i\theta_{\text{fin}} + i\theta_{\text{ini}})], \\ \varphi_j &\rightarrow \varphi_j + 2\theta_j,\end{aligned}\tag{3.14}$$

where θ_j is the value of the phase $\theta(x)$ at the peripheral scattering vertex j and $\theta_{\text{ini}} = \theta(x_{\vec{b}_j} = 0)$ resp. $\theta_{\text{fin}} = \theta(x_{\vec{b}_j} = L_{b_j})$ are its values at the beginning resp. end of the directed bond \vec{b}_j . The increase of the Andreev phase φ_j by $2\theta_j$ is clear from the definition (1.4) as the order parameter $\Delta(x)$ acquires *double* the phase $\Delta(x) \rightarrow \exp[i2\theta(x)]\Delta(x)$ under the gauge transformation described above.

The invariance of the secular equations (3.11) resp. (3.13) under local gauge transformations is shown by inserting the transformations of (3.14) in the expression of the reduced bond-scattering matrix (where $k_F \neq 0$, with the matrices \mathcal{L}^+ , \mathcal{L}^-):

$$S_{B_{\text{red}}}^{\mathbf{k}_F \neq 0} = \mathcal{L}^- \overline{S_C} \mathcal{L}^- \text{diag}[-i \exp(-i\varphi_j)] \mathcal{L}^+ S_C \mathcal{L}^+ \text{diag}[-i \exp(+i\varphi_j)].\tag{3.15}$$

From an explicit notation of the matrices in (3.15) entry-by-entry, invariance under the transformations (3.14) – i.e. gauge invariance – is easily seen.

3.1.2. Star graph without spin-rotation invariance – classes D and $DIII$

Equipped with the design of the Andreev star graph for the classes of preserved spin-rotation invariance explained in the last subsection, we can now generalize to systems of class D and $DIII$ where spin-rotation invariance is *not* preserved.

We choose such systems for the set-up of the Andreev star graph, where neither a magnetic field nor any spin-orbit scatterers are present in the normalconducting region. Thereby, the central scattering matrix leaves spin settings invariant.

Taking the spin degree of freedom into account leads to a four dimensional wave function $\Psi^{(j)}(x_j)$ on each bond b_j . The additional labels \uparrow and \downarrow indicate the respective positions of the spin with regard to the quantization axis:

$$\Psi^{(j)}(x_j) = \begin{bmatrix} e_{\rightarrow,\uparrow,i} e^{ik^+ x_i} + e_{\leftarrow,\uparrow,i} e^{ik^+(L_i-x_i)} \\ e_{\rightarrow,\downarrow,i} e^{ik^+ x_i} + e_{\leftarrow,\downarrow,i} e^{ik^+(L_i-x_i)} \\ h_{\rightarrow,\uparrow,i} e^{-ik^- x_i} + h_{\leftarrow,\uparrow,i} e^{-ik^-(L_i-x_i)} \\ h_{\rightarrow,\downarrow,i} e^{-ik^- x_i} + h_{\leftarrow,\downarrow,i} e^{-ik^-(L_i-x_i)} \end{bmatrix}. \quad (3.16)$$

This wave function $\Psi^{(j)}(x_j)$ is a solution of the BdG equation (1.8) with *zero* order parameter Δ . The wave numbers k^\pm are the same as given by eq. (3.2). The vector $\mathbf{v} = (e_{\leftarrow}, e_{\rightarrow}, h_{\leftarrow}, h_{\rightarrow})^T$ is now $8N$ -dimensional, as the entry e_{\leftarrow} (and likewise e_{\rightarrow} , h_{\leftarrow} , and h_{\rightarrow}) itself has $2N$ components.⁷

$$e_{\leftarrow} = \begin{bmatrix} e_{\leftarrow,\uparrow,1} \\ e_{\leftarrow,\downarrow,1} \\ \vdots \\ e_{\leftarrow,\uparrow,N} \\ e_{\leftarrow,\downarrow,N} \end{bmatrix}. \quad (3.17)$$

The vertex-scattering relations at the center and at the periphery are readily noted down in analogy with the relations (3.4) and (3.5). The bond-scattering matrix exhibits the same structure of partitions as was shown for classes C and CI in (3.7) – merely the dimension of each partition has doubled. Instead of giving a discussion similar to that of the previous subsection 3.1.1 with the minor modification of the extra spin degree of freedom, we present the form of the reduced bond-scattering matrix for classes D and $DIII$ at once. Except for the matrices for Andreev scattering, all entries M_{ij} in matrices of (3.12) are substituted as $M_{ij} \rightarrow M_{ij} \otimes \mathbb{1}_2$:

$$S_{B\text{red}}(k) = [\mathcal{L}(k) \otimes \mathbb{1}_2] [\overline{S_C} \otimes \mathbb{1}_2] [\mathcal{L}(k) \otimes \mathbb{1}_2] \text{diag}(\overline{\mathcal{A}}_1, \dots, \overline{\mathcal{A}}_N) \times \\ \times [\mathcal{L}(k) \otimes \mathbb{1}_2] [S_C \otimes \mathbb{1}_2] [\mathcal{L}(k) \otimes \mathbb{1}_2] \text{diag}(\mathcal{A}_1, \dots, \mathcal{A}_N). \quad (3.18)$$

The diagonal matrices holding the partitions for Andreev reflection are diagonal in bond space, while their entries \mathcal{A}_j and $\overline{\mathcal{A}}_j$ are 2×2 matrices governing the Andreev scattering at vertices j . The specific choices for \mathcal{A}_j depending on the symmetry class are explained in the subsequent subsection.

3.1.3. Requirements on the Andreev scatterers by symmetry

In order to obtain an Andreev graph with universal spectral statistics for the quasi-particle excitations close to the Fermi surface, certain conditions must be

⁷For the vector in directed bond space \mathbf{v} and the reduced scattering matrix $S_{B\text{red}}(k)$ of classes D and $DIII$, we use the same symbol as for their counterparts in classes C and CI as the context will always be unambiguous.

Symmetry class	symmetries of \mathcal{H}	symmetries of $S = \exp(i\mathcal{H}t)$	conditions on $\mathcal{A}_k, \mathcal{B}_k$
D	$\mathcal{H}^\dagger = \mathcal{H} = -\Sigma_x \mathcal{H}^T \Sigma_x$ with $\Sigma_x = \sigma_x \otimes \mathbb{1}_2$	$S^{-1\dagger} = S = \Sigma_x \bar{S} \Sigma_x$ with $\Sigma_x = \sigma_x \otimes \mathbb{1}_2$	$\mathcal{A}_k \mathcal{A}_k^\dagger = \mathbb{1}_2, \mathcal{B}_k = \overline{\mathcal{A}_k}$
$DIII$	as in D and $\mathcal{H} = \tau \mathcal{H}^* \tau^{-1}$ with $\tau = \mathbb{1}_2 \otimes i\sigma_y$	as in D and $S = \tau S^T \tau^{-1}$ with $\tau = \mathbb{1}_2 \otimes i\sigma_y$	as in D and $\mathcal{A}_k = \sigma_y \mathcal{A}_k^\dagger \sigma_y$
C	$\mathcal{H}^\dagger = \mathcal{H} = -\sigma_y \mathcal{H}^T \sigma_y$	$S^{-1\dagger} = S = \sigma_y \bar{S} \sigma_y$	$\mathcal{A}_k \overline{\mathcal{A}_k} = 1, \mathcal{A}_k = -\overline{\mathcal{B}_k}$
CI	$\mathcal{H}^\dagger = \mathcal{H}^T = \mathcal{H} = -\sigma_y \mathcal{H}^T \sigma_y$	$S^{-1\dagger} = S^T = S = \sigma_y \bar{S} \sigma_y$	$\mathcal{A}_k = -\overline{\mathcal{B}_k} = \mathcal{B}_k = i\sigma_k$

Table 3.1.: The symmetries of \mathcal{H} impose conditions on the scattering matrix S . With the form (3.19) chosen for a peripheral scattering matrix S_k , conditions on the scattering matrix S_k at vertex k translate to restrictions on the submatrices (entries) \mathcal{A}_k and \mathcal{B}_k .

fulfilled by the Andreev vertices at the periphery. These restrictions are worked out starting from the symmetries of preserved/broken time reversal and/or spin rotation which classify the BdG Hamiltonian \mathcal{H} into one of the four classes D , $DIII$, C or CI [2]. The quasi-particles close to the Fermi surface – on which we focus our interest – have wave numbers k very close to the Fermi wave number k_F . Setting $k = k_F$ is, thus, a very good approximation. In this approximation, the conversion at the Andreev vertices is complete, i. e., all incident electrons are converted to holes and vice versa (cf. appendix A). The general form of the scattering matrix S_k at vertex k ($1 \leq k \leq N$) is then given by

$$\begin{bmatrix} e \\ h \end{bmatrix}_{k \text{ out}} = \underbrace{\begin{bmatrix} 0 & \mathcal{A}_k \\ \mathcal{B}_k & 0 \end{bmatrix}}_{S_k} \begin{bmatrix} e \\ h \end{bmatrix}_{k \text{ in}}. \quad (3.19)$$

For symmetry classes C and CI , amplitudes e, h and entries $\mathcal{A}_k, \mathcal{B}_k \in \mathbb{C}$ are complex numbers. In the case of classes D and $DIII$, e and h stand for the two component wave functions $\begin{bmatrix} e \uparrow \\ e \downarrow \end{bmatrix}$ and $\begin{bmatrix} h \uparrow \\ h \downarrow \end{bmatrix}$, and $\mathcal{A}_k, \mathcal{B}_k$ are complex 2×2 matrices. Depending on the symmetry class, conditions are derived for $\mathcal{A}_k, \mathcal{B}_k$. The scattering matrix S_k for the Andreev vertex k must respect the same symmetries as the exponential $S = \exp(i\mathcal{H}t)$ of the BdG Hamiltonian \mathcal{H} with the corresponding symmetries for each class. In consequence, the symmetries of the Hamiltonian \mathcal{H} lead to conditions for the entries $\mathcal{A}_k, \mathcal{B}_k$ of the Andreev scattering matrix at vertex k . We summarize the computation in the table 3.1.

The matrices $\mathcal{A}_k, \mathcal{B}_k$ are chosen such that the required conditions for the respective symmetry classes are met. In detail, they are for class D :

$$\mathcal{A}_k = e^{i\alpha_k} \begin{bmatrix} i \sin(\theta_k) e^{-i\varphi_k} & -i \cos(\theta_k) e^{i\eta_k} \\ -i \cos(\theta_k) e^{-i\eta_k} & -i \sin(\theta_k) e^{i\varphi_k} \end{bmatrix}, \quad \mathcal{B}_k = \overline{\mathcal{A}_k}, \quad (3.20)$$

where $0 \leq \theta_k \leq \pi$, $0 \leq \alpha_k < \pi$, and $0 \leq \eta_k, \varphi_k \leq 2\pi$.

Setting $\eta_k = \alpha_k = 0$ accomplishes the transition to class $DIII$:

$$\mathcal{A}_k = \begin{bmatrix} i \sin(\theta_k) e^{-i\varphi_k} & -i \cos(\theta_k) \\ -i \cos(\theta_k) & -i \sin(\theta_k) e^{i\varphi_k} \end{bmatrix}, \quad \mathcal{B}_k = \overline{\mathcal{A}_k}. \quad (3.21)$$

When collecting all periodic orbits which contribute to the self-dual approximation in classes D and $DIII$, we restrict $\sin(\theta_k)$ and $\cos(\theta_k)$ to the values $\pm 1/\sqrt{2}$. This restriction has the enormous advantage of generating a flat integration measure when the ensemble averages for classes D and $DIII$ are performed (see eqs. (3.26) and (3.27)). As a consequence of this restriction, all orbits with the same length also have the same stability amplitude. This restriction is altogether arbitrary; however, with our interest in the *universal* features of the spectrum, this step is justified by the computational ease it entails.

In this case the Andreev scattering matrices read ($\mathcal{B}_k = \overline{\mathcal{A}_k}$ is understood):⁸

$$\mathcal{A}_k^D = \frac{e^{i\alpha_k}}{\sqrt{2}} \begin{bmatrix} i e^{-i\varphi_k} & -i e^{i\eta_k} \\ -i e^{-i\eta_k} & -i e^{i\varphi_k} \end{bmatrix}, \quad \mathcal{A}_k^{DIII} = \frac{1}{\sqrt{2}} \begin{bmatrix} i e^{-i\varphi_k} & -i \sigma_k \\ -i \sigma_k & -i e^{i\varphi_k} \end{bmatrix}. \quad (3.22)$$

For classes C and CI the Andreev scattering matrices at vertex k read:

$$S_k^C = \begin{bmatrix} 0 & -i e^{i\varphi_k} \\ -i e^{-i\varphi_k} & 0 \end{bmatrix}, \quad S_k^{CI} = \begin{bmatrix} 0 & -i \sigma_k \\ -i \sigma_k & 0 \end{bmatrix}, \quad (3.23)$$

again with $0 \leq \varphi_k < 2\pi$.

Within each of the symmetry classes, the ensemble average explores the full range of parameters allowed by the symmetry requirements on the partitions (entries) \mathcal{A}_k and \mathcal{B}_k . For future reference, the ensemble averages for a quantity Q within the four classes of concern are quoted below:

$$\langle Q \rangle_C = \prod_{k=1}^{k_{\max}} \int_0^{2\pi} \frac{d\varphi_k}{2\pi} Q, \quad (3.24)$$

$$\langle Q \rangle_{CI} = \frac{1}{2^{k_{\max}}} \sum_{\substack{\sigma_1, \dots, \sigma_{k_{\max}} \\ \in \{-1, 1\}}} Q, \quad (3.25)$$

$$\langle Q \rangle_D = \prod_{k=1}^{k_{\max}} \int_0^{2\pi} \frac{d\alpha_k}{2\pi} \int_0^{2\pi} \frac{d\varphi_k}{2\pi} \int_0^{2\pi} \frac{d\eta_k}{2\pi} Q, \quad (3.26)$$

$$\langle Q \rangle_{DIII} = \frac{1}{2^{k_{\max}}} \sum_{\substack{\sigma_1, \dots, \sigma_{k_{\max}} \\ \in \{-1, 1\}}} \prod_{k=1}^{k_{\max}} \int_0^{2\pi} \frac{d\varphi_k}{2\pi} Q. \quad (3.27)$$

⁸Here, in the table 3.1, and throughout this subsection $\sigma_k = \pm 1$.

The index k labels the peripheral vertices $k \in \{1, \dots, k_{\max}\}$ involved, where the choice of parameters at different vertices is uncorrelated.

Here, an addendum about the behaviour of the Andreev scattering phases under gauge transformations is in place. It is clear from the definition (1.4) that the superconducting order parameter $\Delta(x)$ acquires *double* the phase $\Delta(x) \rightarrow \exp[i2\theta(x)]\Delta(x)$ when the *local* gauge transformations $\psi(x) \rightarrow \exp[i\theta(x)]\psi(x)$ is applied (where $\theta(x)$ is a space dependent phase). As a consequence, the phases imparted on the quasi-particle wave functions which are Andreev scattered at the periphery are also gauge dependent. However, when it comes to physical quantities, these are all gauge independent. It has been shown at the end of section 3.1.1 that the secular equation (3.13) is indeed independent of the gauge chosen. Consequently, all quantities derived from the quantization condition (3.13) are gauge invariant. For all four symmetry classes under scrutiny in the subsequent sections, we assume $B = 0$ with the gauge $\mathbf{A} = 0$ on the bonds of the star graph.

3.2. Andreev Star Graph with symmetries of class C

In this subsection, we compute the density of states $\rho(k)$ and the form factor $K(t)$ as defined in eq. (1.50)⁹ for an ensemble of Andreev star graphs of symmetry class C with N peripheral vertices. This computation is presented in some detail, as it also serves as a template for the subsequent treatment of all other symmetry classes.

The starting point of the calculation is the quantization condition for the reduced scattering matrix $\det(1 - S_{B_{\text{red}}}(k)) = 0$ with the N -dimensional matrix¹⁰

$$S_{B_{\text{red}}}(k) = \mathcal{L} \overline{S_C} \mathcal{L} \text{diag}(-ie^{-i\varphi_j}) \mathcal{L} S_C \mathcal{L} \text{diag}(-ie^{i\varphi_j}) \quad (3.28)$$

as defined in eq. (3.12). The choice $S_{C,kl} = e^{2\pi ikl/N} / \sqrt{N} (\overline{S_C})_{lm}$ as the central scattering matrix for electrons (holes) has already been motivated before (see subsection 3.1). The matrix $\mathcal{L} = e^{ikL} \mathbb{1}_N$ contains the phases accumulated when the quasi-particle propagates along the bonds (k is the wave number measured from the Fermi wave number). All bond lengths $L_j = L$ can be chosen to have equal lengths. The values $\varphi_j \in [0, 2\pi[$ taken on by the Andreev phases φ_j are explained in the previous subsection 3.1.3 in the context of the ensemble average of class C (see eq. (3.24)).

We now set off for an interpretation of the random-matrix theory prediction for the averaged spectral density $\langle \rho(k) \rangle$ of class C in terms of periodic orbits. As is standard in the field of quantum graphs [10] (and is explained in depth in appendix C), we write the density of states in k -space as $\rho(k) = \rho_{av} + \delta\rho(k)$,

⁹In the original definition (1.50), E measures the distance from the Fermi *energy*. In the present context, k is the difference of the wave number from the Fermi *wave number*.

¹⁰The range for the index j in the diagonal matrices is $1 \leq j \leq N$.

where ρ_{av} is the mean density sufficiently far from the Fermi edge and $\delta\rho$ stands for the deviation thereof. With the form (3.28) for the reduced scattering matrix $\mathcal{S}_{B\text{red}}(k)$, one obtains the following expression for the density of states:

$$\rho(k) = \frac{2NL}{\pi} + \text{Im} \frac{1}{\pi} \frac{d}{dk} \sum_{m=1}^{\infty} \frac{1}{m} \text{tr} \mathcal{S}_{B\text{red}}^m(k). \quad (3.29)$$

The first term is the smooth part $\rho_{av} = 2NL/\pi$ of the spectral density. It is proportional to the ‘‘volume’’ of the system (i. e. total length of the system = number of bonds N times their length L) and is a constant, reflecting the fact that the graph is one dimensional. The deviation from the mean density $\delta\rho(k)$ is expressed in terms of $\text{tr} \mathcal{S}_{B\text{red}}^m(k)$. This intricate relation between density $\delta\rho(k)$ and trace $\text{tr} \mathcal{S}_{B\text{red}}^m$ places it in the focus of all interest. When the individual matrix entries in the expression for the trace $\text{tr} \mathcal{S}_{B\text{red}}^m$ are noted down, one gets:

$$\text{tr} \mathcal{S}_{B\text{red}}^m(k) = \frac{1}{N^m} \sum_{i_1, \dots, i_{2m}}^N \exp \left(i4mkL + i \frac{2\pi}{N} \sum_{j=1}^{2m} (-1)^{j+1} i_j i_{j+1} - im\pi - i \sum_{j=1}^{2m} (-1)^{j+1} \varphi_{i_j} \right), \quad (3.30)$$

where $i_{2m+1} = i_1$. The periodic orbits are uniquely defined by the sequence i_1, i_2, \dots, i_{2m} of the peripheral vertices. Any cyclic permutation of the sequence defines the same periodic orbit. The quasi-particle type at the beginning and the end of the orbit must be identical for the orbit to be periodic. As the particle type changes on each excursion to the periphery, the sequence must have even length $l = 2m$.

The expression (3.30) offers a good opportunity for us to point out the formal similarity of the expansion for the deviation $\delta\rho(k)$ by use of the trace $\text{tr} \mathcal{S}_{B\text{red}}^m(k)$ to a Gutzwiller type trace formula as introduced in eq. (1.40). The following notation supports this affinity:

$$\delta\rho(k) = \frac{1}{\pi} \text{Re} \sum_{p \in \mathcal{P}_{2m}} t_p A_p \exp(iS_p + i\chi_p). \quad (3.31)$$

One can identify and quantify the classical characteristics of the path in the graph context: the sum is over the set \mathcal{P}_{2m} of primitive periodic orbits¹¹ with period $2m_p$ such that $r \times 2m_p = 2m$, where r is the repetition number. The length of the primitive periodic orbit is $t_p = 4mL/r$. Its counterpart in the original Gutzwiller trace formula is the time needed for one passage through the orbit. The stability amplitude $A_p = 1/N^m$ decays exponentially and is equal for all orbits with the same length $l = 2m$. Such models are called

¹¹A *primitive* periodic orbit is defined in the following way: the sequence of vertices defining the orbit *cannot* be written down as a repetition of a shorter sequence (see section 1.6).

uniformly hyperbolic. The action is $S_p = 4mkL + \sum_{j=1}^{2m} (-1)^{j+1} 2\pi i_j i_{j+1}/N$. The phase $\chi_p = -m\pi - \sum_{j=1}^{2m} (-1)^{j+1} \varphi_{i_j}$ is accumulated by the Andreev scatterings at the periphery.

As a guideline to the subsequent steps of the calculation, we offer the agenda:

- The ensemble average for class C is performed, leading to a definite set of orbits robust under this averaging procedure.
- In the footsteps of Berry's diagonal approximation [9], an analogous approximation scheme for the present context – the *self-dual approximation* – is developed. A graphical presentation of the contributing orbits supports the intuition.

When the average (3.24) is applied to the trace (3.30)

$$\langle \text{tr } \mathcal{S}_{B\text{red}}^m(k) \rangle^C = \prod_{j=1}^{2m} \int_0^{2\pi} \frac{d\varphi_{i_j}}{2\pi} \text{tr } \mathcal{S}_{B\text{red}}^m(k), \quad (3.32)$$

only a specific set of periodic orbits survives. These orbits have the following characteristics. Each peripheral vertex v_j where an incoming electron is Andreev scattered to become a hole must be visited again by an incoming hole (equally with the roles of electron and hole interchanged). In this way, the two Andreev processes at vertex v_j contribute factors of $-ie^{-i\varphi_i}$ and $-ie^{i\varphi_i}$, respectively, to the weight of the periodic orbit. Their product – independent of φ_j – is robust under the averaging procedure. Orbits with *unpaired* excursions to the periphery – say, with only a single electron arriving at vertex v_j that generates a phase $ie^{-i\varphi_j}$ – do *not* survive the averaging (3.32).

In the following, we assume all indices i_j of peripheral vertices to be *pairwise different*. This assumption finds its justification as our interest focuses on the short-time behaviour of the spectral form factor $K(t)$ with the aim in recovering the universal random-matrix theory result. To that end, it is sufficient to consider orbits with sequence length $m \ll N$. The traversal time $t = 4mL$ of these periodic orbits is far shorter than the Heisenberg time $t_H = 4NL$ of the star graph. For these orbits (with $2m$ excursions to the periphery where $m \ll N$), it is a good approximation to assume all indices i_j to be pairwise different.

The defining sequence of peripheral vertices for surviving periodic orbits has the form:

$$(i_1, \Pi(i_1), i_2, \Pi(i_2), \dots, i_m, \Pi(i_m)) \quad \text{with} \quad 1 \leq i_1, \dots, i_m \leq N, \quad (3.33)$$

where Π is some permutation of the list $\{i_1, \dots, i_m\}$. For the peripheral vertices where electrons are incident – here labeled by i_1, \dots, i_m – any choice from the N peripheral vertices is possible. However, once this choice is taken, the set of allowed vertices for the holes is fixed by the condition that peripheral vertices

must be visited twice in the above mentioned way, once by an electron and once by a hole. Consequently, any possible permutation Π of the electron indices i_j is an allowed order for the hole excursion vertices.

Taking these considerations into account, we can write for the averaged trace:

$$\begin{aligned} \langle \text{tr } \mathcal{S}_{B^{\text{red}}}^m(k) \rangle^C &= \left(\frac{-1}{N} \right)^m \sum_{\Pi} \sum_{i_1, \dots, i_m}^N \exp \left(i4mkL + \right. \\ &\quad \left. + \frac{2\pi i}{N} \sum_{j=1}^m (i_{(j+1) \bmod m} - i_j) \Pi(i_j) \right), \end{aligned} \quad (3.34)$$

where the sum labeled Π is over all permutations Π of the indices $\{i_1, i_2, \dots, i_m\}$.

We now introduce the *self-dual approximation* for the Andreev star graph. This approximation plays the same role for systems with symmetries of the new classes [2] as does Berry's *diagonal approximation* [9] in the classic Wigner-Dyson context. On the star graph, this approximation takes only those permutations Π into account where the exponential of the trace (3.34) does *not* depend on the indices i_j . In that case the contributions add up coherently when the sum over the indices i_j is carried out. In contrast, for other permutations the sum over i_j leads to destructive averaging. The *self-dual approximation* singles out those orbits whose total phase due to the scattering matrix of the central vertex vanishes. As the phase factors due to central scattering between bonds $i_l \rightarrow i_k$ for electrons and holes are complex conjugates of one another, this requires that the periodic orbits contain equal numbers of scattering events between bonds $i_l \rightarrow i_k$ for electrons as for holes.

An illustration of those orbits of the *self-dual approximation* contributing in class C is given by figure 3.2 (a). The vertices in this diagram correspond to peripheral vertices of the original star graph. The central vertex is omitted for the sake of clarity. The diagram clarifies the nature of the contributing orbits: they traverse the same trajectory twice in the same direction with the roles of electrons and holes interchanged after the first round. Completing one round such that the resulting quasi-particle type differs from the initial quasi-particle type is only possible if the number m of peripheral vertices visited is *odd*. As for their characteristics, these orbits are termed *self-dual orbits*, because they are invariant under electron-hole conjugation. For m even, the construction of such a self-dual orbit fails.

Here (for class C), and for all remaining symmetry classes, we use the convention that the *inner* part of the diagram represents the *first* round, whereas the *outer* part stands for the *second* traversal of the periodic orbit, where the roles of electrons and holes are interchanged. As a guide to the eye, the point of the orbit where the beginning and end of the two rounds match, has been circled in diagram 3.2 (a). Its position is of no physical meaning, as it only deals with the graphical layout of the traversals.

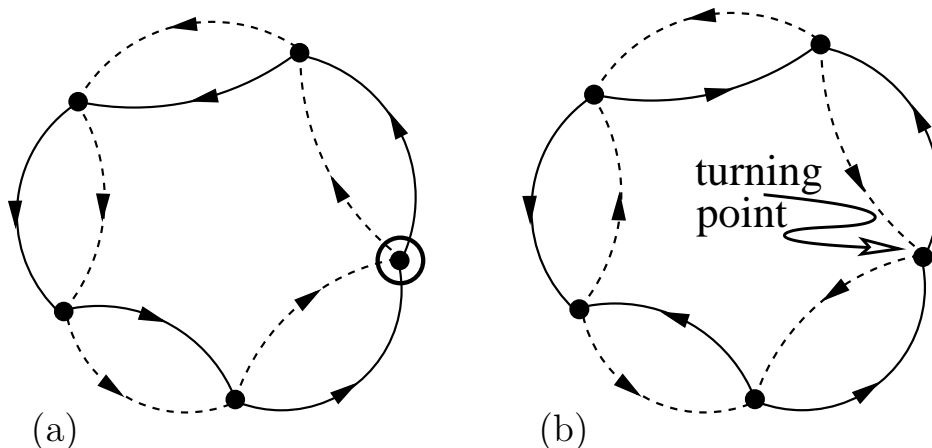


Figure 3.2.: Periodic orbits contributing in the *self-dual approximation* (here $m = 5$). Full lines represent electron propagation while dashed lines stand for hole propagation. The vertices in the diagram correspond to peripheral vertices of the original star graph. The scattering event at the central vertex is not shown for the sake of clarity. From the original star graph set-up, it is clear that every propagation shown includes one encounter with the central scatterer. For class C only the left diagram (a) contributes, whereas for class CI both diagrams contribute (as will be discussed in section 3.3). The diagrams are taken from [89] with minor modifications.

The *self-dual approximation* is crucial for the evaluation of the Andreev star graph of all four symmetry classes. The pictorial representation by figures like the diagram 3.2 provides a powerful intuitive tool for identifying these orbits.

For class C , the self-dual approximation breaks the sum over permutations Π in (3.34) down to a single permutation. By following the orbit in figure 3.2 (a), it is an easy matter to detect the appropriate values $\Pi(i_j)$ in the sequence (3.33). Here, we omit the bookkeeping of the quasi-particle type and cite the sequence of peripheral vertices of the self-dual orbit of class C for m odd ($m = 2l + 1$):

$$\begin{aligned}
 & (i_1, \Pi(i_1), i_2, \Pi(i_2), \dots, i_m, \Pi(i_m)) = \\
 = & (i_1, i_{l+2}, i_2, i_{l+3}, i_3, i_{l+4}, \dots, i_l, i_m, i_{l+1}, i_1, i_{l+2}, i_2, \dots, i_m, i_{l+1}). \quad (3.35)
 \end{aligned}$$

For future reference, we call this *self-dual* orbit described by the sequence (3.35) with two traversals in the same sense (without turning point) as the *self-dual orbit of length $2m$ with class C geometry*.¹² We will make use of this nomenclature when treating the remaining symmetry classes.

¹²Admittedly, “geometry” is a lax use of terminology as the illustrations in figure 3.2 refer to indices i_j which may have vastly different order in configuration space.

For such orbits of length $m \ll N$ within the self-dual approximation, the remaining sum in (3.34) is trivial and gives a factor of $\frac{N!}{(N-m)!}$ which is approximated by N^m . This brings to an end the evaluation of the ensemble averaged trace within the *self-dual approximation*:

$$\langle \text{tr } \mathcal{S}_{B\text{red}}^m(k) \rangle_{\text{sd}}^C = \begin{cases} -\exp(i4mkL) & \text{for } m \text{ odd,} \\ 0 & \text{for } m \text{ even.} \end{cases} \quad (3.36)$$

The graph version of the trace formula (3.29) now allows for an estimate for the deviations from the mean spectral density $\delta\rho(k)$:

$$\langle \delta\rho(k) \rangle^C = \frac{1}{\pi} \text{Im} \frac{d}{dk} \sum_{m=1}^{\infty} \frac{1}{m} \langle \text{tr } \mathcal{S}_{B\text{red}}^m(k) \rangle_{\text{sd}}^C \approx \frac{-4L}{\pi} \sum_{\substack{m=1 \\ m \text{ odd}}}^{m_{\text{max}}} \cos(4mkL). \quad (3.37)$$

As the self-dual approximation breaks down above a certain threshold m_{max} (as the condition $m \ll N$ is violated by m large enough), we must content ourselves with the rough estimate of a truncated sum. In the next step, the wave number

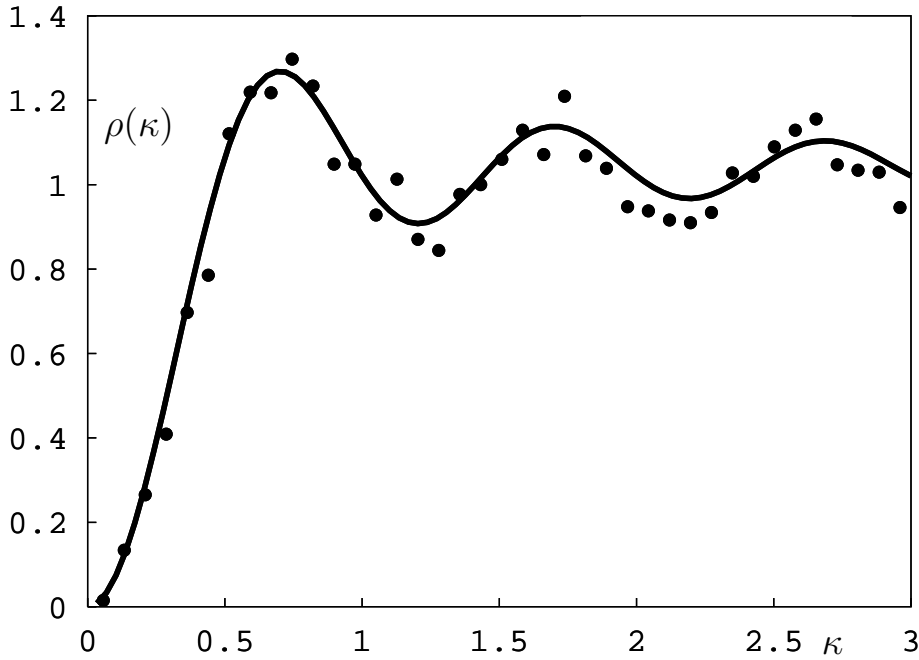


Figure 3.3.: Mean spectral density $\rho(\kappa)$ (κ is the wave number in units of the mean spacing Δk) calculated numerically for a star graph (dots) with $N = 24$ bonds where 8000 realizations contribute to the average. The prediction for the Gaussian RMT ensemble of class C is given by the solid line (see eq. (F.3) for the deviation $\delta\rho(\kappa)$).

k is expressed as a multiple of the mean spacing $\Delta k = \pi/(2NL)$, i.e., $k = \kappa\Delta k$ with dimensionless κ (and $m = 2l + 1$, for m odd):

$$\langle \delta\rho(k) \rangle^C \approx \rho_{\text{av}} \sum_{l=1}^{l_{\text{max}}} \frac{-2}{N} \cos\left(2\pi\kappa \frac{2l+1}{N}\right) \approx \frac{-\rho_{\text{av}}}{\pi} \int_0^{\lambda_{\text{max}}} d\lambda \cos(2\kappa\lambda). \quad (3.38)$$

This result (3.38) is to be contrasted with the universal result obtained by random-matrix theory in [2] for the deviation $\delta\rho(k)$ of class C :

$$\langle \delta\rho(k) \rangle_{\text{RMT}}^C = -\rho_{\text{av}} \frac{\sin(2\pi k)}{2\pi k} = -\frac{\rho_{\text{av}}}{\pi} \int_0^\pi d\lambda \cos(2\pi\lambda). \quad (3.39)$$

We now turn to the computation of the graph version of the form factor:

$$K(t) = 2 \int_{-\infty}^{\infty} dk e^{ikt} \langle \delta\rho(k) \rangle^C = \frac{t_H}{N} \sum_{m=1}^{\infty} K_m \delta(t - mt_H/N), \quad (3.40)$$

where $t_H = 4LN$ is the Heisenberg time of the star graph with N bonds. K_m can be understood as a form factor in discrete time with steps $\Delta t = m/N$. Within the self-dual approximation (3.36), we find the short-time result

$$K_{m,\text{sd}}^C = \begin{cases} -2 & \text{for } m \text{ odd,} \\ 0 & \text{for } m \text{ even} \end{cases} \Rightarrow \overline{K}_{m,\text{sd}}^C = -1, \quad (3.41)$$

where $\overline{K}_{m,\text{sd}}^C$ is the time averaged form factor in self-dual approximation. This result is in perfect agreement with the random-matrix theory prediction for class C (see eq. (F.3)).

Although the time average in eq. (3.41) is self-explanatory, we offer a transparent, pedantic explanation of the averaging procedure as it is useful for the calculations in the other symmetry classes as well:

$$\overline{K} := \frac{1}{T} \int_0^T dt K(t) = \frac{1}{T} \int_0^T dt \frac{t_H}{N} \sum_{m=1}^{\infty} K_m \delta\left(t - \frac{mt_H}{N}\right) = \frac{1}{M} \sum_{m=1}^M K_m, \quad (3.42)$$

where T denotes the time range for the average, which translates to the number M of discrete time steps taken into account (with $T/t_H = M/N$).

As a supplement to the analytical calculation, we present endorsing numerical results. For symmetry class C , results for the spectral density $\rho(k)$ are presented in figure 3.3, whereas the numerical results for the form factor $K(t)$ are stated in figure 3.4.

The special topology of the star graph allows the calculation of the form factor $K(t)$ of far larger graphs ($N = 100$ peripheral vertices) than is possible when computing the spectral density $\rho(k)$ by use of the routine described in chapter 2 ($N = 24$ peripheral vertices). This is why the routine calculating the form factor $K(t)$ is favoured in the sequel for symmetry classes CI , D , and $DIII$.

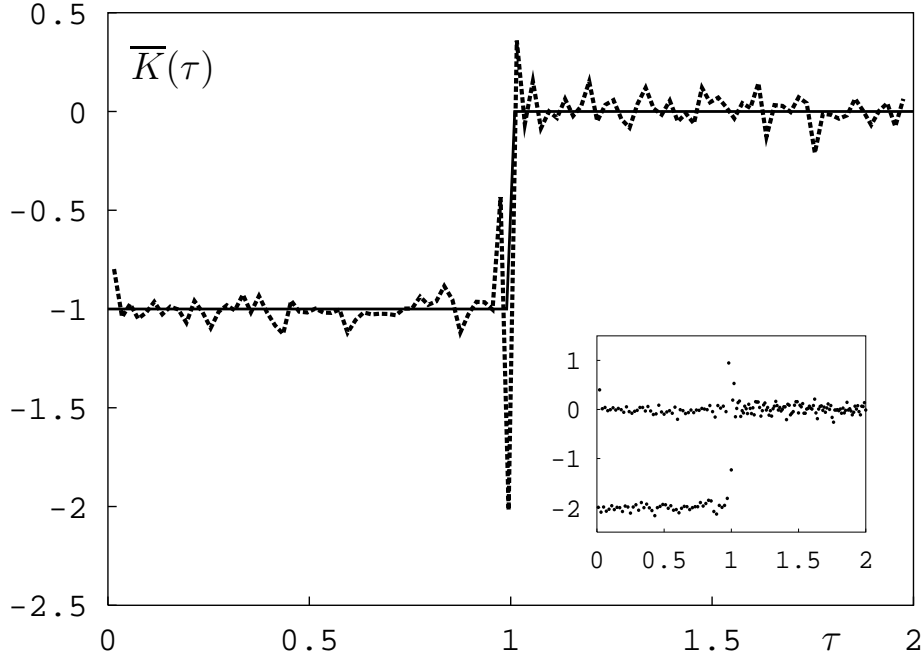


Figure 3.4.: Comparison between the numerically computed form factor and the universal predictions from random-matrix theory for class C (see eq. (F.4)). The numerical result for the star graph with $N = 100$ bonds (obtained by an ensemble average over 50000 configurations) is given in the inset. This result is in remarkable agreement with the coefficients K_m of (3.41). The time averaged form factor $\overline{K}(\tau)$ (dashed line) is in very good accordance with the RMT prediction (full line). Times τ are given in multiples of the Heisenberg time t_H . The data set for this figure is taken from [89].

At this stage, we do not want to interrupt the presentation of the analytical calculation by a description of the numerical calculation of the form factor $K(t)$. Thus, we merely present the numerical results and their comparison to the universal expectations of the respective symmetry class. For a description of the routine, we refer to section 3.6.

3.3. Andreev Star Graph with symmetries of class CI

In this section, the calculation for the form factor of an Andreev graph of symmetry class CI with N peripheral vertices is presented. The origin of the calculation is, as for class C , the quantization condition (3.28). The important difference from the previous case are the allowed values for the Andreev phases.

For class CI , only values $\varphi_l \in \{0, \pi\}$ are allowed in $-\mathrm{i}\exp(\pm\mathrm{i}\varphi_l)$ at vertex l ($1 \leq l \leq N$) as the Andreev phase (see eq. (3.23)). Thus, it comes as no surprise in a system with time-reversal symmetry that *both* electron and hole scattering lead to the same phase factor $-\mathrm{i}\sigma_l = \pm\mathrm{i}$. The calculation of the form factor $K(t)$ calls for an evaluation of the following trace $\mathrm{tr} \mathcal{S}_{B\mathrm{red}}^m(k)$:

$$\mathrm{tr} \mathcal{S}_{B\mathrm{red}}^m(k) = \frac{1}{N^m} \sum_{i_1, \dots, i_{2m}} \prod_{l=1}^{2m} (-\mathrm{i}\sigma_{i_l}) \exp \left[\mathrm{i}4mkL + \mathrm{i}\frac{2\pi}{N} \sum_{j=1}^{2m} (-1)^{j+1} i_j i_{j+1} \right]. \quad (3.43)$$

For generating an ensemble of class CI , the appropriate average (3.25) is employed:

$$\begin{aligned} \langle \mathrm{tr} \mathcal{S}_{B\mathrm{red}}^m(k) \rangle^{CI} &= \frac{1}{2^{2m}} \sum_{\substack{\sigma_{i_1}, \dots, \sigma_{i_{2m}} \\ \in \{-1, 1\}}} \mathrm{tr} \mathcal{S}_{B\mathrm{red}}^m(k) = \\ &= \frac{1}{N^m} \frac{1}{2^{2m}} \sum_{\substack{\sigma_{i_1}, \dots, \sigma_{i_{2m}} \\ \in \{-1, 1\}}} \sum_{i_1, \dots, i_{2m}} \prod_{l=1}^{2m} (-\mathrm{i}\sigma_{i_l}) \times \\ &\quad \times \exp \left[\mathrm{i}4mkL + \mathrm{i}\frac{2\pi}{N} \sum_{j=1}^{2m} (-1)^{j+1} i_j i_{j+1} \right]. \quad (3.44) \end{aligned}$$

With the interest being in the short-time behaviour of the form factor $K(t)$, we take only orbits with $m \ll N$ into account and apply the *self-dual approximation*. The graphical representations of the orbits in figures 3.2 (a) and (b) present a good guide as to which orbits contribute.

Typically in periodic-orbit theory, the relevant orbits in a time-reversal invariant system are twofold. On the one hand, the orbits of the equivalent system where time-reversal symmetry is broken (see figure 3.2 (a)) also contribute in the case of preserved time-reversal symmetry. As this type of orbit is the only one contributing to class C , we refer to it as the *self-dual orbit of class C geometry*. On the other hand, the preserved time-reversal symmetry allows the formation of additional orbits not present in the case when time-reversal symmetry is broken (see figure 3.2 (b)). From now on, this type of orbit characteristic for class CI is referred to as the *self-dual orbit of class CI geometry*.

First, we treat the self-dual orbit of class C geometry. The symbolic code of this type of orbit of length $2m$ states:

$$(i_1, i_2, \dots, i_m, i_1, i_2, \dots, i_m) \text{ with } m \text{ odd.} \quad (3.45)$$

These orbits yield coherent contributions to the trace (3.44). At each vertex l , where one electron and one hole are scattered, the over-all phase acquired is $(-\mathrm{i}\sigma_l)^2 = -1$. The (trivial) evaluation of the sum over the indices i_1, \dots, i_{2m} with the restriction to the specific permutation Π (explained in eq. (3.35))

contributes a factor of N^m to the trace (3.44). Equally elementary is the sum over all choices of $\sigma_1, \dots, \sigma_{2m}$. Altogether, the contribution of orbits with class C geometry of length $2m$ (m odd) reads

$$(-1)^m \exp(i4mkL) = -\exp(i4mkL). \quad (3.46)$$

We now come to the second type of orbits, the self-dual orbit of class CI geometry, which contribute for m both odd and even. For a given orbit length $2m$, there exist m different periodic orbits. They distinguish themselves by the m possible choices for the turning point, as indicated in figure 3.2 (b). In symbolic notation, these m orbits read (bookkeeping of the quasi-particle type is suppressed):

$$\begin{aligned} & (i_1, i_2, i_3, \dots, i_m, i_1, i_m, i_{m-1}, \dots, i_2) && \text{where } \mu = 1, \\ & (i_2, i_3, i_4, \dots, i_m, i_1, i_2, i_1, i_m, i_{m-1}, \dots, i_3) && \text{where } \mu = 2, \\ & (i_3, i_4, i_5, \dots, i_m, i_1, i_2, i_3, i_2, i_1, i_m, i_{m-1}, \dots, i_4) && \text{where } \mu = 3, \\ & \vdots \\ & (i_\mu, i_{\mu+1}, \dots, i_m, i_1, i_2, \dots, i_{\mu-1}, i_\mu, i_{\mu-1}, \dots, i_1, i_m, i_{m-1}, \dots, i_{\mu+1}), \\ & && \mu \text{ general,} \\ & \vdots \\ & (i_m, i_1, i_2, i_3, \dots, i_{m-2}, i_{m-1}, i_m, i_{m-1}, i_{m-2}, \dots, i_1) && \text{where } \mu = m. \end{aligned} \quad (3.47)$$

All these m orbits are distinct from each other and are labeled by the index $\mu \in \{1, \dots, m\}$. For an easier notation in the sequel, it proves helpful to introduce a set of new indices $\{k_1, \dots, k_{2m}\}$. They are fixed by the following identification (with general μ in the description (3.47)) of self-dual orbits:

$$\begin{aligned} & (\mu, \mu + 1, \dots, m, 1, 2, \dots, \mu - 1, \mu, \mu - 1, \dots, 1, m, m - 1, \dots, \mu + 1) =: \\ & (k_1, k_2, \dots, k_m, k_{m+1}, \dots, k_{2m-1}, k_{2m}). \end{aligned} \quad (3.48)$$

It is obvious from this identification that the first m indices k_1, \dots, k_m are chosen according to the respective value of μ . Then, the remaining m indices k_{m+1}, \dots, k_{2m} are fixed by the self-duality of the orbit. It is clear that different values for μ have different values for $k_1(\mu), \dots, k_{2m}(\mu)$ as consequence. With the convention (3.48), the sequence of peripheral vertices of a self-dual orbit for any value of μ ($1 \leq \mu \leq N$) can be cited as

$$(i_{k_1(\mu)}, i_{k_2(\mu)}, \dots, i_{k_{2m}(\mu)}). \quad (3.49)$$

This sequence (3.49) is a compact symbolic notation for the self-dual orbits of length $2m$ with class CI geometry with a turning point and two traversals in opposite senses. Orbits of this nature will also be of relevance in the case of the other class with preserved time-reversal symmetry – class $DIII$ (see section 3.5).

The self-dual restriction of vertices $i_{k_{l+m}}$ of the second round (to the appropriate “partner vertex” of the first traversal i_{k_l}) is achieved by introducing m Kronecker $\delta_{i_{k_{l+m}}, i_{k_l}}$ into the expression (3.44). As above, each vertex i_k involved contributes a total phase of $(-i\sigma_{i_k})^2 = -1$. The subsequent evaluation of the sum over the m free indices and the choices of σ_{i_k} is trivial and the contribution of an orbit of class *CI* geometry (of length $2m$) reads

$$(-1)^m m \exp(i4mkL). \quad (3.50)$$

Collecting the contributions from the self-dual orbits of both class *C* and class *CI* geometry results in the following expression for the trace within the *self-dual approximation*:

$$\langle \text{tr } \mathcal{S}_{B\text{red}}^m(k) \rangle_{\text{sd}}^{\text{CI}} = \exp(i4mkL) \begin{cases} \times (-m-1) & \text{for } m \text{ odd,} \\ \times m & \text{for } m \text{ even.} \end{cases} \quad (3.51)$$

With the value of the trace (3.51) and its link (3.29) to the spectrum $\langle \delta\rho(k) \rangle$ at hand, the form factor is

$$\begin{aligned} K(t) &= 2 \int_{-\infty}^{\infty} dk e^{ikt} \langle \delta\rho(k) \rangle^{\text{CI}} = \\ &= \int_{-\infty}^{\infty} \frac{dk}{2\pi} \frac{t_H}{N} \sum_{m=1}^{\infty} e^{ikt-i4mkL} [-1 + (-1)^m(2m+1)] = \\ &= \frac{t_H}{N} \sum_{m=1}^{\infty} K_m \delta(t - mt_H/N). \end{aligned} \quad (3.52)$$

Thus, the discrete version of the form factor K_m (in discrete time steps $t/t_H = m/N$) for class *CI* in the self-dual approximation is given by:

$$K_{m,\text{sd}}^{\text{CI}} = -1 + (-1)^m(2m+1). \quad (3.53)$$

Inserting this form factor $K_{m,\text{sd}}^{\text{CI}}$ in the time average (3.42) yields:

$$\begin{aligned} \overline{K}_{m,\text{sd}}^{\text{CI}} &= \frac{1}{T} \int_0^T dt \frac{t_H}{N} \sum_{m=1}^{\infty} K_{m,\text{sd}}^{\text{CI}} \delta\left(t - \frac{mt_H}{N}\right) \\ &= \frac{1}{M} \sum_{m=1}^M [-1 + (-1)^m(2m+1)] = -1. \end{aligned} \quad (3.54)$$

The time averaged form factor $\overline{K}_{m,\text{sd}}^{\text{CI}} = -1$ is in good agreement with the random-matrix theory result (F.10). In fact, it is the first term of the expansion (F.11):

$$K^{\text{CI}}(t) = -1 + \frac{1}{2}t + \mathcal{O}(t^2). \quad (3.55)$$

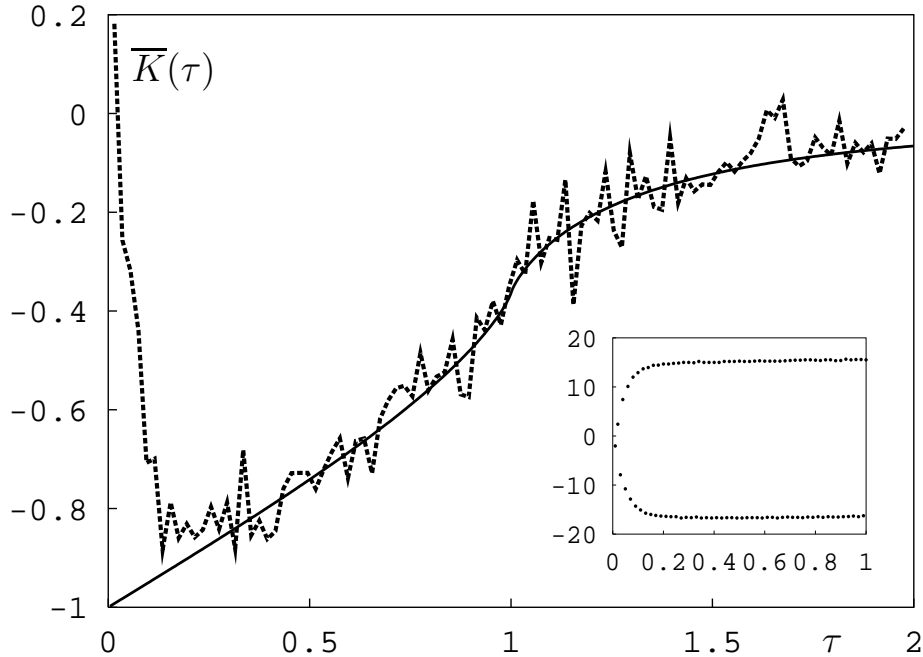


Figure 3.5.: Numerical results for the form factor $K(\tau)$ calculated for the star graph with class CI symmetries with $N = 100$ bonds (averaged over 50000 configurations) are compared to universal predictions (F.10) from RMT for class CI . The inset gives the numerical results, while their average $\overline{K(\tau)}$ (dashed line) is observed to be in very good agreement with the RMT prediction (full line). Times τ are given in multiples of the Heisenberg time t_H . The data set for this figure is taken from [89]. The deviations for very small times τ can be attributed to short periodic orbits which lead to non-universal results. The breakdown of the *self-dual approximation* (3.53) can be observed in the numerical data in the inset, as data points obviously follow the *self-dual* result (3.53) only for τ small.

3.4. Andreev Star Graph with symmetries of class D

In the sequence of the different symmetry classes treated, we now come to symmetry class D where neither spin-rotation invariance nor time-reversal symmetry is preserved. The set-up of a class D Andreev star graph with N peripheral vertices also incorporates the spin degrees of freedom (as was explained in subsection 3.1.2) resulting in the $2N$ -dimensional reduced bond-scattering

matrix:¹³

$$\begin{aligned} \mathcal{S}_{B\text{red}}(k) &= \mathcal{L}(k) \overline{\mathcal{S}_C} \mathcal{L}(k) \text{diag}(\overline{\mathcal{A}_1^D}, \dots, \overline{\mathcal{A}_N^D}) \times \\ &\times \mathcal{L}(k) \mathcal{S}_C \mathcal{L}(k) \text{diag}(\mathcal{A}_1^D, \dots, \mathcal{A}_N^D). \end{aligned} \quad (3.56)$$

The submatrix \mathcal{A}_k^D for Andreev scattering from holes to electrons at vertex k is given by:

$$\mathcal{A}_k^D = \frac{e^{i\alpha_k}}{\sqrt{2}} \begin{bmatrix} ie^{-i\varphi_k} & -ie^{i\eta_k} \\ -ie^{-i\eta_k} & -ie^{i\varphi_k} \end{bmatrix}, \quad 1 \leq k \leq N, \quad (3.57)$$

and the reverse scattering process, i.e. from electrons into holes, is described by the complex conjugate matrix $\overline{\mathcal{A}_k^D}$. Here, for class D , it is understood that the matrices \mathcal{L} , \mathcal{S}_C , $\overline{\mathcal{S}_C}$ are $2N$ -dimensional matrices whose entries M_{ij} are known from the treatment of classes C and CI with the replacement $M_{ij} \rightarrow M_{ij} \otimes \mathbb{1}_2$. As is standard in the field of quantum graphs, the secular equation $\det(1 - \mathcal{S}_{B\text{red}}(k)) = 0$ supplies an expression for the density of states:

$$\rho(k) = \frac{4NL}{\pi} + \text{Im} \frac{1}{\pi} \frac{d}{dk} \sum_{m=1}^{\infty} \frac{1}{m} \text{tr} \mathcal{S}_{B\text{red}}^m(k). \quad (3.58)$$

Note that for star graphs of class D , the smooth part $\rho_{\text{av}} = 4NL/\pi$ has doubled with respect to class C (cf. eq. (3.29)); this comes as no surprise as the spin degree of freedom is now taken into account (see eq. (C.9) and the comments thereafter in appendix C). Consequently, the Heisenberg time now also has double the value $t_H = 8LN$. As in the previous subsections treating the cases of classes C and CI , the quantity of major interest is the trace $\text{tr} \mathcal{S}_{B\text{red}}^m(k)$ which reads as a sum over periodic orbits:

$$\begin{aligned} \text{tr} \mathcal{S}_{B\text{red}}^m(k) &= \frac{1}{N^m} \sum_{i_1, \dots, i_{2m}}^N \exp \left[i4mkL + i \frac{2\pi}{N} \sum_{j=1}^{2m} (-1)^{j+1} i_j i_{j+1} \right] \times \\ &\times \text{tr} \left[\prod_{l=1}^m \overline{\mathcal{A}_{i_{2l-1}}^D} \mathcal{A}_{i_{2l}}^D \right]. \end{aligned} \quad (3.59)$$

What is new for class D is the necessity to evaluate the trace over the spin degrees of freedom.

We apply the class D ensemble average, as explained by eq. (3.26), to the trace (3.59):

$$\langle \text{tr} \mathcal{S}_{B\text{red}}^m(k) \rangle^D = \prod_{j=1}^{2m} \int_0^{2\pi} \frac{d\alpha_{i_j}}{2\pi} \int_0^{2\pi} \frac{d\varphi_{i_j}}{2\pi} \int_0^{2\pi} \frac{d\eta_{i_j}}{2\pi} \text{tr} \mathcal{S}_{B\text{red}}^m(k). \quad (3.60)$$

¹³The term ‘‘diag’’ for diagonal matrix in the eq. (3.56) refers to the N -dimensional bond space while the entries \mathcal{A}_j^D , $\overline{\mathcal{A}_j^D}$ are non-diagonal in spin space.

As for the other symmetry classes, only a specific set of periodic orbits survives this average. We will work out those characteristics of the relevant orbits in the following. By now, we are familiar with the approximations in use: the short-time behaviour of the spectral form factor $K(t)$ calls for the restriction on the length m of orbits, $m \ll N$. In this regime of orbit lengths, we can restrict ourselves to the *self-dual approximation* for the Andreev star graph.

As in class C , it is the inspection of the respective Andreev scattering matrix at a peripheral vertex k that leads to an understanding of which pairs of scattering processes survive the averaging (3.60). For the Andreev vertex k at the periphery, the scattering situation is summarized by the two scattering matrices:

$$\begin{bmatrix} e_{\uparrow} \\ e_{\downarrow} \end{bmatrix}_{k \text{ out}} = \underbrace{\frac{e^{i\alpha_k}}{\sqrt{2}} \begin{bmatrix} ie^{-i\varphi_k} & -ie^{i\eta_k} \\ -ie^{-i\eta_k} & -ie^{i\varphi_k} \end{bmatrix}}_{\mathcal{A}_k^D} \begin{bmatrix} h_{\uparrow} \\ h_{\downarrow} \end{bmatrix}_{k \text{ in}}, \quad (3.61)$$

$$\begin{bmatrix} h_{\uparrow} \\ h_{\downarrow} \end{bmatrix}_{k \text{ out}} = \underbrace{\frac{e^{-i\alpha_k}}{\sqrt{2}} \begin{bmatrix} -ie^{i\varphi_k} & ie^{-i\eta_k} \\ ie^{i\eta_k} & ie^{-i\varphi_k} \end{bmatrix}}_{\overline{\mathcal{A}_k^D}} \begin{bmatrix} e_{\uparrow} \\ e_{\downarrow} \end{bmatrix}_{k \text{ in}}. \quad (3.62)$$

Contributing pairs of scatterings (which are robust under the class D ensemble average) are found by matching an entry of the scattering matrix (3.61) with the appropriate entry in the scattering matrix (3.62) such that their product is independent of any of the parameters α_k , φ_k , and η_k . Such products are referred to as “coherent” from now onwards. On inspection of these scattering prescriptions (3.61) and (3.62), one recognizes that the parameter α_k here plays the role of the Andreev phase φ_k at vertex k in the context of a class C graph.¹⁴ The α_k -average requires that each peripheral vertex k which has been visited by an electron (of either spin direction) must be revisited by a hole (and likewise with the roles of electrons and holes interchanged). To put it differently, the parameters α_k determine the *geometry* of the orbit, which is as in class C . Thus, as an intermediary result, we obtain from the α_k -average:

$$\begin{aligned} \langle \text{tr } \mathcal{S}_{B^{\text{red}}}^m(k) \rangle^D &= \frac{1}{N^m} \sum_{\Pi} \sum_{i_1, \dots, i_m}^N \exp \left[i4mkL + \right. \\ &\quad \left. + \frac{2\pi i}{N} \sum_{j=1}^m (i_{(j+1) \bmod m} - i_j) \Pi(i_j) \right] \times \\ &\quad \left\langle \text{tr} \left(\mathcal{A}_{\Pi(i_m)}^D \overline{\mathcal{A}}_{i_m}^D, \dots, \mathcal{A}_{\Pi(i_1)}^D \overline{\mathcal{A}}_{i_1}^D \right) \right\rangle_{\text{w.r.t } \varphi_{i_k}, \eta_{i_k}}. \end{aligned} \quad (3.63)$$

Thereby, we see that in the *self-dual approximation*, the parameter α_k enforces the same sequence of visited peripheral vertices as was worked out for class C

¹⁴The Andreev phase φ_k in section 3.2 (class C) has *no* relation to the phase φ_k seen here in eqs. (3.61) and (3.62).

(see the symbolic code (3.35)). Thus, α_k governs *which* vertices must be revisited on the second traversal after the end of the first round. The contributing orbits are of the kind as depicted in figure (3.2) with an *odd* number of peripheral vertices visited. Thus, the *geometry* of the orbit (ignoring the spin degrees of freedom) is the same as the geometry of a class C type star graph.

With the sequence of visited vertices fixed by the self-dual approximation, the trace over the spin degrees of freedom reads (for $m = 2l + 1$):

$$\prod_{j=1}^m \int_0^{2\pi} \frac{d\varphi_{i_j}}{2\pi} \int_0^{2\pi} \frac{d\eta_{i_j}}{2\pi} \text{tr} \left[(\overline{\mathcal{A}_{i_{l+1}}^D} \mathcal{A}_{i_m}^D) (\overline{\mathcal{A}_{i_l}^D} \mathcal{A}_{i_{m-1}}^D) \dots \dots (\overline{\mathcal{A}_{i_1}^D} \mathcal{A}_{i_{l+1}}^D) (\overline{\mathcal{A}_{i_m}^D} \mathcal{A}_{i_l}^D) \dots (\overline{\mathcal{A}_{i_{l+2}}^D} \mathcal{A}_{i_1}^D) \right] = 1. \quad (3.64)$$

We can anticipate the result by identifying all coherent contributions to the trace (3.64). These coherent contributions are given by matching entries in the scattering prescriptions (3.61) and (3.62). Coherence demands that the product of an entry taken from the scattering matrix in (3.61) and an appropriate “partner” entry of the matrix (3.62) be *independent* of the parameters φ_{i_k} and η_{i_k} at any vertex i_k on the itinerary.

In the self-dual approximation, the orbit is made up of the double round (as illustrated in figure 3.2 (a)) of total length $2m$. For such an orbit of *class C geometry*, one is free to choose any spin position for the first m segments of the orbit, i. e., for the first round. As every entry in the scattering matrix (3.61) can be complemented by exactly one “partner” entry of the matrix (3.62) to form a product independent of the parameters η_k and φ_k , the spin directions of quasi-particles of the second round are fixed by the choice taken for the first traversal.

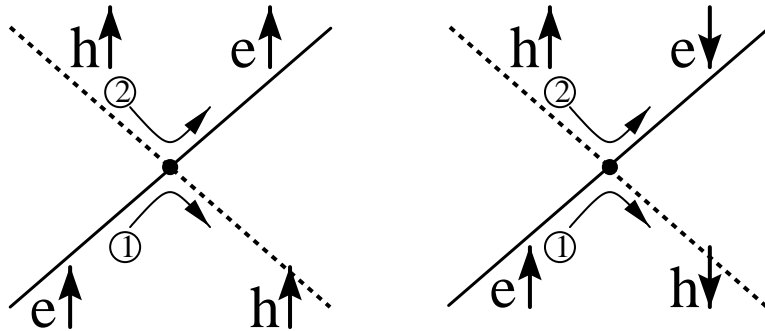


Figure 3.6.: Spin directions of quasi-particles scattered at the vertex k on the first round dictate the spin directions allowed during the second round. Only those pairs of scatterings survive the class D ensemble average in which the initial and final spin directions of the first round are identical to those of the second round (irrespective of their relative orientation).

Examples of coherent combinations of two scatterings at a single vertex on a self-dual orbit are illustrated in figure 3.6. Instead of a graphical representation of the full orbit as in figure 3.2, we show the zoom-in of a single peripheral vertex. The parts belonging to the first and second round are labeled such that the first round fragment is drawn at the bottom and its counterpart of the second round above.

While the examples shown in figure 3.6 are not exhaustive, all coherent combinations of scatterings at a given vertex i_k on the self-dual orbit have the following pattern:

$$\left(\begin{array}{c} \{e\} \\ \{h\} \end{array} \right)_{\tau_1} \rightarrow \left(\begin{array}{c} \{h\} \\ \{e\} \end{array} \right)_{\tau_2} \Bigg|_{\substack{\text{at vertex } i_k, \\ \text{first round}}} \Rightarrow \left(\begin{array}{c} \{h\} \\ \{e\} \end{array} \right)_{\tau_1} \rightarrow \left(\begin{array}{c} \{e\} \\ \{h\} \end{array} \right)_{\tau_2} \Bigg|_{\substack{\text{at vertex } i_k, \\ \text{second round}}}, \quad (3.65)$$

where τ_1, τ_2 stand for spin directions \uparrow, \downarrow and e (h) stands for electron (hole). The product of the accumulated phases of the scattering combinations (3.65) surviving the class D average is unity. From the rule (3.65) for the relative spin orientation at vertex k , the spin systematics for orbits relevant to class D can be read off: on the first round, one is free to choose the m spin directions for each part of an orbit of overall length $2m$ between two scattering events. However, once these m spin directions are set, the m spins in the second round must be aligned parallel to their respective partners of round one. This results in a total of 2^m choices for spin directions. All coherent products of entries from the scattering matrices in (3.61) and (3.62) have weight $1/2$. Consequently, the averaged trace of the spin degrees of freedom in (3.64) equals unity. Thus, in the self-dual approximation with all coherent contributions from the spin degrees of freedom taken into account, the trace (3.63) states:

$$\langle \text{tr } \mathcal{S}_{B\text{red}}^m(k) \rangle^D = \exp(i4mkL) \times \begin{cases} +1 & \text{for } m \text{ odd,} \\ 0 & \text{for } m \text{ even.} \end{cases} \quad (3.66)$$

This expression, inserted in eq. (3.58), yields the deviation $\langle \delta\rho(k) \rangle$, or more directly the form factor:

$$\begin{aligned} K(t) &= 2 \int_{-\infty}^{\infty} dk \exp(ikt) \langle \delta\rho(k) \rangle \\ &= \frac{t_H}{N} \sum_{m=1}^{\infty} \delta\left(t - \frac{mt_H}{2N}\right) K_m = \frac{1}{N} \sum_{m=1}^{\infty} \delta\left(\frac{t}{t_H} - \frac{m}{2N}\right) K_m, \end{aligned} \quad (3.67)$$

where, again, a discrete form factor K_m has been defined and which reads in the *self-dual approximation*:

$$K_{m,\text{sd}}^D = [(-1)^{m+1} + 1] / 2 = \begin{cases} +1 & \text{for } m \text{ odd,} \\ 0 & \text{for } m \text{ even.} \end{cases} \quad (3.68)$$

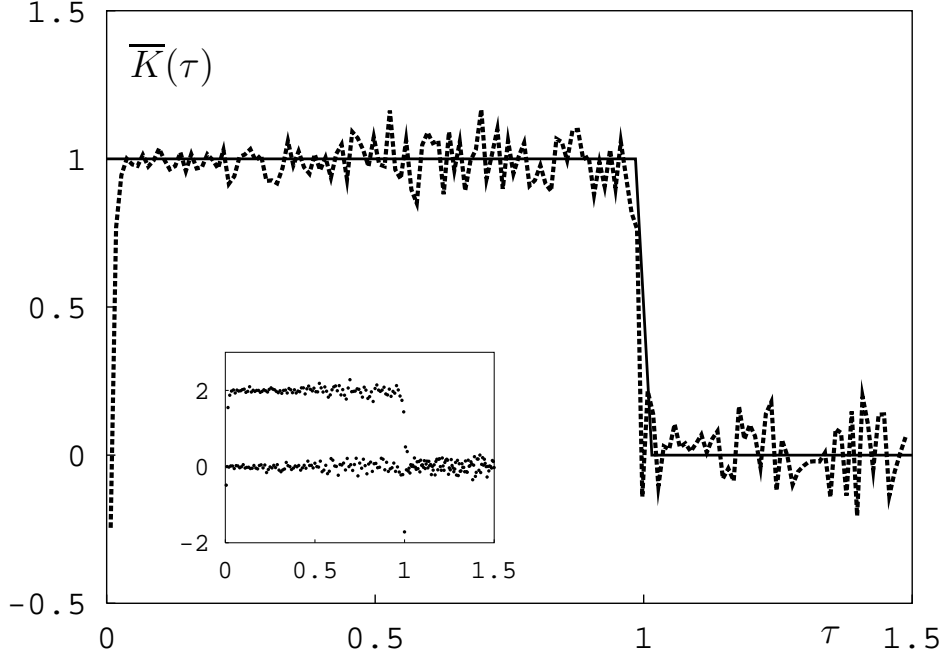


Figure 3.7.: The form factor $K(\tau)$ calculated for the star graph with class D symmetries with $N = 100$ bonds (averaged over 50000 configurations) is compared to universal predictions from random-matrix theory for class D (see eq. (F.5)). The inset gives the numerical results, while their average $\overline{K}(\tau)$ (dashed line) is observed to be in very good agreement with the RMT prediction (full line). Again, all times τ are given in multiples of the Heisenberg time t_H .

Here, the discrete time step is $\Delta t = t/t_H = m/2N$ (see eq. (3.67)). The time averaged form factor is found with aid of the averaging (3.42):

$$\overline{K}_{m,\text{sd}}^D = \frac{1}{T} \int_0^T dt \frac{t_H}{N} \sum_{m=1}^{\infty} K_m \delta\left(t - \frac{mt_H}{2N}\right) = \frac{2}{M} \sum_{m=1}^M K_{m,\text{sd}}^D = 1. \quad (3.69)$$

This result (3.69) for the time averaged form factor $\overline{K}_{m,\text{sd}}^D$ in the self-dual approximation agrees perfectly with the random-matrix theory prediction (F.3) for class D .

3.5. Andreev Star Graph with symmetries of class $DIII$

The computation of the form factor of an Andreev star graph with N peripheral vertices in the last remaining symmetry class – class $DIII$ – is the most elaborate. In the self-dual approximation, the *geometry* of the orbits is analogous to

the *CI* case, where both orbits *with* a turning point as well as orbits with two parallel traversals but *without* a turning point contribute. The term “geometry” is used to indicate the sequence of peripheral vertices visited (dictated by the condition of coherence for the phases of the central scatterer) omitting any reference to the spin alignment. With respect to the spin degrees of freedom, the coherent contributions outnumber the possibilities studied for a class *D* type graph.

The calculation of the form factor will be organized according to the following outline:

- The sequence of peripheral vertices visited in the self-dual approximation is stated (the *geometry*). Helpful, in this context, is the analogous line of reasoning for the other class where time-reversal symmetry is conserved (class *CI*).
- All pairs of spin scattering processes robust under the *DIII* ensemble average at a single peripheral vertex k on the self-dual itinerary are identified.
- The respective contributions of the different types of orbits in self-dual approximation (with and without a turning point) are computed.
- Finally, the agreement between the time averaged form factor and the RMT prediction is shown.

The starting point of the calculation is (as has been for class *D*) a $2N$ -dimensional reduced bond-scattering matrix:¹⁵

$$\begin{aligned} \mathcal{S}_{B\text{red}}(k) &= \mathcal{L}(k) \overline{S_C} \mathcal{L}(k) \text{diag}(\overline{\mathcal{A}_1^{DIII}}, \dots, \overline{\mathcal{A}_N^{DIII}}) \times \\ &\times \mathcal{L}(k) S_C \mathcal{L}(k) \text{diag}(\mathcal{A}_1^{DIII}, \dots, \mathcal{A}_N^{DIII}), \end{aligned} \quad (3.70)$$

where the matrices S_C , $\overline{S_C}$, and $\mathcal{L}(k)$ have been explained in the context of class *D* (see eq. (3.56)). Distinct for the graph with symmetries of class *DIII* are the submatrices \mathcal{A}_k^{DIII} ($\overline{\mathcal{A}_k^{DIII}}$) for Andreev scattering at the peripheral vertices k that preserve time-reversal symmetry yet break spin-rotation invariance. They have been defined in eq. (3.22) and are quoted here for completeness:

$$\mathcal{A}_k^{DIII} = \frac{1}{\sqrt{2}} \begin{bmatrix} \text{ie}^{-i\varphi_k} & -i\sigma_k \\ -i\sigma_k & -\text{ie}^{i\varphi_k} \end{bmatrix}. \quad (3.71)$$

Starting from the quantization condition $\det(1 - \mathcal{S}_{B\text{red}}(k)) = 0$, the deviation $\delta\rho(k)$ from the mean density of states is

$$\delta\rho(k) = \text{Im} \frac{1}{\pi} \frac{d}{dk} \sum_{m=1}^{\infty} \frac{1}{m} \text{tr} \mathcal{S}_{B\text{red}}^m(k), \quad (3.72)$$

¹⁵In order to avoid an overload of notation, we use the same symbol $\mathcal{S}_{B\text{red}}(k)$ here as for symmetry class *D* (without any additional superscript indicating the symmetry class *DIII*), because the context is unambiguous.

while the smooth part of the density is $\rho_{\text{av}} = 4NL/\pi$, and the associated Heisenberg time has the same value $t_H = 8LN$ as in class D . The corresponding trace formula

$$\text{tr } \mathcal{S}_{B\text{red}}^m(k) = \frac{1}{N^m} \sum_{i_1, \dots, i_{2m}}^N e^{i4mkL + i\frac{2\pi}{N} \sum_{j=1}^{2m} (-1)^{j+1} i_j i_{j+1}} \text{tr} \left[\prod_{l=1}^m \overline{\mathcal{A}_{i_{2l-1}}^{DIII}} \mathcal{A}_{i_{2l}}^{DIII} \right] \quad (3.73)$$

is subjected to the ensemble average of class $DIII$, which has been defined in eq. (3.27):

$$\langle \text{tr } \mathcal{S}_{B\text{red}}^m(k) \rangle^{DIII} = \frac{1}{2^{2m}} \sum_{\substack{\sigma_{i_1}, \dots, \sigma_{i_{2m}} \\ \in \{-1, 1\}}} \prod_{k=1}^{2m} \int_0^{2\pi} \frac{d\varphi_{i_k}}{2\pi} \text{tr } \mathcal{S}_{B\text{red}}^m(k). \quad (3.74)$$

The main part of the present chapter is dedicated to the extraction of all the orbits robust under the average (3.74). We work in the regime of orbit length m with $m \ll N$ and restrict ourselves to the *self-dual approximation* in order to determine the short-time behaviour of the spectral form factor $K(t)$ for the Andreev star graph.

The geometry of the orbits

With the spin degrees of freedom put aside for the time being, we first discuss the allowed sequences of peripheral vertices (the *geometry*) of the $2m$ -periodic self-dual orbits. The restriction as to which sequence is allowed is set by the condition of coherence of the phases from the central scatterer.

As in class CI (the other symmetry class with preserved time-reversal symmetry), *two* different types of orbits contribute in the self-dual approximation. First, the self-dual orbit present in all symmetry classes for m odd is the orbit with class C geometry and whose sequence of peripheral vertices has already been laid down in the code (3.35) (with $m = 2l + 1$ odd):

$$(i_1, i_{l+2}, i_2, i_{l+3}, i_3, i_{l+4}, \dots, i_l, i_m, i_{l+1}, i_1, i_{l+2}i_2, \dots, i_m, i_{l+1}). \quad (3.75)$$

The illustration of this type of orbit (with class C geometry, without turning point) is given in figure 3.2 (a). Second, one has for both m odd as well as even another m distinct self-dual orbits of class CI geometry. These orbits have different turning points (see figure 3.2 (b)) and exist only for *preserved* time-reversal symmetry. The general expression for the itinerary is

$$(i_{k_1(\mu)}, i_{k_2(\mu)}, \dots, i_{k_{2m}(\mu)}), \quad (3.76)$$

where the indices k_1, \dots, k_{2m} are chosen by the identification

$$(\mu, \mu + 1, \dots, m, 1, 2, \dots, \mu - 1, \mu, \mu - 1, \dots, 1, m, m - 1, \dots, \mu + 1) =: (k_1, k_2, \dots, k_{2m-1}, k_{2m}). \quad (3.77)$$

Each value of μ ($1 \leq \mu \leq m$) labels one of the m different possibilities for the turning point of the self-dual orbit.

Common to both types of self-dual orbits is the fact that only m of the $2m$ peripheral indices can be chosen freely, while the other m indices are fixed by self-duality. Both types of self-dual orbits contribute to the trace of the scattering matrix (3.74):¹⁶

$$\langle \text{tr } \mathcal{S}_{B \text{ red}}^m(k) \rangle_{\text{sd}}^{DIII} \propto \text{tr} \left\langle \left[(\overline{\mathcal{A}}_{i_{l+1}} \mathcal{A}_{i_m}) (\overline{\mathcal{A}}_{i_l} \mathcal{A}_{i_{m-1}}) \dots (\overline{\mathcal{A}}_{i_1} \mathcal{A}_{i_{l+1}}) (\overline{\mathcal{A}}_{i_m} \mathcal{A}_{i_l}) \dots (\overline{\mathcal{A}}_{i_{l+2}} \mathcal{A}_{i_1}) \right] \right\rangle \quad (3.78)$$

$$+ \sum_{\mu=1}^m \left\langle \text{tr} \left[\prod_{j=1}^m \overline{\mathcal{A}}_{i_{k_{2j}(\mu)}} \mathcal{A}_{i_{k_{2j-1}(\mu)}} \right] \right\rangle, \quad (3.79)$$

where the brackets stand for averaging over the spin degrees of freedom; the first term (3.78) is generated by the self-dual orbits of *class C geometry*, while the m different orbits of *class CI geometry* (with a turning point) make up for the second term (3.79).

Both terms need careful investigation as to which settings of quasi-particle spin directions along the orbits contribute coherently. As a first step to the solution for the entire orbit, we analyze the scattering situation at a *single* vertex k on the itinerary.

Coherent pairs of spin scatterings at one vertex k

Recall the scattering situations at a given peripheral vertex k , which are given by the scattering matrix in (3.22) and the complex conjugate matrix:

$$\begin{bmatrix} e_{\uparrow} \\ e_{\downarrow} \end{bmatrix}_{k \text{ out}} = \frac{1}{\sqrt{2}} \underbrace{\begin{bmatrix} i e^{-i\varphi_k} & -i\sigma_k \\ -i\sigma_k & -i e^{i\varphi_k} \end{bmatrix}}_{\mathcal{A}_k^{DIII}} \begin{bmatrix} h_{\uparrow} \\ h_{\downarrow} \end{bmatrix}_{k \text{ in}}, \quad (3.80)$$

$$\begin{bmatrix} h_{\uparrow} \\ h_{\downarrow} \end{bmatrix}_{k \text{ out}} = \frac{1}{\sqrt{2}} \underbrace{\begin{bmatrix} -i e^{i\varphi_k} & i\sigma_k \\ i\sigma_k & i e^{-i\varphi_k} \end{bmatrix}}_{\overline{\mathcal{A}}_k^{DIII}} \begin{bmatrix} e_{\uparrow} \\ e_{\downarrow} \end{bmatrix}_{k \text{ in}}, \quad (3.81)$$

with $\varphi_k \in [0, 2\pi[$ and $\sigma_k = \pm 1$ according to the ensemble average (3.74) for class *DIII*. The coherent contributions are found by forming pairs of matrix entries from (3.80) and/or (3.81) such that their product is independent of the parameters φ_k and σ_k . One can distinguish two groups of coherent combinations of spin scattering processes: first, pairings of processes where each process *flips* the spin direction (described by the entries $\pm i\sigma_k$) and second, such pairings of

¹⁶In order to avoid an overload of notation, we drop the superscript *DIII* and write \mathcal{A}_{i_k} instead of $\mathcal{A}_{i_k}^{DIII}$ in the sequel.

processes *preserving* the spin direction during the scattering process (described by the entries $\pm i \exp(\mp i \varphi_k)$). The first group counts ten distinct pairings, the second four. We spare the reader an exhaustive gallery of all processes allowed, instead citing figure 3.8 as pictorial examples of processes where spin direction is *preserved* and figure 3.9 for those processes where the spin is *flipped*. As examples, we show only those processes where an electron with spin up (e_\uparrow) is incident.

The coherent pairings of scattering events – illustrated by the figures 3.8 and 3.9 – sets restrictions on the relative spin orientations for the two segments of the self-dual orbit meeting at a given vertex k . The relative orientation of spins on corresponding segments of the first and second round traversals at the vicinity of vertex k are locked to one another. If the spins of the two incident electrons paired at vertex k are parallel, the spins of the outgoing quasi-particles are also parallel. The same holds for anti-parallel alignment of spins from the two parts of the trajectory: anti-parallel alignment between the two incident quasi-particles at vertex k (on the first and second traversal, respectively) results in anti-parallel alignment of the outgoing quasi-particles.

The resulting weight factor to the periodic orbit contributed by the pairing of scattering processes on the self-dual orbits depends on whether

- the quasi-particles incident on the same vertex k during the two rounds are of the same *type* or not and whether
- the *spin directions* are flipped by the scatterer or not.

Summarily, we find that the contributing factor is $-1/2$ if the incident quasi-particles at vertex k on the two rounds are of the *same type* *and* if their spin is *flipped* by the scatterer. All other pairings of scattering processes robust against averaging yields a factor of $1/2$. With this quintessential rule, we can

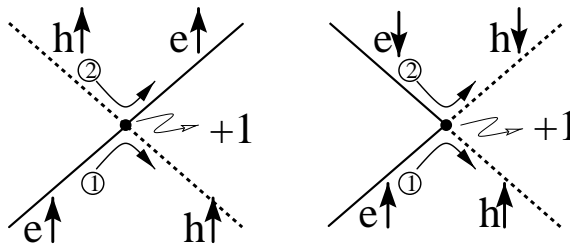


Figure 3.8.: Zoom-in on a single vertex where the spin directions are *not* changed during the scattering processes. While the process on the left is also allowed in class D , the pairing of scattering processes on the right is allowed in class $DIII$ only. The lower part of the diagram represents a cutting from the *first* traversal of the self-dual orbit while the upper part is from the *second* traversal. The sign of the overall weight factor contributed by the depicted pairing of scattering processes is also given.

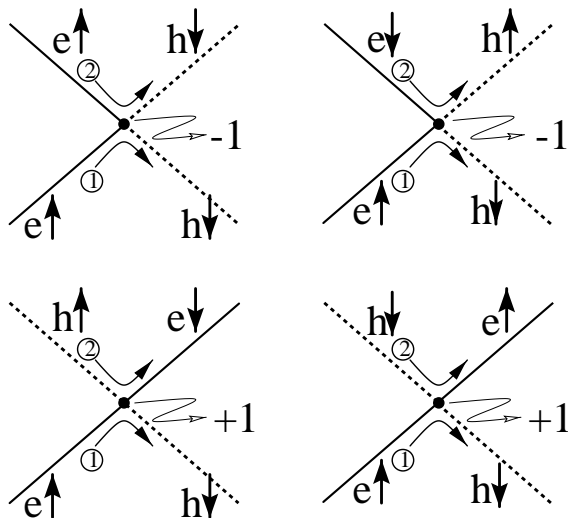


Figure 3.9.: The four processes sketched above are examples of the ten distinct pairings where the spins are flipped. Shown here are all combinations with an electron e_{\uparrow} incident on the first round (cf. leg on the bottom left part of each diagram). To the right of the scattering vertex is indicated the sign of the overall weight accumulated by the respective pairing of scattering processes.

now assemble all self-dual orbits robust under the ensemble average (3.74) of class *DIII*.

Finally, something must be said about the *types* of quasi-particles incident at a given vertex k on the two traversals of the self-dual orbit. For orbits of class *C* geometry with total length $2m$, one always has quasi-particles of *different type* incident on any peripheral vertex. For possible coherent pairs of scattering events, this calls for matching of entries of the two *different* scattering matrices (3.80) and (3.81). However, in the case of orbits with class *CI* geometry, the possibility arises that *identical types* of quasi-particles are incident on a vertex k such that two entries of *either* matrix (3.80) *or* (3.81) must be matched, depending on the respective quasi-particle type.

The self-dual orbits of class *DIII*

With the systematics of the allowed scattering processes at the *individual vertices* at hand, we are now ready to *assemble* the contributing self-dual orbits for the class *DIII* Andreev star graph. For an orientation, we give the following outline for three types of orbits:

- Orbits of *class C geometry* of total length $2m$ where the two traversals have the same direction (*no turning point*, only m odd),

- orbits of *class CI geometry* of total length $2m$ where the spin directions are *flipped* at the turning point and
- orbits of *class CI geometry* of total length $2m$ where the spin directions are *preserved* at the turning point.

Following this outline, we begin with the orbit of *class C geometry* of total length $2m$ (m odd). The spin directions on the m segments of the first traversal can be chosen freely, adding up to a total of 2^m possibilities. This said, the spin directions on the remaining m segments (making up the second traversal) are fixed to stand *parallel* to their partners of the first traversal. This parallel alignment is enforced such that at each vertex k where the spin direction is preserved by one scattering process, the quasi-particles of the other traversal touching this vertex k must stand parallel to their partners. Antiparallel spin orientation between “partner” quasi-particles (belonging to different traversals) is forbidden if the spin is *preserved* by the scattering process at the vertex. *Only* for the *single* orbit where spin-directions are flipped at *every* vertex are antiparallel orientation between “partner” quasi-particles of the two traversals allowed.

Thus, in total, we have $2^m + 1$ spin configurations adding coherently to the self-dual expression (3.78). The weight factor contributed by each of the m elementary pairings of scatterings at the vertices is always $+1/2$, as the incident quasi-particles are never of the same type. Consequently, the first type of orbits itemized in the outline – the orbits of class *C* geometry of length $2m$ (m odd) – yield the following contribution to the trace (3.78) in the self-dual approximation:

$$e^{i4mkL} \frac{1 + 2^m}{2^m} [(-1)^{m+1} + 1] / 2, \quad (3.82)$$

where the last factor is unity for m odd and zero otherwise.

Following the outline, we now discuss orbits of *class CI geometry* of total length $2m$ where the spin directions are *flipped* at the turning point. It is shown in the following that this type of orbits *does not* contribute to the trace in (3.79) due to cancellation – for *every* given spin configuration exists a partner orbit with opposite weight. This cancellation is best explained by means of figure 3.10 (for a start, we restrict the argument to m odd and modify the lines of reasoning for m even in due course). First, we focus on the pairing of scattering processes at the turning point itself. To the right of the turning point, the scattering situation is assumed to be fixed while to the left, the alternatives *A* and *B* are considered. The coherent weight of either pairing alternative *A* or *B* at the turning point is $(-i\sigma_k)(i\sigma_k)/2 = 1/2$. The different spin alignments in *A* and *B* lead to the claimed cancellation. In order to verify this claim, we follow the orbit starting with either alternative *A* (h_\uparrow) or alternative *B* (h_\downarrow) in an anti-clockwise direction until the turning point is reached from the other side. Alternative *A* (*B*) demands for an even (odd) number of spin flips. It is worth

remembering that when the incident electrons on a given vertex are of the *same* type, each process where spins are *flipped* (*preserved*) results in a factor of $-1/2$ ($+1/2$). As the number of spin flips for A and B differs by *exactly one*, the two alternatives A and B cancel each other out.

This argument for cancellation is independent of the special choice for the scattering situation on the right hand side of the turning point in the figure 3.10. Modifying this scattering situation just demands a consistent relabeling of the rest of the diagram.

Cancellation of orbits of *class CI geometry* where the spin directions are *flipped* at the turning point is also at work for m *even*. The illustration in figure 3.10 must then be modified by adding or removing one segment of the self-dual path. For m even, one has two quasi-particles of the *same type* incident on the turning point. Identical incident quasi-particles together with a spin flip lead to the weight $(-i\sigma_k)^2/2 = -1/2$. Despite this difference, the two alternatives A and B with different spin directions continue to exist, leading once again to cancellation of orbits. This concludes the second point of the outline: orbits of *class CI geometry* where the spin directions are *flipped* at the turning point do *not* contribute to the trace (3.79).

We now come to the third category of self-dual orbits – namely the orbits of *class CI geometry* of total length $2m$ where the spin directions are *preserved* at the turning point. The kind of processes paired to the left and right of the turning point vertex depend on whether m is even or odd. With the spin direction preserved, we must look for φ_k -independent products of the entries $\pm ie^{\pm i\varphi_k}$ of the scattering matrices (3.80) and (3.81). For m odd (even), the incident quasi-particle types are different (identical) such that their spins must point in the

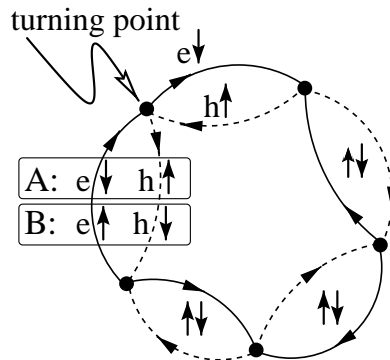


Figure 3.10.: Two partner orbits A and B are shown. Independent of the spin configurations at other parts of the orbit (schematically indicated by $\uparrow\downarrow$), the two alternatives A and B (drawn in the same picture, framed by boxes) are orbits with opposite weight leading to cancellation. The total length of the orbit is $2m$ and the example shown has $m = 5$.

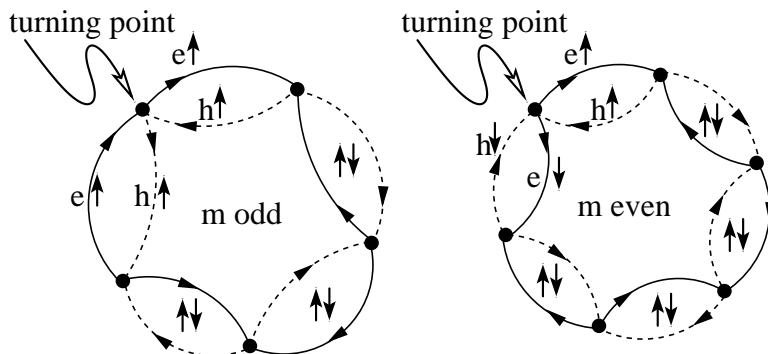


Figure 3.11.: Spin directions for self-dual orbits of *class CI geometry* where the spin direction is *preserved* at the turning point. As examples, the orbit for m odd ($m = 5$) is shown on the left, while m even ($m = 6$) is shown on the right.

same (opposite) direction. A representative sketch of both situations is given in figure 3.11 for both m odd ($m = 5$) and m even ($m = 6$).

The weight of a representative of these orbits is read off the diagrams in figure 3.11. The factors due to the pairing of scatterings at the turning point are $+1/2$ for both m odd and even. On the remaining vertices, the total number of spin flipping scatterings must be *even* (*odd*) for m odd (even) – whatever be the spin directions on intermediary segments. When quasi-particles of the *same* type are incident on all the intermediary vertices, each spin flip results in a weight factor of $-1/2$. Counting the necessary numbers of spin flips along the itinerary in order to match the setting on the two path segments adjacent to the turning point provides information of the overall weight of the orbit. Orbits with m odd [even] have weight $(1/2)^m$ [$-(1/2)^m$]. For l spin flips along the $m - 1$ vertices, one has $\binom{m-1}{l}$ distinct orbits contributing.

Collecting the contributions from all types of self-dual orbits, we find the *DIII* ensemble average of the trace:

$$\begin{aligned} \langle \text{tr } \mathcal{S}_{B_{\text{red}}}^m(k) \rangle_{\text{sd}}^{\text{DIII}} &= e^{i4mkL} \left[\left(1 + \frac{1}{2^m}\right) + \frac{1}{2^m} \sum_{\substack{l=0 \\ l \text{ even}}}^{m-1} \binom{m-1}{l} \right] [1 - (-1)^m] / 2 \\ &+ e^{i4mkL} \left[- \sum_{\substack{l=0 \\ l \text{ odd}}}^{m-1} \binom{m-1}{l} \right] [1 + (-1)^m] / 2. \end{aligned} \quad (3.83)$$

This expression for the trace, when inserted in the graph version of the trace formula (3.72), gives the spectral quantity $\langle \delta\rho(k) \rangle$ which, on its part, yields the form factor after a Fourier transform:

$$K(t) = 2 \int_{-\infty}^{\infty} dk \exp(ikt) \langle \delta\rho(k) \rangle = \frac{1}{N} \sum_{m=1}^{\infty} \delta\left(\frac{t}{t_H} - \frac{m}{2N}\right) K_{m,\text{sd}}^{\text{DIII}} \quad (3.84)$$

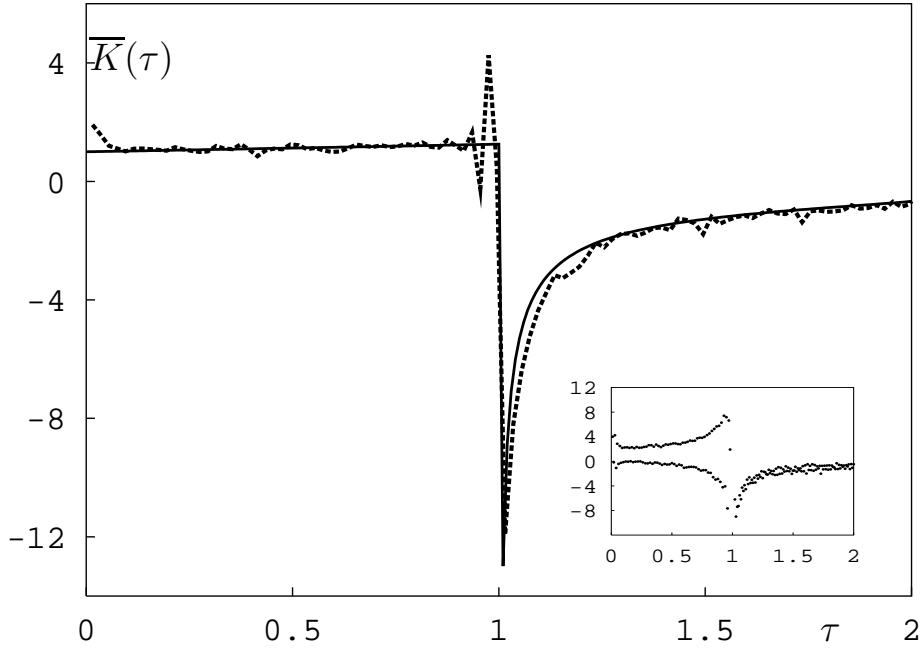


Figure 3.12.: Also for class $DIII$, the numerically computed form factor $K(\tau)$ is in excellent agreement with its RMT counterpart. The star graph with class $DIII$ symmetries with $N = 100$ bonds has been averaged over 50000 configurations. The inset gives the numerical results, their average $\overline{K}(\tau)$ is given by the dashed line. The full line gives the RMT prediction, more precisely, *double* the value as stated in eq. (F.16) (see the text for an explanation of this extra factor of 2 due to degeneracy). All times τ are given in multiples of the Heisenberg time t_H .

with the discrete form factor K_m in the *self-dual approximation*:¹⁷

$$K_{m,\text{sd}}^{DIII} = (-1)^{m+1} \frac{m}{4} + \left(1 + \frac{1}{2^m}\right) \frac{1 - (-1)^m}{2} \longrightarrow \frac{1}{2} - (-1)^m \frac{m+2}{4}. \quad (3.85)$$

As for class D , the discrete time step here too is $\Delta t = t/t_H = m/2N$ and the time averaged form factor states (analogous to eq. (3.42)):

$$\overline{K}_{m,\text{sd}}^{DIII} = \frac{1}{T} \int_0^T dt \frac{t_H}{N} \sum_{m=1}^{\infty} K_{m,\text{sd}}^{DIII} \delta\left(t - \frac{mt_H}{2N}\right) = \frac{2}{M} \sum_{m=1}^M K_{m,\text{sd}}^{DIII} = 1. \quad (3.86)$$

This result is in full agreement with the random-matrix theory prediction for the short-time behaviour of the form factor. In order to see this agreement, we point out that we follow the convention of [2] in appendix F insofar as all

¹⁷In the final result, we have approximated $2^{-m} \rightarrow 0$, neglecting the single orbit of class C geometry where spins are flipped at *every* vertex.

eigenenergy levels are counted without multiplicity. However, as the square of the time-reversal operator in class *DIII* is the *negative* of the identity operator, every eigenvalue is *doubly degenerate* by Kramers' rule [93]. This degeneracy is taken into account if one reinstates a factor of 2 in the result obtained for the form factor $K^{DIII}(t)$ in eq. (F.16), which leads to the short-time expansion given below:

$$K^{DIII}(t) = 1 + \frac{1}{4}t + \mathcal{O}(t^3). \quad (3.87)$$

It is the first term of this expansion which is reproduced by the result (3.86) of the semiclassical analysis presented in this section.

3.6. The numerical routine used in computing the form factor

Throughout the previous sections 3.2 – 3.5, numerical results for the form factor $K(t)$ backed up the analytical calculation. The numerical results are in very good agreement with the random-matrix theory predictions for the form factors $K(t)$ of the respective symmetry classes (which are presented in appendix F). In the current section, we give a brief account of the numerical routine employed in generating the form factor $K(t)$.

The routine for computing the form factor is based on the observation that the (discrete version of) the form factor K_m is directly related to the trace of the m -th power of the reduced bond-scattering matrix:

$$K_m \propto \text{tr} \mathcal{S}_{B\text{red}}^m(k=0), \quad (3.88)$$

which is seen from the trace formula (3.29) for the spectrum $\rho(k)$ in combination with its link to the form factor $K(t)$ by a Fourier transform (1.50).

The crucial advantage of the routine in calculating the form factor is its sheer speed in comparison to the routine employed in the search for the spectral density $\rho(k)$ (which we described in section 2.4). The lesser numerical cost of the routine for the form factor becomes clear from an estimate of the numbers of operations needed by each of the routines in order to obtain their respective results. One diagonalization of an N -by- N -matrix needs $\mathcal{O}(N^3)$ operations [94]. The routine for the calculation of the density $\rho(k)$ needs about $M = 20$ such diagonalizations for the computation of a *single* eigenvalue k_n (see section 2.4 for details). For an Andreev star graph with N peripheral vertices (leading to an N -dimensional reduced bond-scattering matrix $\mathcal{S}_{B\text{red}}$), the calculation of ν eigenvalues of a single realization needs about νMN^3 operations.

This is to be contrasted with the numerical cost needed for a series of values of the (time-discrete) form factor K_m . In this case, the reduced bond-scattering matrix $\mathcal{S}_{B\text{red}}$ must be diagonalized only *once*, yielding all eigenvalues. The

subsequent computation of the trace of the m -th power $\text{tr } \mathcal{S}_{B \text{ red}}^m$ necessitates only the multiplication of the N eigenvalues found by the diagonalization. Thus, it is obvious that the routine for evaluating the (discrete) form factor K_m is much faster, facilitating the calculation of larger systems (with more peripheral vertices) within larger ensembles (by use of more configurations).

Unrelated to the question of which numerical routine to use is the following comment on the star graph topology. It is the special connectivity of the star graph that suggests the usage of the *reduced* bond-scattering matrix $\mathcal{S}_{B \text{ red}}(k)$ instead of the bond-scattering matrix $\mathcal{S}_B(k)$ – this reduces the size of the matrix under scrutiny by a factor of *four*.

3.7. Andreev Billiards

Andreev billiards are at the origin of the reductionist modeling of Andreev graphs. This is why a generalization of the results obtained for Andreev graphs to Andreev *billiards* is desirable. As the author’s own contribution to the topic of Andreev billiards has been minimal, this section is to be understood as a kind of outlook beyond the work on Andreev quantum graphs, reviewing the publication [89] in some detail.

The novel element in superconducting-normalconducting hybrid systems, *Andreev reflection*, has been discussed extensively in the introductory section 1.1.3. There it was explained that in the absence of a magnetic field, electrons (holes) sufficiently close to the Fermi energy are reflected as holes (electrons) which then retrace the electron (hole) trajectory backwards (retroreflection). In chaotic billiards, essentially all trajectories eventually hit the superconducting interface, thus leading to a periodic orbit bouncing back and forth between two points on the superconducting interface [88]. Thus, a conventional chaotic billiard (without magnetic field) that is coupled to a superconductor has a combined electron-hole dynamics that is no longer chaotic. The resulting trajectories are all periodic, leading to nonuniversal behaviour like the proximity-induced hard gap [23, 95, 96] for time-reversal invariant systems. Here, however, we want to recover *universal* spectral statistics, which is possible *only* if the *combined* electron-hole dynamics is chaotic and periodic orbits are isolated as in conventional chaotic (hyperbolic) systems.

Andreev billiards in class C

In Andreev billiards of class C , where time-reversal symmetry is broken by a perpendicular magnetic field B , the *combined* electron-hole dynamics is chaotic and periodic orbits are isolated. This comes in natural, as the retroreflected hole (electron) does not retrace the trajectory of the incoming electron (hole) since both electron and hole trajectories are curved in the *same* direction (in the expression for the Lorentz force $(q/m)\mathbf{v} \times \mathbf{B}$ *both* charge q and effective

mass m change signs when replacing an electron by a hole). This situation has been given a graphical illustration in figure 3.1, part (a) at the opening of the chapter on star graphs.

With isolated periodic orbits in a hyperbolic system one is allowed to express the semiclassical density of states by a Gutzwiller-type trace formula (analogous to eq. 1.40) as a sum over the isolated periodic orbits p of the *combined* electron-hole dynamics of the Andreev billiard,

$$\delta\rho(E) = \frac{1}{\pi\hbar} \operatorname{Re} \sum_p t_p A_p e^{iS_p(E)/\hbar + i\chi}. \quad (3.89)$$

The orbit amplitudes A_p are products of electron and hole contributions,

$$A_p = A_p^{(e)} A_p^{(h)}, \quad (3.90)$$

while the orbit actions are sums of electron and hole actions,

$$S_p(E) = S_p^{(e)}(E) + S_p^{(h)}(E). \quad (3.91)$$

The factor t_p stands for the traversal time of the *complete* orbit and reflects the arbitrary starting point of the orbit (see eq. (1.39) in the middle of the GTF derivation in section 1.3) and χ denotes the accumulated Andreev phases.

Coherent contributions to the form factor can be expected from those periodic orbits where the same trajectory is run through twice in the same direction with the roles of electrons and holed interchanged on the second traversal. We recognize these types of orbits as *self-dual* orbits; their counterparts on graphs have shown up repeatedly in sections 3.2 – 3.5. The *self-dual* orbits are invariant under electron-hole conjugation and the dynamical contributions to their action largely cancel due to the relation $S_p^{(e)}(E) = -S_p^{(h)}(-E)$, such that $S_p(E) \simeq Et_p$.

Moreover, the stability amplitudes of electron $A_p^{(e)}$ and hole $A_p^{(h)}$ are just complex conjugates of one another. This is obvious from the form of the semiclassical Green function $G_{\text{sc}}(q_A, q_B, E)$ stated in eq. (1.28), where transition from electron to hole entails $K_{\text{sc}}^{(h)}(q_A, q_B, t) = [K_{\text{sc}}^{(e)}(q_A, q_B, t)]^*$ and $E \rightarrow -E$ for the energy. Consequently, one has $A_p = |A_p^{(e)}|^2$ in total. The accumulated Andreev phase is $(-i)^{2s} = -1$ with s an odd integer. Keeping only the *self-dual* periodic orbits (i. e. the restriction to the *self-dual approximation*) we find

$$\delta\rho(E)_{\text{sd}} = -\frac{1}{\pi\hbar} \operatorname{Re} \sum_p t_p |A_p^{(e)}|^2 e^{iEt_p/\hbar}. \quad (3.92)$$

For the form factor as defined in eq. (1.50), this leads to

$$K(t)_{\text{sd}} = -2 \sum_p t_p |A_p^{(e)}|^2 \delta(t - t_p). \quad (3.93)$$

This expression reveals the similarity to the diagonal approximation for the Wigner-Dyson form factor (1.46). However, here only *one* factor t_p arises.

It is important to notice that the HOA sum rule does not apply directly to the sum over self-dual orbits. The original HOA sum rule as stated in eq. (1.47) deals with *squares* of amplitudes of all periodic orbits. Here we have a sum over the *amplitudes* $|A_p^{(e)}|^2$ *themselves* of all self-dual orbits (deceivingly similar to a square of amplitudes).

To deal with this difficulty, a *virtual billiard* is introduced with the same dynamics as the Andreev billiard except that there is *no* particle-hole conversion at the SN interface. Thus, the virtual billiard is an ordinary chaotic billiard with unusual reflection conditions at the SN-interface (retroreflections). Primitive periodic orbits of the virtual billiard involve either even or odd numbers of retroreflections. Reintroducing electron-hole conversion, one observes that *even* orbits lead to non-self-dual periodic orbits in the Andreev billiard. This observation falls in lines with the impossibility in constructing self-dual orbits with m peripheral excursions for m *even* (on the class C type Andreev star graph in section 3.2). Twofold traversals of *odd* orbits are periodic and self-dual in the Andreev billiard as the roles of electron and hole are interchanged in the second traversal. We can now interpret the sum over self-dual orbits in (3.93) as a sum over *odd* orbits of the virtual billiard. Since on average *half* of its orbits are odd, the HOA sum rule for the virtual billiard gives

$$\sum_{p \in [t, t+\Delta t]} |A_p^{(e)}|^2 = \frac{\Delta t}{2t}. \quad (3.94)$$

This modified HOA sum rule (3.94), when inserted in the periodic-orbit representation of the form factor in self-dual approximation (3.93), yields

$$K(t)_{\text{sd}} = -1 \quad (3.95)$$

in agreement with the RMT result (F.3) for short times. The self-dual approximation is expected to hold for $t_0, t_A \ll t \ll t_H$ where t_0 is the traversal time of the shortest periodic orbits and t_A is the so-called Andreev time. The Andreev time t_A is the typical time before the quasi-particle hits the interface. It is a natural limit for short times, as for times t below the Andreev time $t < t_A$, the superconductor typically has not been probed by the orbit. The upper boundary $t \ll t_H$ is understood as in the case of the diagonal approximation for the Wigner-Dyson classes (presented in section 1.4). The *self-dual approximation* must break down as classical correlations between orbits *not* related by self-duality become important with increasing orbit length.

Andreev billiards in class CI

The reasoning is more involved when we consider Andreev billiards of class CI . In class CI , time-reversal symmetry implies that the holes necessarily retrace the electron trajectory, thus leading to non-isolated periodic orbits and nonuniversal spectral statistics (as surveyed in section 1.1.3).

In order to find the universal spectral statistics of class CI , the Andreev billiard is coupled to N *individual* one-channel leads. The reason why this configuration of the Andreev billiards (with N leads containing one channel each) displays universal statistics is found by mapping this system to Andreev star graphs of type CI . The quantization condition for Andreev billiards with N leads is $\det(\mathbb{1} - \mathcal{S}(E)) = 0$ as worked out in [88]. In this context, $\mathcal{S}(E)$ is the $N \times N$ Andreev billiard scattering matrix $\mathcal{S}(E) = S_{NC}(E)D_- S_{NC}^*(-E)D_+$. The scattering matrix $S_{NC}(E)$ describes the coupling of the N channels by the dynamics in the normal region. The matrices D_{\pm} describing the Andreev scattering in the leads are diagonal, $D_{\pm} = -i \text{diag}(e^{\mp i\alpha_j})$, with a specific Andreev phase $\alpha_j \in \{0, \pi\}$ chosen for each lead.

A detailed correspondence between the CI -type star graph treated in section 3.3 and the billiard of the configuration described above is obtained by substituting the quantum graph expressions with the scattering matrix S_C (explained by eq. (3.6)) with a more general central scattering matrix $S_{NC}(E)$: $\mathcal{L}S_C\mathcal{L} \rightarrow S_{NC}(E)$ and $\mathcal{L}S_C^*\mathcal{L} \rightarrow S_{NC}^*(-E)$. Thus, the form factor of these billiards is obtained in the self-dual approximation in complete analogy with the star graph of class CI .

This concludes the section on Andreev billiards showing universal spectral statistics of the symmetry classes C and CI , respectively. While these billiards are of course interesting in their own right, the arguments laid out above also show how modeling these billiards by quantum graphs helps in forming an intuition about the contributing orbits in the self-dual approximation.

3.8. Summary

The work in this chapter is dedicated to a semiclassical analysis of the universal spectral form factors of superconducting-normalconducting hybrid systems in the ergodic limit which belong to the new symmetry classes C , CI , D , and $DIII$.

The semiclassical method applied is based on a Gutzwiller type trace formula linking the spectrum of the quantum mechanical system to the classical orbits of the system and their properties.

As we evaluate the trace formula on a quantum graph – an especially transparent model in identifying and evaluating periodic orbits – the basic scattering mechanism of superconducting-normalconducting hybrid systems, Andreev reflection, must be incorporated on the quantum graph. This introduction of Andreev reflection is the novel ingredient put forward by this thesis to the realm of quantum graphs. For quantum graphs incorporating the mechanism of Andreev reflection, we use the term “Andreev quantum graph”. These graphs then permit a semiclassical analysis of the universal spectral statistics for ergodic superconducting-normalconducting hybrid systems belonging to the new symmetry classes C , CI , D , and $DIII$.

With the aid of Andreev quantum graphs, it has been shown that the universal spectral statistics of Gaussian random-matrix models within the new symmetry classes [2] is correctly reproduced by semiclassical theory. As spectral quantity of choice for the analysis, we have used an appropriate generalization of the form factor as defined in eq. (1.50). Its value is computed by evaluating a graph version of the Gutzwiller trace formula. The analytical findings based on periodic-orbit theory are supported by numerical results which show excellent agreement with the random-matrix theory predictions.

The novel element developed for the analysis of the orbits relevant for the spectrum by a Gutzwiller trace formula is the *self-dual approximation*. The *self-dual approximation* is a modification of Berry's diagonal approximation [9] for application to superconducting-normalconducting hybrid systems. The terminology "self-dual" is derived from the characteristics of the orbits taken into account by this approximation: these orbits are traversed *twice* such that each segment of the orbit is once traversed by an electron and once by a hole. Thus, such orbits are invariant under electron-hole conjugation, which motivates our terming them *self-dual*.

Inspired by the successful semiclassical interpretation of the universal spectral form factor of the novel symmetry classes on the Andreev graph model, one has set out to do the same for *Andreev billiards* where a superconductor is adjacent to a normalconducting billiard with underlying non-integrable classical dynamics. The semiclassical results obtained for Andreev billiards of symmetry class *C* and *CI* – again in the *self-dual approximation* – reproduce the universal spectral statistics predicted by random-matrix theory [89]. As decisive condition for recovering the universal spectral statistics is found to be that the *combined* electron-hole dynamics of the Andreev system must be classically chaotic.

A. The superconducting-normalconducting (SN) interface

As a supplement to the introductory chapter on Andreev scattering 1.1.3, this appendix presents the computational background for the physical phenomena discussed in the introduction. This appendix is based on the seminal paper by Blonder *et al* [90] where the Andreev scattering off a superconducting-normalconducting (SN) interface was studied in one dimension (the perpendicular to the interface). Here, we include two dimensions and allow for a complex value of the superconductor order parameter Δ (see figure A.2). It is a straightforward matter to derive the characteristic physics of the SN interface by *matching boundary conditions* of the quasi-particle wave functions at the interface.

The physics at the NS-interface is described by the Bogoliubov-deGennes equation

$$\begin{bmatrix} h_0(\mathbf{r}) & \Delta(\mathbf{r}) \\ \Delta^*(\mathbf{r}) & -h_0(\mathbf{r}) \end{bmatrix} \psi(\mathbf{r}) = E \psi(\mathbf{r}) \quad (\text{A.1})$$

with

$$h_0(\mathbf{r}) = -\hbar^2 \frac{\partial_x^2 + \partial_y^2}{2m} - \mu + V(\mathbf{r}) \quad \text{and} \quad \Delta(\mathbf{r}) = \Theta(x) \Delta_0 e^{i\varphi}. \quad (\text{A.2})$$

The functional form of the order parameter $\Delta(\mathbf{r})$ is appropriate for the physical system under scrutiny, where a semi-infinite normalconducting metal (N) for $x < 0$ meets a semi-infinite superconductor (S) for $x > 0$ at the interface situated at $x = 0$ (see figure A.2). It is known in the literature as “rigid boundary condition” [20].

The translational invariance of the interface in the y direction (leading to preserved momentum $\hbar k_{\parallel}$ for the component parallel to the interface) allows a separation of variables and motivates the plane wave ansatz below:

$$\psi(\mathbf{r}) = e^{ik_{\parallel}y} \psi_{\text{BTK}}(x), \quad (\text{A.3})$$

where we have anticipated by the subscript “BTK” that this ansatz inserted in the BdG equation (A.1) leads to an effective equation for $\psi_{\text{BTK}}(x)$, depending

only on the variable x :

$$\begin{bmatrix} \tilde{h}_0(x) & \Delta(x) \\ \Delta^*(x) & -\tilde{h}_0(x) \end{bmatrix} \psi_{\text{BTK}}(x) = E \psi_{\text{BTK}}(x), \quad (\text{A.4})$$

where in $\tilde{h}_0(x)$, the dependence on the coordinate y has been absorbed in the chemical potential: $\tilde{h}_0(x) = -\hbar^2 \partial_x^2 / 2m - \tilde{\mu} + V(x)$ with $\tilde{\mu} = \mu - \hbar^2 k_{\parallel}^2 / 2m$. The form of eq. (A.4) is identical to the one considered in the appendix of [90]. The solutions of the “effective” equation (A.4) for the side $x < 0$ of the semi-infinite normalconducting metal are linear combinations of

$$\psi_{\pm q^+} = \begin{bmatrix} 1 \\ 0 \end{bmatrix} \exp(\pm i q^+ x) \quad \text{and} \quad \psi_{\pm q^-} = \begin{bmatrix} 0 \\ 1 \end{bmatrix} \exp(\pm i q^- x) \quad (\text{A.5})$$

with

$$\hbar q^{\pm} = \sqrt{2m} \sqrt{\tilde{\mu} \pm E}. \quad (\text{A.6})$$

On the side of the superconductor ($x > 0$), the solution of eq. (A.4) is a linear combination of

$$\psi_{\pm k^+} = \begin{bmatrix} u_0 e^{i\varphi} \\ v_0 \end{bmatrix} \exp(\pm i k^+ x) \quad \text{and} \quad \psi_{\pm k^-} = \begin{bmatrix} v_0 e^{i\varphi} \\ u_0 \end{bmatrix} \exp(\pm i k^- x) \quad (\text{A.7})$$

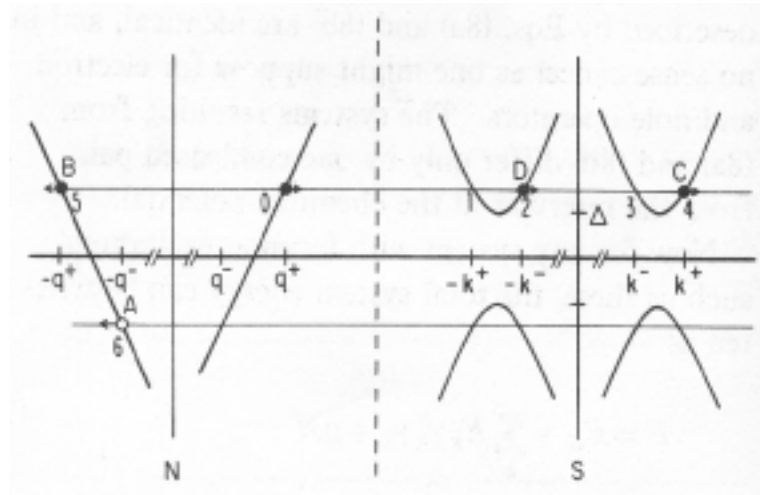


Figure A.1.: Schematic plot of the dispersion relations (A.6) in the normal metal (indicated by N) and (A.8) in the superconductor (indicated by S). The open (closed) circles denote holes (electrons), and the arrows point in the direction of the group velocities. Shown is an electron incident from the normalconducting metal (0), resulting in transmitted (2,4) and reflected (5,6) quasi-particles. Diagram and caption taken from [90].

with the wave numbers

$$\hbar k^\pm = \sqrt{2m} \sqrt{\tilde{\mu} \pm \sqrt{E^2 - \Delta_0^2}} \quad (\text{A.8})$$

and the quasi-particle amplitudes

$$1 - v_0^2 = u_0^2 = \frac{1}{2} \left[1 + \frac{(E^2 - \Delta^2)^{1/2}}{E} \right]. \quad (\text{A.9})$$

We are interested in constructing the scattering states for the situation when an electron impinges on the interface coming from the normal metal, assuming that the interface is free of elastic scatterers $V(x=0) = 0$. Note that all directions of incoming, reflected, and transmitted waves are defined by their group velocity $v_g = dE/d(\hbar k)$ (see also figure A.1). This motivates the following ansatz for the scattering situation when an electron is incident with unit amplitude from the normalconducting side onto the interface:

$$\begin{aligned} \psi_{\text{inc}}(x) &= \begin{bmatrix} 1 \\ 0 \end{bmatrix} e^{iq^+x}, \\ \psi_{\text{refl}}(x) &= a \begin{bmatrix} 0 \\ 1 \end{bmatrix} e^{iq^-x} + b \begin{bmatrix} 1 \\ 0 \end{bmatrix} e^{-iq^+x}, \\ \psi_{\text{trans}}(x) &= c \begin{bmatrix} u_0 e^{i\varphi} \\ v_0 \end{bmatrix} e^{ik^+x} + d \begin{bmatrix} v_0 e^{i\varphi} \\ u_0 \end{bmatrix} e^{-ik^-x}. \end{aligned} \quad (\text{A.10})$$

Demanding continuity for the wave function at the interface $\psi_{\text{inc}}(0) + \psi_{\text{refl}}(0) = \psi_{\text{trans}}(0)$ and its derivative $\psi'_{\text{inc}}(0) + \psi'_{\text{refl}}(0) = \psi'_{\text{trans}}(0)$ and carrying out the necessary algebraic reduction leads to expressions for the coefficients a, b, c , and d . In the limiting case, when the involved wave numbers approach the Fermi

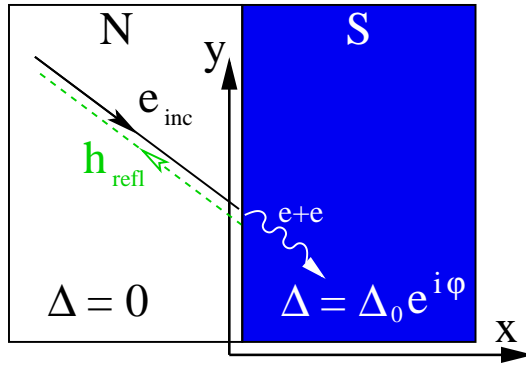


Figure A.2.: Andreev reflection of an electron at the SN-interface in the plane $x = 0$, with the superconductor (S) occupying the region $x > 0$.

wave number $k^+ = k^- = q^+ = q^- = k_F$, one finds:

$$a = \frac{v_0}{u_0} e^{-i\varphi} = e^{-i\arccos(E/\Delta)} e^{-i\varphi} \rightarrow -i e^{-i\varphi} \quad \text{for } E/\Delta \rightarrow 0,$$

$$b = 0, \quad c = \frac{e^{-i\varphi}}{u_0}, \quad d = 0. \quad (\text{A.11})$$

Upon reinstating the functional dependence on the parallel coordinate y , this leads to the following reflected and transmitted wave functions:

$$\psi_{\text{refl}}(\mathbf{r}) = \begin{bmatrix} 0 \\ -i e^{-i\varphi} \end{bmatrix} e^{iq^-x} e^{ik_{\parallel}y}, \quad \psi_{\text{trans}}(\mathbf{r}) = \begin{bmatrix} 1 \\ -i e^{-i\varphi} \end{bmatrix} e^{ik^+x} e^{ik_{\parallel}y}. \quad (\text{A.12})$$

From the wave function of the Andreev reflected hole $\psi_{\text{refl}}(\mathbf{r})$, we can read off all the characteristic features: all three component of the velocity change signs and the hole is *retroreflected* along the path of the incident electron, with the additional phase $-\pi/2 - \varphi$ imparted onto the hole by the superconductor.

B. Method of stationary phase

Semiclassical analysis relies crucially on the saddle-point approximation of integrals of the type

$$I = \int_{-\infty}^{\infty} d^d x A(x) \exp(is\Phi(x)), \quad (\text{B.1})$$

where $\Phi(x)$ is a real-valued function and s is a large, real parameter. We first restrict ourselves to the one-dimensional version ($d = 1$). For large s the phase oscillates rapidly. Thus the phase averages to zero *nearly* everywhere. Exceptions are the surroundings of the extremal points x_0 where the phase is *stationary*: $\Phi'(x_0) = 0$, $\Phi''(x_0) \neq 0$. From that condition originates the name of this approximation scheme: *method of stationary phase*. Expanding $\Phi(x)$ to second order at the point x_0 allows for

$$I = \int_{-\infty}^{\infty} dx A(x) \exp\left(is\left(\Phi(x_0) + \frac{1}{2}\Phi''(x_0)(x - x_0)^2 + \dots\right)\right). \quad (\text{B.2})$$

It is assumed that $A(x)$ is regular and varies only slowly around x_0 , such that it may be regarded as constant, and we obtain

$$I \approx A(x_0) \exp(is\Phi(x_0)) \int_{-\infty}^{\infty} dx \exp\left(is\frac{\Phi''(x_0)}{2}(x - x_0)^2\right). \quad (\text{B.3})$$

The integral on the right hand side is known as a Fresnel integral, leading us to

$$I \approx \sqrt{\frac{2\pi}{s|\Phi''(x_0)|}} A(x_0) \exp\left(is\Phi(x_0) + \frac{i\pi}{4}\text{sgn}(\Phi''(x_0))\right). \quad (\text{B.4})$$

This approximation (B.4) is called the *stationary phase approximation*. It is a standard technique and is used repeatedly for the derivation of the Gutzwiller trace formula sketched in section (1.3).

Generalizing this method to d dimensions is straightforward. With the symmetric matrix $D(x_0)$ of second order derivatives of $\Phi(x)$ at the stationary phase point x_0

$$D_{ij}(x_0) = \frac{\partial^2}{\partial x_i \partial x_j} \Phi(x) \Big|_{x=x_0} \quad (\text{B.5})$$

one obtains the following estimate for the d -dimensional version (B.1):

$$I \approx \sum_{x_0} \left(\frac{2\pi i}{s} \right)^{d/2} \frac{A(x_0)}{\sqrt{|\det(D(x_0))|}} \exp \left(i s \Phi(x_0) - \frac{i\pi}{2} m(x_0) \right). \quad (\text{B.6})$$

As an additional generalization, we allowed for several stationary points x_0 of $\Phi(x)$ which are all summed over. The index $m(x_0)$ counts the number of negative eigenvalues of the matrix of second order derivatives $D(x_0)$. We have assumed in the derivation of (B.6) that $D(x_0)$ has no zero eigenvalues.

In the context of semiclassical analysis, the large parameter s is identified with the inverse of Planck's constant $s = \frac{1}{\hbar}$, while the action S or Hamilton's principal function W is identified with the real-valued function $\Phi(x)$.

This presentation of the stationary phase approximation is along the lines of that in [21].

C. The trace formula for quantum graphs

Here we present a detailed derivation of the graph version trace formula (1.58)¹

$$\rho(k) = \frac{1}{2\pi} \frac{d}{dk} \left[\sum_{i=1}^M \phi_i(k) \right] + \frac{1}{\pi} \lim_{\varepsilon \rightarrow 0} \text{Im} \frac{d}{dk} \sum_{n=1}^{\infty} \frac{1}{n} \text{tr} S_B(k + i\varepsilon)^n \quad (\text{C.1})$$

starting from the quantization condition for eigenvalues k of quantum graphs:

$$\det(1 - \mathcal{S}_B(k)) = 0 \quad (\text{C.2})$$

with the $M \times M$ bond-scattering matrix $\mathcal{S}_B(k)$. M is the number of directed bonds times the number of components of the wave function. For agreement with the notation in the introductory chapter (1.6), we set $M = 2B$, while particle-hole and spin degrees of freedom lead to a multiple value for M .

Following Kottos *et al* [11], we denote the eigenvalues of the unitary matrix $\mathcal{S}_B(k)$ by $e^{i\phi_i(k)}$ ($i = 1, 2, \dots, M$). The quantization condition is now equivalent to

$$\phi_i(k) = 2\pi n \quad \text{with} \quad n \in \mathbb{Z} \quad (\text{C.3})$$

and the density of states is

$$\rho(k) = \sum_{l=1}^{\infty} \delta(k - k_l) = \sum_{i=1}^M \sum_{n \in \mathbb{Z}} \delta[\phi_i(k) - 2\pi n] \left| \frac{d\phi_i(k)}{dk} \right|. \quad (\text{C.4})$$

For the derivation of the trace formula one starts from the spectral determinant

$$\zeta_B(k) = \det(1 - \mathcal{S}_B(k)) \quad (\text{C.5})$$

as its logarithm is easily expanded in a trace formula

$$\log \zeta_B(k) = \text{tr} \log(1 - \mathcal{S}_B(k)) = - \sum_{n=1}^{\infty} \frac{1}{n} \text{tr} \mathcal{S}_B^n(k). \quad (\text{C.6})$$

This expansion is at the heart of the graph version of periodic-orbit theory, as

$$\text{tr} \mathcal{S}_B^n = \sum_{i_1, \dots, i_n=1}^M \mathcal{S}_{B, i_1 i_2} \mathcal{S}_{B, i_2 i_3} \dots \mathcal{S}_{B, i_n i_1} \quad (\text{C.7})$$

¹ $\varepsilon > 0$ is assumed throughout.

is easily interpreted as a sum over periodic orbits visiting the n directed bonds $i_1 i_2 \dots i_n$ one after the other. For the interpretation just given, a single component wave function and $M = 2B$ is assumed. In the case of multiple component wave functions on the bonds (taking particle-hole and/or spin degrees of freedom into account), one must read the indices $i_1 i_2 \dots i_n$ as multi-indices comprising information about the actual directed bond, the quasi-particle type, and the spin direction.

Rewriting the spectral determinant as a real amplitude times a phase factor gives

$$\zeta_B(k) = \exp \left[i \frac{\Theta(k)}{2} \right] 2^M \prod_{i=1}^M \sin \frac{\phi_i(k)}{2} \quad (\text{C.8})$$

with

$$\Theta(k) = \sum_{i=1}^M \phi_i(k) - M\pi = \frac{1}{i} \log \det (-\mathcal{S}_B(k)) = k \sum_{i=1}^M L_i + \text{const.} \quad (\text{C.9})$$

The last equality follows easily from writing the bond-scattering matrix as the product $\mathcal{S}_B(k) = D(k)T$ where $D(k)_{ij} = \delta_{ij} e^{ikL_{ij}2}$ and T depends only on the vertex scattering matrices $\sigma^{(j)}$. We have assumed that the $\sigma^{(j)}$ do not depend on k for the graphs defined and analyzed in this thesis.

First we prove that the first term on the right hand side in (C.1) is the mean density of state ρ_{av} . The Helmholtz equation on the line with Dirichlet boundary conditions at two points separated by a length L has eigenvalues $k = n\pi/L$ ($n = 1, 2, \dots$) and therefore a mean density of states $\rho_{\text{av}} = L/\pi$. This is just the description of the minimalist graph with two directed bonds and a one-component wave function ($M = 2$). Consequently, each directed bond has a contribution $L/2\pi$ (multiplied by the number of components of the wave function) to the mean density. Now summing up the contributions of all elements L_i ($i = 1, 2, \dots, M$) and comparing the resulting expression $\sum_{i=1}^M L_i/2\pi$ with the derivative of $\Theta(k)$ with respect to k as given by (C.9) proves that the first term in (C.1) is indeed the mean density of state ρ_{av} .

More elaborate is the proof concerning the fluctuating part of the spectrum $\delta\rho(k)$. With the mean length $\bar{L} = \sum_{i=1}^M L_i/M$, the logarithmic derivative of the spectral determinant is

$$\frac{d}{dk} \log \zeta_B(k + i\varepsilon) = i \frac{M\bar{L}}{2} + \sum_{i=1}^M \frac{d}{dk} \log \sin \frac{\phi_i(k + i\varepsilon)}{2}. \quad (\text{C.10})$$

Kottos *et al* now argue in [11] that since $\sin \frac{\phi_i(k)}{2}$ is real on the real axis, the imaginary part of its logarithmic derivative is a sum over delta-distributions

²When particle-hole or spin degrees of freedom are taken into account, this matrix – appropriately enlarged as $D \rightarrow D \otimes \mathbb{1}_d$ – is still diagonal (where d is the number of components of the wave function).

located at the zeros of $\sin \frac{\phi_i(k)}{2}$. Indeed the logarithmic derivative of the sin-functions should be considered as a distribution. An integration over k along the real axis is a sum over contributions from its singularities k_s where $\phi_i(k_s) = 2\pi s$. The contribution from one singularity k_s can be obtained by expanding $k + i\varepsilon = k_s + \Delta k + i\varepsilon$ (the positive imaginary part is mandatory here to avoid crossing a branch cut line of the logarithm, see below)

$$\begin{aligned} \left. \frac{d}{dk} \log \sin \frac{\phi_i(k + i\varepsilon)}{2} \right|_{k_s} &= \frac{\cos \frac{\phi_i(k+i\varepsilon)}{2}}{\sin \frac{\phi_i(k+i\varepsilon)}{2}} \frac{\phi'_i(k + i\varepsilon)}{2} = \frac{(-1)^s \phi'_i(k_s)}{(-1)^s \phi'_i(k_s) (\Delta k + i\varepsilon)} \\ &= \frac{1}{\Delta k + i\varepsilon} = \mathcal{P} \frac{1}{\Delta k} - i\pi \delta(\Delta k). \end{aligned} \quad (\text{C.11})$$

Thus, after isolating the imaginary part from the real part (given by the principal value \mathcal{P}), the link between the density of states $\rho(k)$ and the logarithmic derivative of the spectral determinant $\zeta_B(k)$ becomes manifest:

$$\text{Im} \frac{d}{dk} \log \zeta_B(k) = \frac{M\bar{L}}{2} - \pi \rho(k) \quad (\text{C.12})$$

leading, in combination with the expansion (C.6), to the trace formula for the graph:

$$\boxed{\rho(k) = \frac{M\bar{L}}{2\pi} + \text{Im} \frac{d}{dk} \sum_{n=1}^{\infty} \frac{1}{\pi n} \text{tr} \mathcal{S}_B^n(k + i\varepsilon).} \quad (\text{C.13})$$

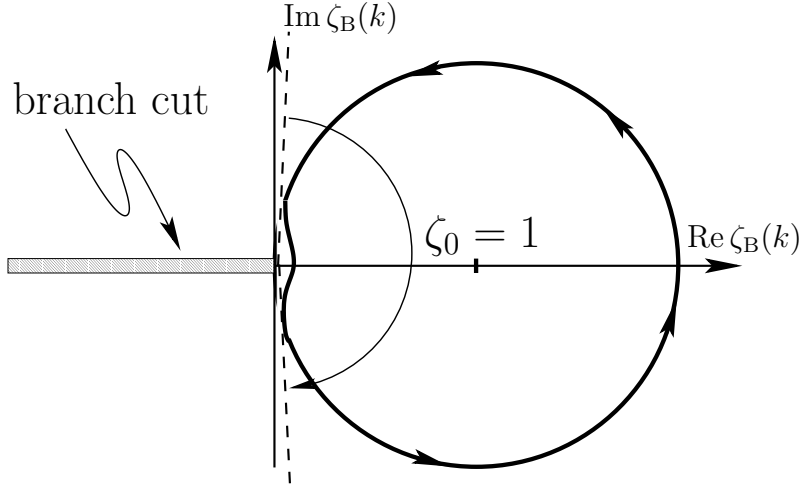


Figure C.1.: On the choice of a positive imaginary part $k \rightarrow k + i\varepsilon$ in the trace formula (C.13). For details we refer to the text below.

Finally, a few words should be said about why one has to choose a positive imaginary part $k \rightarrow k + i\varepsilon$. To simplify the reasoning, let the bond matrix be one-dimensional $\mathcal{S}_B(k) = \exp[i\phi(k)]$. The spectral determinant in this case is

$$\zeta_B(k) = 1 - e^{i\phi(k)}. \quad (\text{C.14})$$

The phase $\phi(k)$ is strictly monotonically increasing with k (for a line with some boundary conditions on two points $\phi(k) = 2Lk + c$; for the general case see appendix D) and the complex number $\zeta_{\text{B}}(k)$ moves *anti-clockwise* along the unit circle centered at $\zeta_0 = 1$. As pictorial support to the line of reasoning, we refer the reader to figure (C.1). The branch cut of the logarithm is usually taken along the negative real axis such that $\log |z|e^{i\phi} = \log |z| + i\phi$ where $-\pi < \phi \leq \pi$. The spectral determinant as a function of real k (without the increment $i\varepsilon$) would cross the branch point along the imaginary axis from positive to negative imaginary part. Thus the imaginary part of the logarithm jumps from $\frac{\pi}{2}$ to $-\frac{\pi}{2}$. This jump is hinted at by the arrow between the two (nearly) vertical dashed lines in figure (C.1). These step function-like jumps of the phase of the spectral determinant $\zeta_{\text{B}}(k)$ passing the origin give the sum over delta distributions after differentiation. Now, the logarithm of the spectral determinant near the branch point is analytic for $\text{Re} \zeta > 0$, which can only be achieved by avoiding the branch point by $k \rightarrow k + i\varepsilon$. This infinitesimal imaginary part has a shortening of the radius as consequence [$i\phi(k + i\varepsilon) = i\phi(k) - \varepsilon \partial_k \phi$] such that the complex number $\zeta_{\text{B}}(k)$ passes the branch point unscathed. This situation is illustrated exaggeratedly in direct vicinity of the origin in fig (C.1).

In principle, it is possible to choose a different branch cut – as long as it does not intersect with the unit circle around $\zeta_0 = 1$, the argument remains unchanged. However, if the branch cut is chosen to cross the circle, new jumps in the imaginary part of $\log \zeta_{\text{B}}(k)$ are introduced which are completely unrelated to the spectrum (thus such a choice is not allowed). Besides, the choice of the positive increment $k \rightarrow k + i\varepsilon$ is compulsive. Choosing a negative imaginary part $k \rightarrow k - i\varepsilon$ would not allow us to expand the function since we cross a branch cut line. The argument is completely analogous for any dimension of the bond-scattering matrix. In the final result, the limit $\varepsilon \rightarrow 0$ is trivial for each summand in the series for finite dimensional bond-scattering matrices \mathcal{S}_{B} . In contrast, for summing up the whole series (C.13) or for infinite dimensional scattering matrices, the limit should be explicitly mentioned in the trace formula.

D. Monotonic anti-clockwise movement of eigenphases $\theta_n(E)$

For the construction of the algorithm in section (2.4), the constant anti-clockwise motion of the eigenphases $\theta_n(E)$ of the bond-scattering matrix $S_B(E)$ (see eq. (2.9)) when the energy E is increased is essential. In this appendix the proof of

$$\frac{d\theta_n}{dE} > 0 \quad \text{with } n = 1, \dots, \dim(S_B(E)) \quad (\text{D.1})$$

is presented. The proof starts out with the eigenvalue equation

$$S_B(E)|n(E)\rangle = e^{i\theta_n(E)}|n(E)\rangle \quad (\text{D.2})$$

where $|n(E)\rangle$ is eigenket with norm $\sqrt{\langle n(E)|n(E)\rangle} = 1$. To investigate the energy dependence of the phases θ_n , the derivate with respect to the energy E is taken on both sides of

$$\langle n(E)|S_B(E)|n(E)\rangle = e^{i\theta_n(E)}\langle n(E)|n(E)\rangle = e^{i\theta_n(E)} \quad (\text{D.3})$$

leading to

$$\begin{aligned} \langle n'(E)|S_B(E)|n(E)\rangle + \langle n(E)|S_B(E)|n'(E)\rangle + \\ + \langle n(E)|S'_B(E)|n(E)\rangle = i \frac{d\theta_n(E)}{dE} e^{i\theta_n(E)}. \end{aligned} \quad (\text{D.4})$$

The first two terms cancel by use of the eigenvalue equation (D.2) and the normalization of the eigenket $\langle n'(E)|n(E)\rangle + \langle n(E)|n'(E)\rangle = \frac{d}{dE}\langle n(E)|n(E)\rangle = 0$. The derivative of the bond-scattering matrix $S_B(E)$ (see eq. (2.9)) with respect to the energy E affects only the diagonal matrix D as the scattering matrix T is energy independent. The matrix $S_B(E)$, its partitions and entries are defined in section (2.2) (see equations (2.9), (2.10), and (2.11)).

$$\begin{aligned} \frac{dS_B(E)}{dE} &= i \left[\begin{array}{cc} \frac{\partial k^+}{\partial E} \text{diag}(L_m e^{ik^+ L_m}) & 0 \\ 0 & -\frac{\partial k^-}{\partial E} \text{diag}(L_m e^{-ik^- L_m}) \end{array} \right] T \\ &= i \left[\begin{array}{cc} \frac{\partial k^+}{\partial E} \text{diag}(L_m) & 0 \\ 0 & -\frac{\partial k^-}{\partial E} \text{diag}(L_m) \end{array} \right] S_B(E). \end{aligned} \quad (\text{D.5})$$

Investing this derivative (D.5) in the relation (D.4), writing \mathcal{L} for $\text{diag}(L_m)$ and employing the eigenequation (D.2) leads to:

$$\langle n(E) | \begin{bmatrix} \frac{\partial k^+}{\partial E} \mathcal{L} & 0 \\ 0 & -\frac{\partial k^-}{\partial E} \mathcal{L} \end{bmatrix} e^{i\theta_n(E)} | n(E) \rangle = \frac{d\theta_n(E)}{dE} e^{i\theta_n(E)}. \quad (\text{D.6})$$

While $|n(E)\rangle$ is member of the eigenbasis of $S_B(E)$, the matrix sandwiched on the left hand side of equation (D.6) is diagonal in the product space of directed bonds and quasi-particle type; a ket in this basis is denoted by $|b_m, \tau\rangle$ where b_m labels the directed bond and τ stands either for p (particle) or h (hole). Using the completeness relation for the $|b_m, \tau\rangle$ -basis, we find

$$\begin{aligned} \frac{d\theta_n(E)}{dE} &= \sum_{b_m, \tau} \langle n(E) | b_m, \tau \rangle \langle b_m, \tau | \begin{bmatrix} \frac{\partial k^+}{\partial E} \mathcal{L} & 0 \\ 0 & -\frac{\partial k^-}{\partial E} \mathcal{L} \end{bmatrix} | b_m, \tau \rangle \langle b_m, \tau | n(E) \rangle = \\ &= \sum_{b_m, \tau} |\langle n(E) | b_m, \tau \rangle|^2 \underbrace{\langle b_m, \tau | \begin{bmatrix} \frac{\partial k^+}{\partial E} \mathcal{L} & 0 \\ 0 & -\frac{\partial k^-}{\partial E} \mathcal{L} \end{bmatrix} | b_m, \tau \rangle}_{>0}. \end{aligned} \quad (\text{D.7})$$

As all lengths L_m of bonds on the graph are positive quantities and as the eigenket $|n(E)\rangle$ with norm 1 *cannot* have vanishing overlap with *all* $|b_m, \tau\rangle$ -kets, it is proven that

$$\frac{d\theta_n(E)}{dE} > 0. \quad (\text{D.8})$$

It may be noticed that the physical dimension of the computed quantity (D.7) is that of a time (with $\hbar = 1$) (see also the matrix sandwiched on the right hand side of (D.7)). This is reminiscent of the calculation of the Wigner-Smith time delay for scattering processes through open systems where derivatives of the scattering matrix $S(E)$ with respect to the energy are used (see [97] and Refs. [1] and [2] in [97]).

An analogous relation $\frac{d\theta_n(k)}{dk} > 0$ is used by Kottos *et al* [11] when the level statistics of *energy* levels is linked to the statistics of *eigenphases*.

E. The Schur orthogonality relations

In this section we explain the relations (2.19) with the help of group theory, starting with the relation

$$\int_G dU U_{ij}(U^{-1})_{lk} = \frac{\delta_{ik}\delta_{jl}}{2N} \quad \text{with } U \in G = \text{Sp}(2N) \quad (\text{E.1})$$

where the indices $i, j, k, l = 1, \dots, 2N$ here and throughout this section. The presentation draws from [98]. Relation (E.1) is a special case of the Schur orthogonality relations [98]. We start out by forming

$$M = \int_G dU U m U^{-1}, \quad (\text{E.2})$$

where m is an arbitrary $2N \times 2N$ matrix and dU is the invariant Haar measure of the group G . The integrand is a matrix-valued function and the relation (E.2) is to be handled entry-by-entry. Conjugating by an arbitrary matrix $V \in \text{Sp}(2N)$ and exploiting the invariance of the Haar measure yields:

$$V M V^{-1} = \int_G dU (VU) m (VU)^{-1} = M \Rightarrow V M = M V. \quad (\text{E.3})$$

Thus M commutes with all $V \in \text{Sp}(2N)$. For such M , Schur's lemma guarantees that M is scalar: $M = \mu \text{id}$. The factor μ is readily determined by evaluating the trace using its cyclicity: $2N\mu = \text{tr } M = \int_G dU \text{tr}(U m U^{-1}) = \text{tr } m$. So we find for the entries of M :

$$M_{ik} = \frac{\text{tr } m}{2N} \delta_{ik} \quad (\text{E.4})$$

The choice for the matrix m is taken such that the entries of U are picked out as called for by (E.1). m has only one single non-vanishing entry 1 in row j and column l : $m_{ab} = \delta_{aj}\delta_{bl}$.

$$M_{ik} = \int_G dU (U m U^{-1})_{ik} = \int_G dU U_{ij}(U^{-1})_{lk} = \frac{\delta_{ik}\delta_{jl}}{2N} \quad (\text{E.5})$$

which completes the proof of (E.1).

Likewise, the first of the relations (2.19)

$$\int_G dU U_{ij} = \int_G dU U_{ij} \mathbb{1} = 0 \quad (\text{E.6})$$

also resorts to the Schur orthogonality relations. The set of $2N \times 2N$ matrices $\{U\}$ fulfilling the condition $(U^{-1})^\dagger = U = J(U^{-1})^T J^{-1}$ (with J the symplectic unit) forms a fundamental representation of $\text{Sp}(2N)$. The trivial representation of $G = \text{Sp}(2N)$ is the representation which maps all group elements to the unit matrix. The integral (E.6) over such a combination of *inequivalent* irreducible representations vanishes due to the Schur orthogonality relations [98].

F. Form factors of the new ensembles

In this appendix the spectral form factor

$$K(t) = 2 \int_{-\infty}^{\infty} dE e^{-2\pi i E t} \langle \delta\rho(E) \rangle \quad (\text{F.1})$$

as defined by (1.51) is computed for the four classes C , CI , D , and $DIII$. The universal predictions for the averaged fluctuating part of the density $\langle \delta\rho(E) \rangle$ were calculated in [2].

As a starting point for calculating $K(t)$, the inverse of (F.1) is taken:

$$\langle \delta\rho(E) \rangle = \int_0^{\infty} dt \cos(2\pi E t) K(t). \quad (\text{F.2})$$

For classes C and D , one can read off the results given in [2]¹

$$\langle \delta\rho(E) \rangle = \pm \frac{\sin(2\pi E)}{2\pi E} = \pm \int_0^1 dt \cos(2\pi E t) \quad (\text{F.3})$$

and the form factors

$$K^C(t) = -\Theta(1-t) \quad (\text{F.4})$$

$$K^D(t) = \Theta(1-t) \text{ with } t > 0. \quad (\text{F.5})$$

For classes CI and $DIII$, we compare (F.2) with the full one-point function $g(E)$ presented in [2] to obtain $K(t)$. A detailed account of the calculation for class CI is given. For class $DIII$, we merely cite the result as the calculation closely follows the lines of the class CI case.

Using the relation $1 + \langle \delta\rho(\omega) \rangle = \langle \rho(\omega) \rangle = -\text{Im} \langle g(\omega) \rangle / \pi$, together with the form of the full one-point function presented in [2]

$$\langle g(E) \rangle = -i\pi + i \int_1^{\infty} du \int_{-1}^1 dv e^{i\pi E(u-v)} \frac{\sqrt{1-v^2}}{\sqrt{u^2-1}} \frac{1}{u-v} \quad (\text{F.6})$$

one obtains:

$$\begin{aligned} \langle \delta\rho(E) \rangle &= -\frac{1}{\pi} \text{Re} \int_1^{\infty} du \int_{-1}^1 dv \frac{e^{i\pi E(u-v)}}{u-v} \frac{\sqrt{1-v^2}}{\sqrt{u^2-1}} = \\ &= -\frac{1}{\pi} \int_1^{\infty} du \int_{-1}^1 dv \int_0^{\infty} dt \delta\left(t - \frac{u-v}{2}\right) \frac{\cos(2\pi E t)}{2t} \frac{\sqrt{1-v^2}}{\sqrt{u^2-1}} = \\ &= \int_0^{\infty} dt \cos(2\pi E t) K(t). \end{aligned} \quad (\text{F.7})$$

¹The positive sign applies for class D and the negative sign for class C .

Thus, we need to evaluate the following expression for the form factor $K^{CI}(t)$:

$$K^{CI}(t) = -\frac{1}{2\pi t} \int_1^\infty du \int_{-1}^1 dv \delta\left(t - \frac{u-v}{2}\right) \sqrt{\frac{1-v^2}{u^2-1}}. \quad (\text{F.8})$$

A brief glance at the argument of the δ -function motivates the coordinate transformation:

$$x = \frac{u-v}{2}, \quad s = \frac{u+v}{2} \quad \text{with} \quad \frac{\partial(u,v)}{\partial(x,s)} = 2. \quad (\text{F.9})$$

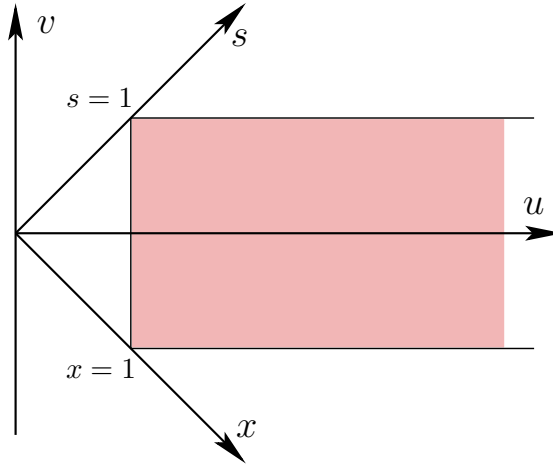


Figure F.1.: The integration domain of (F.8) is shaded and coordinates before and after the transformation are given.

The ranges of the new variables are $x \in \mathbb{R}_0^+$ and $s \in [\max(1-x, x-1), x+1]$. After the coordinate transformation the form factor reads:

$$\begin{aligned} K^{CI}(t) &= -\frac{1}{\pi t} \int_0^\infty dx \delta(t-x) \int_{\max(1-x, x-1)}^{1+x} ds \sqrt{\frac{1-(s-x)^2}{(s+x)^2-1}} = \\ &= -\frac{1}{\pi t} \int_{\max(1-t, t-1)}^{1+t} ds \sqrt{\frac{1-(s-t)^2}{(s+t)^2-1}}. \end{aligned} \quad (\text{F.10})$$

The exact expression (F.10) can be approximated by

$$\begin{aligned} K^{CI}(t) &= -1 + \frac{1}{2}t + \mathcal{O}(t^2) \quad \text{for } t \text{ close to zero and by} \\ K^{CI}(t) &= -\frac{1}{4t^2} + \mathcal{O}\left(\frac{1}{t^3}\right) \quad \text{for } t \text{ very large.} \end{aligned} \quad (\text{F.11})$$

We now turn to the form factor of class *DIII*. The starting point is again the

full one-point function as stated in [2]:

$$\begin{aligned} \langle g(E) \rangle &= -i\pi + i\pi \int_1^\infty du \frac{u}{\sqrt{u^2 - 1}} e^{2i\pi Eu} \\ &\quad - i \int_1^\infty du \int_{-1}^1 dv \frac{\sqrt{u^2 - 1}}{\sqrt{1 - v^2}} \frac{e^{2\pi i E(u-v)}}{u - v}. \end{aligned} \quad (\text{F.12})$$

The two integrals in (F.12) are treated separately. Again, using $\langle \rho(\omega) \rangle = -\text{Im} \langle g(\omega) \rangle / \pi$, one obtains from the first integral in (F.12) the contribution

$$K_1(t) = -\Theta(t - 1) \frac{t}{\sqrt{t^2 - 1}} \quad (\text{F.13})$$

to the form factor. The second contribution

$$K_2(t) = \frac{1}{\pi t} \int_1^\infty du \int_{-1}^{-1} dv \int_0^\infty dt \delta(t - (u - v)) \frac{\sqrt{u^2 - 1}}{\sqrt{1 - v^2}} \quad (\text{F.14})$$

bears close structural resemblance to the integral expression (F.8) of class *CI* and yields:

$$K_2(t) = \frac{1}{2\pi t} \int_{\max(t-2, 2-t)}^{2+t} ds \sqrt{\frac{(s+t)^2 - 4}{4 - (s-t)^2}}. \quad (\text{F.15})$$

Summing up the contributions $K_1(t)$ and $K_2(t)$ gives the form factor for class *DIII*:

$$K^{DIII}(t) = -\Theta(t - 1) \frac{t}{\sqrt{t^2 - 1}} + \frac{1}{2\pi t} \int_{\max(t-2, 2-t)}^{2+t} ds \sqrt{\frac{(s+t)^2 - 4}{4 - (s-t)^2}}. \quad (\text{F.16})$$

For comparison to the results obtained from periodic-orbit theory, the approximation of the form factor (F.16) for t close to zero is useful:

$$K^{DIII}(t) = \frac{1}{2} + \frac{1}{8}t + \mathcal{O}(t^3). \quad (\text{F.17})$$

For very large values of t one finds the approximation:

$$K^{DIII}(t) = -\frac{1}{t^2} + \mathcal{O}\left(\frac{1}{t^4}\right). \quad (\text{F.18})$$

Bibliography

- [1] Y. Imry, *Introduction to Mesoscopic Physics* (Oxford University Press, Oxford, 1997).
- [2] A. Altland and M. R. Zirnbauer, Phys. Rev. B **55**, 1142 (1997).
- [3] E. P. Wigner, Ann. Math. **67**, 325 (1958).
- [4] F. J. Dyson, J. Math. Phys. **3**, 1199 (1962).
- [5] J. J. M. Verbaarschot and I. Zahed, Phys. Rev. Lett. **70**, 3853 (1993).
- [6] J. J. M. Verbaarschot, Phys. Rev. Lett. **72**, 2531 (1994).
- [7] A. Altland, B. D. Simons, and M. R. Zirnbauer, Phys. Rep. **359**, 283 (2002).
- [8] M. C. Gutzwiller, J. Math. Phys. **12**, 343 (1971).
- [9] M. V. Berry, Proc. R. Soc. Lond. A **400**, 229 (1985).
- [10] T. Kottos and U. Smilansky, Phys. Rev. Lett. **79**, 4794 (1997).
- [11] T. Kottos and U. Smilansky, Annals of Physics **274**, 76 (1999).
- [12] J. Bardeen, L. N. Cooper, and J. R. Schrieffer, Phys. Rev. **108**, 1175 (1957).
- [13] L. N. Cooper, Phys. Rev. **104**, 1189 (1956).
- [14] P. G. de Gennes, *Superconductivity of Metals and Alloys* (W.A. Benjamin, New York, 1966).
- [15] N. N. Bogoliubov, Sov. Phys. JETP **7**, 41 (1958).
- [16] J. B. Ketterson and S. N. Song, *Superconductivity* (Cambridge University Press, Cambridge, 1999).
- [17] A. Altland, *Quantum field theory in condensed matter physics*, Lecture notes, 2001.
- [18] A. F. Andreev, Sov. Phys. JETP **19**, 1228 (1964).

- [19] N. W. Ashcroft and N. D. Mermin, *Solid State Physics* (Saunders College Publishing, Fort Worth, 1976).
- [20] C. W. J. Beenakker, *Rev. Mod. Phys.* **69**, 731 (1997).
- [21] H.-J. Stöckmann, *Quantum Chaos* (Cambridge University Press, Cambridge, 1999).
- [22] I. Kosztin, D. L. Maslov, and P. M. Goldbart, *Phys. Rev. Lett.* **75**, 1735 (1995).
- [23] J. Melsen, P. Brouwer, K. Frahm, and C. Beenakker, *Europhys. Lett.* **35**, 7 (1996).
- [24] G. Eilenberger, *Z. Phys. B* **214**, 195 (1968).
- [25] K. D. Usadel, *Phys. Rev. Lett.* **25**, 507 (1970).
- [26] J. Eroms *et al.*, *Europhys. Lett.* **58**, 569 (2002).
- [27] M. L. Mehta, *Random Matrices* (Academic Press, New York, 1991), 2nd edition.
- [28] O. Bohigas, M. J. Giannoni, and C. Schmit, *Phys. Rev. Lett.* **52**, 1 (1984).
- [29] M. R. Zirnbauer, *J. Math. Phys.* **37**, 4986 (1996).
- [30] C. E. Porter, *Statistical Theory of Spectra: Fluctuations* (Academic Press, New York, 1965).
- [31] T. Guhr, A. Müller-Groeling, and H. A. Weidenmüller, *Phys. Rep.* **299**, 189 (1998).
- [32] F. Haake, *Quantum Signatures of Chaos* (Springer, Berlin, 2000).
- [33] *Chaos and Quantum Physics (Les Houches Session LII)*, edited by M.-J. Giannoni, A. Voros, and J. Zinn-Justin (Elsevier, North-Holland, Amsterdam, 1989).
- [34] D. A. Ivanov, *J. Math. Phys.* **43**, 126 (2002).
- [35] M. R. Zirnbauer, *Random Matrices, Symmetry Classes, and Dual Pairs*, James H. Simons Workshop, Stony Brook, 2002; see: <http://tonic.physics.sunysb.edu/~verbaarschot/simons/talks/zirnbauer/index.html>.
- [36] R. Bundschuh, C. Cassanello, D. Serban, and M. R. Zirnbauer, *Nucl. Phys. B* **532**, 689 (1998).
- [37] R. Bundschuh, C. Cassanello, D. Serban, and M. R. Zirnbauer, *Phys. Rev. B* **59**, 4382 (1999).

- [38] M. Bocquet, D. Serban, and M. R. Zirnbauer, Nucl. Phys. B **578**, 628 (2000).
- [39] T. Senthil and M. P. A. Fisher, Phys. Rev. B **61**, 9690 (2000).
- [40] J. T. Chalker and P. D. Coddington, J. Phys. C **21**, 2665 (1988).
- [41] V. Kagalovsky, B. Horovitz, Y. Avishai, and J. T. Chalker, Phys. Rev. Lett. **82**, 3516 (1999).
- [42] I. A. Gruzberg, A. W. W. Ludwig, and N. Read, Phys. Rev. Lett. **82**, 4524 (1999).
- [43] E. J. Beamond, J. Cardy, and J. T. Chalker, preprint cond-mat/0201080, 2002.
- [44] E. J. Beamond, A. L. Owczarek, and J. Cardy, preprint cond-mat/0210359, 2002.
- [45] T. Senthil, J. B. Marston, and M. P. A. Fisher, Phys. Rev. B **60**, 4245 (1999).
- [46] F. Merz and J. T. Chalker, Phys. Rev. B **65**, 054425 (2002).
- [47] F. Merz and J. T. Chalker, Phys. Rev. B **66**, 054413 (2002).
- [48] M. C. Gutzwiller, J. Math. Phys. **8**, 1979 (1967).
- [49] M. C. Gutzwiller, J. Math. Phys. **10**, 1004 (1969).
- [50] M. C. Gutzwiller, J. Math. Phys. **11**, 1791 (1970).
- [51] M. C. Gutzwiller, *Chaos in Classical and Quantum Mechanics* (Springer, New York, 1990).
- [52] R. P. Feynman and A. R. Hibbs, *Quantum Mechanics and Path Integrals* (McGraw-Hill, New York, 1965).
- [53] A. Einstein, Verhandlungen der Deutschen Physikalischen Gesellschaft **19**, 82 (1917).
- [54] Y. C. de Verdière, Compositio Mathematica **27**, 83 (1973).
- [55] J. J. Duistermaat and V. W. Guillemin, Inv. Math. **29**, 39 (1975).
- [56] H.-J. Stöckmann and J. Stein, Phys. Rev. Lett. **64**, 2215 (1990).
- [57] D. Wintgen and H. Friedrich, Phys. Rev. Lett. **57**, 571 (1986).
- [58] D. Wintgen, Phys. Rev. Lett. **58**, 1589 (1987).
- [59] A. Holle *et al.*, Phys. Rev. Lett. **61**, 161 (1988).

- [60] J. H. Hannay and A. M. O. de Almeida, *J. Phys. A* **17**, 3429 (1984).
- [61] O. Agam, B. L. Altshuler, and A. V. Andreev, *Phys. Rev. Lett.* **75**, 4389 (1995).
- [62] E. B. Bogomolny and J. P. Keating, *Phys. Rev. Lett.* **77**, 1472 (1996).
- [63] H. Schanz and U. Smilansky, *Phys. Rev. Lett.* **84**, 1427 (2000).
- [64] M. Sieber and K. Richter, *Phys. Scr.* **T90**, 128 (2001).
- [65] M. Sieber and K. Richter, *Phys. Rev. Lett.* **89**, 206801 (2002).
- [66] P. A. Braun, F. Haake, and S. Heusler, *J. Phys. A: Math. Gen.* **35**, 1381 (2002).
- [67] P. W. Anderson, *Phys. Rev. B* **23**, 4828 (1981).
- [68] R. Klesse and M. Metzler, *Phys. Rev. Lett.* **79**, 721 (1997).
- [69] J. E. Avron, P. Exner, and Y. Last, *Phys. Rev. Lett.* **72**, 896 (1994).
- [70] P. Exner, *Phys. Rev. Lett.* **74**, 3503 (1995).
- [71] F. Scheck, *Mechanik* (Springer-Verlag, Berlin, 1990), 2nd edition.
- [72] H. Schanz and U. Smilansky, *Spectral Statistics for Quantum Graphs: Periodic Orbits and Combinatorics*, Proceedings of the Australian Summer School on Quantum Chaos and Mesoscopics, 1999.
- [73] T. Kottos and H. Schanz, *Physica E* **9**, 523 (2001).
- [74] T. Kottos and U. Smilansky, *Phys. Rev. Lett.* **85**, 968 (2000).
- [75] F. Barra and G. Gaspard, *Phys. Rev. E* **65**, 016205 (2002).
- [76] T. Kottos and U. Smilansky, preprint nlin/0207049, 2002.
- [77] T. Kottos and H. Schanz, preprint nlin. CD/0301021, 2003.
- [78] G. Berkolaiko, H. Schanz, and R. S. Whitney, Form factor for a family of quantum graphs: An expansion to third order, preprint nlin. CD/0205014, 2001.
- [79] G. Berkolaiko and J. P. Keating, *J. Phys. A: Math. Gen.* **32**, 7827 (1999).
- [80] G. Berkolaiko, E. B. Bogomolny, and J. P. Keating, *J. Phys. A: Math. Gen.* **34**, 335 (2001).
- [81] M. R. Zirnbauer, *J. Phys. A: Math. Gen.* **29**, 7113 (1996).

- [82] U. Smilansky, in *Les Houches 1994 – Session LXI – Mesoscopic quantum physics, Les Houches*, edited by E. Akkermans, G. Montambaux, J.-L. Pichard, and J. Zinn-Justin (Elsevier, Amsterdam, 1994), Chap. Semiclassical quantization of chaotic billiards – a scattering approach, pp. 373–433.
- [83] E. Doron and U. Smilansky, *Phys. Rev. Lett.* **68**, 1255 (1992).
- [84] R. A. Jalabert, in *The semiclassical tool in mesoscopic physics* (International School of Physics *Enrico Fermi*, Varenna, 1999).
- [85] D. H. Sattinger and O. L. Weaver, *Lie Groups and Algebras with Applications to Physics, Geometry and Mechanics* (Springer, New York, 1985).
- [86] M. R. Zirnbauer, *J. Phys. A* **29**, 7113 (1996).
- [87] M. R. Zirnbauer, private communication, 2001.
- [88] W. Ihra, M. Leadbeater, J. Vega, and K. Richter, *Eur. Phys. J. B* **21**, 425 (2001).
- [89] S. Gnutzmann, B. Seif, F. von Oppen, and M. R. Zirnbauer, preprint cond-mat/0207388, 2002.
- [90] G. E. Blonder, M. Tinkham, and T. M. Klapwijk, *Phys. Rev. B* **25**, 4515 (1982).
- [91] G. Tanner, *J. Phys. A* **34**, 8485 (2001).
- [92] G. Berkolaiko, H. Schanz, and R. Whitney, *Phys. Rev. Lett.* **88**, 523 (2002).
- [93] J. J. Sakurai, *Modern Quantum Mechanics* (Addison-Wesley, Reading, Massachusetts, 1994), revised edition.
- [94] W. H. Press, S. A. Teukolsky, W. T. Vetterling, and B. P. Flannery, *Numerical Recipes in C* (Cambridge University Press, Cambridge, 1992), 2nd edition.
- [95] D. Taras-Semchuk and A. Altland, *Phys. Rev. B* **64**, 014512 (2001).
- [96] A. Altland, B. D. Simons, and J. P. D. Taras-Semchuk, *Adv. Phys.* **49**, 321 (2000).
- [97] R. O. Vallejos, A. O. O. de Almeida, and C. H. Lewenkopf, *J. Phys. A: Math. Gen.* **31**, 4885 (1998).
- [98] A. W. Knap, *Lie Groups Beyond an Introduction* (Birkhäuser, Boston, 1996).

Danke

Zuallererst gilt mein Dank meinem Betreuer Prof. Dr. Martin R. Zirnbauer für die Themenstellung der Arbeit und seine stete Unterstützung und Betreuung, wobei er mir gleichzeitig immer großzügigen wissenschaftlichen und persönlichen Freiraum gegeben hat.

Ebenso möchte ich Prof. Dr. Felix von Oppen danken, dessen unermüdliche Diskussionsbereitschaft und Ermutigung für das Gelingen meiner Arbeit wesentlich war. Verbunden bin ich ihm auch dafür, daß er mich auch nach seinem Ruf nach Berlin weiter angeleitet hat. Für die Gastfreundschaft in Berlin danke ich ihm und seiner Familie.

Allen Mitarbeitern der Arbeitsgruppe Zirnbauer - besonders meinen Bürokollegen – danke ich für die freund(schaft)liche Arbeitsatmosphäre.

Für ihre Geduld bei der wissenschaftlichen Zusammenarbeit bedanke ich mich bei Dr. Stéphane Nonnenmacher, Dr. Rochus Klesse und Dr. Sven Gnutzmann. Ebenso danke ich ihnen für ihre wertvollen Korrekturvorschläge zum Manuskript meiner Arbeit. Siddhartha Lal is gratefully acknowledged as an amiable member of the proofreading department. Für sein Interesse danke ich Dr. Holger Schanz, dessen Anregungen ein wichtiges Puzzleteil zum Gelingen der Arbeit darstellten. Andreas Sindermann hat mir bei zahlreichen Fragen der Computerkunst geholfen.

Ich hätte mir gewünscht, daß Dr. Suzanne Krebs und Prof. Dr. Dr. Klaus Wittstadt den Abschluß meiner Arbeit noch erlebt hätten.

Bertram Klein, Anuradha Bhat, Siddhartha Lal, Heide, Ingrid & Gerhard Auers, Birgit Ocken, Annett Dittrich, Bettina Sauer, Birgit Kriener, Johannes Berg, Corinna Kollath, Sebastian Ernst, Christoph Singelstein, Michael Schröter, Petra Picken, Leo Wiest, Martin Rost, Alexander Linke, Marc Timme, Stefan Großkinsky, Stefan Bosch, Julie Barillet, Felix Stoehr, Michael Reder, Tanja Ihle, Björn Kirchner, Hsiao-Ching Cho, Hui Xia, Ying Feng, Marc Schlenso, Marion Guibault, Stéphane Nonnenmacher, Sabine Schiedermaier, Clemens Treter, Christian Geiselmann, Tanja Herrler, Ernestine Henger, Sonja Levensen, Tobias Leismann, Anneke Greta Prananto, Tim Storck, Etta Meyer, Peter Müller, Dorothee Gottwald und Antonia Hoffmann sind mit mir während meiner Kölner Zeit durch dick und dünn gegangen.

Meinem Vertrauensdozenten der Studienstiftung Professor Dr. Wulf Schiefenhövel bin ich für seine Förderung tief verbunden. Die Anregungen in seiner Gruppe haben mein Studium und meinen Berufsweg entscheidend mitgeprägt.

Meiner Familie und insbesondere meinen Eltern danke ich für ihre Unterstützung während Diplom- und Promotionsstudium.

Deutsche Zusammenfassung

Die vorliegende Arbeit ist im Bereich der mesoskopischen Physik angesiedelt. Es wird die Spektralstatistik von normalleitend-supraleitenden Hybridsystemen mit nicht-integrabler klassischer Dynamik untersucht. Wenn diese Systeme aus einem normalleitenden Billiard in Kontakt mit einem Supraleiter bestehen, werden sie als Andreev-Billiards bezeichnet.

Aufbauend auf der Symmetrieklassifizierung von Altland und Zirnbauer [2], die eine stochastische Beschreibung von derartigen normalleitend-supraleitenden Hybridsystemen mittels Ensembles von Zufallsmatrizen formuliert, stellt diese Arbeit eine semiklassische Interpretation der Vorhersagen der Zufallsmatrix-Theorie dar.

Grundlagen

Zuerst werden die Methoden und Konzepte vorgestellt, die für die Formulierung der Problemstellung und die anschließende Lösung derselben notwendig sind. Dabei führen wir zuerst in die theoretische Beschreibung der Supraleitung ein, die sich auf die Molekularfeldnäherung nach Bogoliubov stützt.

Daraufhin beschreiben wir die physikalischen Systeme, die im Rahmen der vorliegenden Arbeit untersucht werden: normalleitend-supraleitende Hybridsysteme. Diese bestehen aus einem normalleitenden Billiard, das in Kontakt mit einem Supraleiter gebracht wird. Wesentlich wird die Phänomenologie dieser Systeme vom Streumechanismus an der Grenzfläche zwischen Normalleiter und Supraleiter bestimmt, der unter dem Terminus *Andreev-Streuung* bekannt ist. Er basiert darauf, daß durch den Ordnungsparameter des Supraleiters elektronenartige und lochartige Anregungen gekoppelt werden. Aufgrund dieses Effekts werden an der Grenzfläche die aus dem normalleitenden Bereich einfallenden Elektronen (Löcher) als Löcher (Elektronen) in den normalleitenden Bereich zurückgestreut.

Ein weiterer umfangreicher Teil der Einleitung beschäftigt sich mit der Vorstellung der *Zufallsmatrix-Theorie*. Nach einem historischen Abriss konzentrieren wir uns auf die Symmetrieklassen [2], die im Zusammenhang mit normalleitend-supraleitenden Hybridsystemen eine herausragende Rolle spielen.

Die semiklassische Analyse der oben genannten Hybridsysteme nimmt Anleihe bei der *Spurformel* von Gutzwiller [8, 48–50]. Diese Spurformel liefert einen

Zusammenhang zwischen dem Quantenspektrum eines chaotischen Systems und seinen klassischen periodischen Orbits und ihren Eigenschaften. Desweiteren wurde von Berry gezeigt [9], wie *universelle* (d. h. von den Systemspezifika unabhängige) Vorhersagen der Zufallsmatrix-Theorie durch die Anwendung der Theorie periodischer Orbits rekonstruiert werden können. Die hierfür verwendete Approximation ist als *Diagonalnäherung* bekannt.

Die Theorie periodischer Orbits wird besonders transparent im Rahmen des verwendeten Modells der *Quanten-Graphen* [10, 11], dessen Einführung den Abschluß des ersten Kapitels bildet. Die Quanten-Graphen erlauben es, eine *exakte* Quantisierungsbedingung $\det(1 - \mathcal{S}_B) = 0$ mit Hilfe der sogenannten Bond-Streumatrix \mathcal{S}_B anzugeben. Die Entwicklung dieser Säkulargleichung führt unmittelbar zu einer Spurformel vom Gutzwillerschen Typ.

Numerische Untersuchungen an Andreev Graphen

Im Modell der Quanten-Graphen propagiert die quantenmechanische Wellenfunktion in eindimensionalen Leitern, die an Vertizes verbunden sind, wo die eintreffenden Wellenfunktionen gestreut werden. Die vorliegende Arbeit statet die Quanten-Graphen auf den Vertizes mit dem Mechanismus der Andreev-Streuung aus. Dies erlaubt uns die semiklassische Analyse der neuen Symmetrieklassen [2] mittels der Theorie periodischer Orbits auf Graphen. Für derartige Graphen verwenden wir die Bezeichnung *Andreev-Quanten-Graphen*.

Für die numerische Untersuchung werden Ensembles von Andreev-Graphen durch die Wahl zufälliger Streubedingungen auf den Vertizes generiert. Hierbei lassen wir uns von dem Vorgehen von Kottos *et al* [73] leiten, die Ensembles für Teilchen mit Schrödinger-Dynamik konstruiert haben.

Die Herleitung der zu wählenden Form der Vertexstreumatrizen $\sigma^{(j)}$ für die jeweiligen Vertizes j wird in einiger Ausführlichkeit präsentiert.

Im Anschluß daran wird die numerische Routine zur Auswertung der Graphen-Spektren vorgestellt, die sich auf eine Darstellung der Bond-Streumatrix \mathcal{S}_B der Graphen in einer Darstellung mittels ihrer Eigenphasen stützt.

Anhand der Spektren für die derart erzeugten Ensembles von Graphen konnte für große Graphen gute Übereinstimmung mit Vorhersagen der Zufallsmatrix-Theorie der zugehörigen Symmetrieklasse gezeigt werden. Abweichungen hiervon werden auf Beiträge kurzer, systemspezifischer (und damit nicht-universeller Orbits) zurückgeführt.

Andreev-Stern-Graphen

Nachfolgend werden Andreev-Billiards mit Symmetrien der Klassen C , CI , D und $DIII$ durch Andreev-Stern-Graphen modelliert.

Diese Graphen verknüpfen sternförmig einen zentralen Vertex mit N peripheren Vertices, an denen Andreev-Streuung stattfindet. Bei der Konstruktion der Sterngraphen unterscheidet man zwischen den beiden Symmetrieklassen C und CI , für die die Spinrotationsinvarianz erhalten ist, und den verbleibenden Symmetrieklassen D und $DIII$, in denen diese Invarianz nicht gewahrt ist. Im letzteren Fall berücksichtigt die Formulierung des Sterngraphs neben den Freiheitsgraden von Elektronen und Löchern zusätzlich auch die Spinfreiheitsgrade. Die jeweiligen Steubedingungen für die Andreevstreuung an den peripheren Vertices werden aus den durch die entsprechenden Symmetrieklassen gegebenen Bedingungen hergeleitet.

Für die Andreev-Stern-Graphen mit den verschiedenen Symmetrien wird in dieser Arbeit mit Hilfe der Theorie periodischer Orbits der spektrale Formfaktor (definiert als die Fourier-Transformierte der Zustandsdichte $\rho(E)$) für kurze Zeiten t in Übereinstimmung mit der Zufallsmatrix-Vorhersage [2] reproduziert.

Essentielles Hilfsmittel hierbei ist die sogenannte *selbst-duale Näherung*, die nur derartige Orbits berücksichtigt, in denen jedes Teilstück eines Orbits sowohl von einem Elektron wie auch von einem Loch durchlaufen wird. Diese *selbst-duale Näherung* ist in der Anwendung auf die neuen Symmetrieklassen [2] das Analogon zu Berrys diagonaler Näherung [9] im Kontext der klassischen Wigner-Dyson Ensembles.

Sämtliche Ergebnisse konnten durch numerische Arbeit bestätigt werden. Dabei zeigen die numerischen Ergebnisse hervorragende Übereinstimmung mit den Vorhersagen der Zufallsmatrix-Theorie [2]. Gleichzeitig sind die analytischen Ergebnisse der Theorie periodischer Orbits, die für kurze Zeiten t gültig sind, im Einklang mit den numerischen Ergebnissen.

Abschließend konnte für die Symmetrieklassen C und CI das Konzept der *selbst-dualen Näherung* auf die ursprünglichen Andreev-Billiards übertragen werden.

Abstract

The present thesis investigates the spectral statistics of superconducting-normalconducting hybrid systems. These hybrid systems are formed by a normal-metal non-integrable billiard being placed adjacent to a superconductor. The symmetry classification scheme of such systems due to Altland and Zirnbauer is at the basis of the thesis. For the mesoscopic systems described above, we give a semiclassical interpretation of the random-matrix theory prediction (by Altland and Zirnbauer) using periodic-orbit theory. Periodic-orbit theory links the quantum spectrum of a system with its classical periodic orbits. The model of choice for the treatment of the hybrid systems are quantum graphs. For an implementation of the hybrid character, the so-called Andreev scattering process is incorporated on the vertices of the graph.

After an introduction to the concepts and methods used (chapter 1), a numerical treatise shows us how to generate an ensemble of graphs by appropriately choosing random scattering conditions at the vertices (chapter 2). The spectrum of these graphs coincides perfectly with the random-matrix theory predictions in the limit of large graphs.

Models of Andreev graphs with symmetries of the classes C , CI , D , and $DIII$ are formulated with the aid of Andreev star graphs (chapter 3). By the use of periodic-orbit theory, the short-time behaviour of the spectral form factor (the Fourier transform of the spectral density) is calculated semiclassically and shows excellent agreement with the predictions of Altland and Zirnbauer. All analytical calculations are supplemented with numerical results which are in perfect agreement with the analytical results and the random-matrix theory predictions. For symmetry classes C and CI , the approximation schemes developed with the help of quantum graphs have been carried over to the original physical system of Andreev billiards.

Kurzzusammenfassung

Die vorliegende Arbeit untersucht die Spektralstatistik von normalleitend-supraleitenden Hybridsystemen mit nicht-integrabler klassischer Dynamik. Bestehen diese Systeme aus einem normalleitenden Billiard in Kontakt mit einem Supraleiter, werden diese Systeme auch als Andreev-Billiards bezeichnet.

Aufbauend auf der Symmetrieklassifizierung von Altland und Zirnbauer, die für die stochastische Beschreibung der oben genannten Hybridsysteme Ensembles von Zufallsmatrizen formuliert, stellt diese Arbeit eine semiklassische Interpretation der Vorhersagen der Zufallsmatrix-Theorie dar. Dabei stützt sie sich auf die Gutzwillersche Spurformel, mit deren Hilfe ein Zusammenhang zwischen dem Quantenspektrum eines chaotischen Systems und seinen klassischen periodischen Orbits hergestellt wird.

Die Modellierung der physikalischen Systeme wird mittels Quanten-Graphen bewerkstelligt, die im Rahmen der vorliegenden Arbeit zusätzlich mit dem Mechanismus der sogenannten Andreev-Streuung ausgestattet sind.

Nach einer Einleitung in die Grundlagen (Kapitel 1) wird in einer numerischen Abhandlung gezeigt, wie Ensembles von Andreev-Graphen durch die Wahl zufälliger Streubedingungen auf den Knotenpunkten generiert werden können (Kapitel 2). Die Spektren für die derart erzeugten Graphen-Ensembles zeigen für große Graphen Übereinstimmung mit Vorhersagen der zugehörigen Zufallsmatrix-Theorie.

Nachfolgend werden Andreev-Billiards mit Symmetrien der Klassen C , CI , D und $DIII$ durch sternförmige Andreev-Graphen modelliert (Kapitel 3). Für dieses System konnte mithilfe der Theorie periodischer Orbits im Bereich kurzer Zeiten der spektrale Formfaktor (Fourier-Transformierte der Zustandsdichte) in Übereinstimmung mit den Vorhersagen von Altland und Zirnbauer reproduziert werden. Sämtliche analytisch gefundenen Ergebnisse wurden durch entsprechende numerische Arbeit bestätigt. Für die Symmetrieklassen C und CI wurden die im Rahmen der Graphen entwickelten Näherungen auf das ursprüngliche Andreev-Billiard übertragen.

Erklärung

Ich versichere, daß ich die von mir vorgelegte Dissertation selbständig angefertigt, die benutzten Quellen und Hilfsmittel vollständig angegeben und die Stellen der Arbeit – einschließlich Tabellen, Karten und Abbildungen –, die anderen Werken im Wortlaut oder dem Sinn nach entnommen sind, in jedem Einzelfall als Entlehnung kenntlich gemacht habe; daß diese Dissertation noch keiner anderen Fakultät oder Universität zur Prüfung vorgelegen hat; daß sie – abgesehen von unten angegebenen Teilpublikationen – noch nicht veröffentlicht worden ist sowie, daß ich eine solche Veröffentlichung vor Abschluß des Promotionsverfahrens nicht vornehmen werde. Die Bestimmungen dieser Promotionsordnung sind mir bekannt. Die von mir vorgelegte Dissertation ist von Prof. Dr. Martin R. Zirnbauer betreut worden.

Köln, den 14. März 2003

Teilpublikation:

S. Gnutzmann, B. Seif, F. von Oppen and M. R. Zirnbauer, *Universal spectral statistics of Andreev billiards: semiclassical approach*, preprint cond-mat/0207388, accepted for publication in Phys. Rev. E..

Name	Burkhard E. R. Seif
Geburtsdatum	17.01.1974
Geburtsort	Freiburg im Breisgau
Familienstand	ledig
Staatsangehörigkeit	deutsch

Schulbildung

09/1980 - 07/1984	Goethe-Grundschule in Würzburg
09/1984 - 06/1990	Wirsberg-Gymnasium in Würzburg
07/1990 - 12/1990	William-Parker-School in Hastings, England
01/1991 - 07/1993	Wirsberg-Gymnasium in Würzburg
07/1993	Abitur

Zivildienst

07/1993 - 11/1994	in Brüssel am Institut Robert Schuman und bei l'Arche Bruxelles
-------------------	--

Hochschulstudium

11/1994 - 08/1996	Grundstudium Physik an der Universität Würzburg
08/1996	Vordiplom
10/1996 - 01/1999	Hauptstudium der Physik an der Technischen Universität München
01/1999	Diplomprüfung
seit 03/1999	Promotionsstudium an der Universität zu Köln
1996 – 1999	Stipendiat der Studienstiftung des deutschen Volkes und nach Bayerischem Begabtenförderungsgesetz